Metabolic control of sensory neuron survival by the p75 neurotrophin receptor in Schwann cells

By Rose M. Follis

Dissertation

Submitted to the Faculty of the

Graduate School of Vanderbilt University

in partial fulfillment of the requirements

for the degree of

DOCTOR OF PHILOSOPHY

In

Neuroscience

February 28, 2021

Nashville, Tennessee

Approved:

Dr. Ronald Emeson, Ph.D.

Dr. Jun Li, M.D., Ph.D.

Dr. Ned Porter, Ph.D.

Dr. Bruce Carter, Ph.D.

Dedication

To family, friends, and the world’s baristas.

Acknowledgements

No science is ever done in isolation. As I wrote this, I was constantly reminded of how many people have contributed to the experiments within these pages. However, since this monster is already clocking in at 170 pages, I'll spare you a full account and just go for a few shout outs.

Starting at home, the Carter lab, I'd like to thank our head honcho, Bruce, for his leadership, guidance, and pumpkin porter. Also, all my awesome Carter lab coworkers who joined me in hours long debates on how to figure out if your randomization is random, if mice think we are alien overlords or don't think about us at all, and why on the heck every incubation in science is 5 minutes (I vote superstition).

I'd also like to thank those that kept us feed and funded (the VBI, Biochemistry Department, and NIH). As well as those that had to put up with my horrible handwriting (the staff of the EM and TPSR cores), horrible paperwork skills (Roz, Jen, and Beth), and endless questions when this project went in down unexpected paths (too many to name, if I'm honest). Also, my committee past and present.

Lastly, I would like to thank all friends and family. May they all be less tormented from here on out by my grumpy mutterings detailing cannibal mice and core computers with Windows Vista installed.

Table of Contents

List of Tables

Table **Page**

List of Figures

List of Abbreviations

7-DHC- 7-dehydrocholesterol

8-DHC- 8-dehydrocholesterol

ABCA1/D1- ATP-binding cassette transporter A1/D1

AMN- adrenomyeloneuropathy

AR-CMT2- Autosomal Recessive CMT 2

AREs-antioxidant response elements

ASM- acid sphingomyelinase

BBB- blood-brain barrier

BDNF- brain derived neurotrophic factor

BNB- blood-nerve barrier

CDK5- cyclin-dependent kinase 5

CIPN- chemotherapy-induced peripheral neuropathy

CMT- Charcot-Marie-Tooth Disease

CNS- Central Nervous System

CTX- Cerebrotendinous xanthomatosis

DAG- diacylglycerol

Dhh- Desert hedgehog

DN- diabetic neuropathy

DNA- deoxyribonucleic acid

doxmethSA- deoxymethylsphinganine

doxSA- deoxysphinganine

DRG-dorsal root ganglion

EIF2α- Eukaryotic Initiation Factor 2 alpha

ER- Endoplasmic Reticulum

ErbB 2/3- erb-b receptor tyrosine kinase 2/3

FA- fatty acid

FFA- free fatty acids

GM3- monosialodihexosylganglioside

GPL-glycerophospholipids

GSK3β- glycogen synthase kinase-3

HMG-CoA- 3-hydroxy-3-methylglutaryl-coenzyme-A

HNE- 4-hydroxy-2-noneal

HNPP- hereditary neuropathy with liability to pressure palsy

HSAN1- Hereditary Sensory and Autonomic Neuropathy

IKK- IκB Receptor Kinase

IL1-R-interleukin-1 receptor

IRE1α-inositol-requiring enzyme 1 α

IRS- insulin receptor

iSC-intermediate Schwan cell

IκBβ- inhibitor of nuclear factor kappa B β

JNK- c-jun N-terminal kinase

LDLR- low density lipoprotein receptor

LOX-1 -oxLDL receptor

LXR- Liver X Receptor

lysoGb3- lysoglobotriaosylceramide/globotriaosylsphingosine

Maf- mitogen-activated protein

MAPK/ERK- mitogen-activated protein kinases

MDA- malondialdehyde

MLCL- monolysocardiolipin

MLD-Metachromatic Leukodystrophy

MPZ/P0- Myelin Protein Zero

mTOR- mechanistic target of rapamycin

NADPH- Nicotinamide adenine dinucleotide phosphate

NCC- neural crest cell

NFκB- nuclear factor kappa-light-chain-enhancer of activated B cells

NGF- nerve growth factor

NOND- naturally occurring neuronal death

Non-M- non-myelinating

NPD- Niemann-Pick Disease

Nrf2- eythroid 2 (NFE2)-related factor 2

NRG1- neuregulin I

NT-3- neurotrophin-3

NT-4- neutrotrophin 4

p75 - Nerve Growth Factor Receptor / NGFR/ p75 neurotrophin receptor

PCD- programed cell death

Perk- protein kinase RNA-like endoplasmic reticulum kinase

Pex5- peroxisome biogenesis factor peroxin 5

PKC- protein kinase C

PMP22- Peripheral Myelin Protein 22

PNS- Peripheral Nervous System

PP1- protein phosphatase 1

Pro-M- pro-myelinating

PUFAs- polyunsaturated fatty acids

RD- Refsum disease

RNA-ribonucleic acid

ROS- reactive oxygen species

S1P- sphingosine-1-phosphate

SCG-satellite glia cell

SCP-Schwann cell precursor

SC-Schwann cell

SFN- small-fiber neuropathy

SLOS- Smith-Lemli-Opitz Syndrome

SPL- sphingosine 1-phosphate lyase

SREBP- sterol-responsive element binding protein

TAG- triacylglycerol

TD- Tangier disease

Thy 1- Thy-1 Cell Surface Antigen

TLR-Toll like receptor

TNFR- tumor necrosis factor receptor

TrkA/B/C- tropomyosin-related kinase A/B/C

UPR- Unfolded Protein Response pathway

VLCFA- Very Long-Chain Fatty Acid

X-ALD- X-linked Adrenoleukodystrophy

Chapter I

Introduction

Overview

> *We remark…..an external pale thin cell-membrane, have a granulated but not a fibrous aspect, the inner surface of which constantly exhibits cell-nuclei in the very early period of the development of the nerve; but in the somewhat more advanced stage, when the white substance is developed, they are only occasionally found…..The white, fat-like substance to which the peculiar appearance and the distinct outline of the nerves is chiefly referable, is deposited upon the inner surface of this cell-membrane….The rest of the cell cavity appears to be filled up with a firm substance, namely, the band discovered by Remak.*
>
> Translated from Theodor Schwann's Mikroskopische Untersuchungen, 1839

Since their discovery in the mid-1800s by Theodor Schwann, Schwann cells have, for the most part, been studied within the context of their, admittedly hard-to-ignore, roles in axon conduction and regeneration. The ensheathment of medium to large caliber peripheral axons by Schwann cells with myelin, compacted layers of specialized membrane bilayer, reduces axonal capacitance, forms the nodes of Ranvier, and guides axon channel segregation. Together, this allows for increased axonal signaling speed and efficiency, through saltatory conduction, and is instrumental in the organization and honing of the peripheral nervous system (PNS) (Mirsky et al., 2002; Jessen, Mirsky and Salzer, 2008). Consequently, the importance of Schwann cells to PNS pathobiology cannot be overstated, with numerous neuropathies either caused, or perpetuated by, dysfunctional myelin formation and/or maintenance (Chrast Roman et al., 2011; Li, 2015; Duncan and Radcliff, 2016). Equally, the ability of Schwann cells to reprogram into precursor-like cells after nerve injury and to promote regeneration far beyond what is achievable by their Central Nervous System (CNS) counterparts, oligodendrocytes, has been instrumental in advancing CNS regenerative therapies (Jessen et al., 2016).

However, a rapidly enlarging pool of data suggests that Schwann cell metabolic dysfunction, leading to the accumulation of cytotoxic lipid species may be a significant component of many peripheral nerve pathologies. In this work, Chapter 1 will first provide an overview of the complex interactions between Schwann cells and neurons in the developing nerve and summarize recent findings that implicate Schwann cell lipid metabolic dysfunction in broad range of inherited and acquired neuropathies. In Chapters 2-5, I will detail my own findings, that deletion of the p75 neurotrophin receptor in Schwann cells leads to a significant loss of sensory neurons during development due to the dysregulation of cholesterol biosynthesis and subsequent accumulation of neurotoxic 7-dehydrocholesterol in peripheral nerves. Lastly, Appendix I will describe a separate project investigating the role of NFκB signaling in inherited neuropathy. Appendix II contains supplemental tables, and a bibliography.

Introduction

The Impact of Neuropathy

Neuropathy, sometimes also referred to as peripheral neuropathy, is defined as any disorder characterized by peripheral nerve abnormalities, whether these abnormalities are inherited (genetic), acquired (metabolic/toxic insult), or idiopathic (of unknown origin). Common abnormalities include structural alterations to peripheral neurons (axon degeneration and metabolic/conductive disruption), Schwann cells (de-/dysmyelination), or both (Hughes, 2002; Azhary et al., 2010). These abnormalities typically result in electrophysiological and impaired nerve conduction. Depending on the severity and type of neuropathy, these disorders can result in neuropathic pain, loss of sensation, muscle weakness, autonomic dysregulation, and skeletal abnormalities. In the United States it is estimated that 14.8% of persons over 40 have neuropathy, with that number expected to increase due to the rising prevalence of Type 2 diabetes mellitus (Gregg et al., 2004). Diabetic neuropathy is not only the most common form of acquired sensory neuropathy, but a leading risk factor for severe diabetic complications (Hicks and

Selvin, 2019). Therefore, the development of new treatments for neuropathies is both of medical and economic importance, especially given the rising age of world populations. Unfortunately, our understanding of the complex pathological mechanisms underlying neuropathy is far from complete. Additionally, while clinical presentation and diagnosis of many neuropathies occurs in adulthood, the underlying etiology is often present years before diagnosis, in many cases even during PNS development when the survival and establishment of neurons and Schwann cells are heavily interdependent (Azhary et al., 2010). This makes attaining a more complete understanding of the complex nature of peripheral nerve formation and metabolism a key priority in advancing neuropathy treatment discovery.

Cells of the Peripheral Nervous System

Neurons

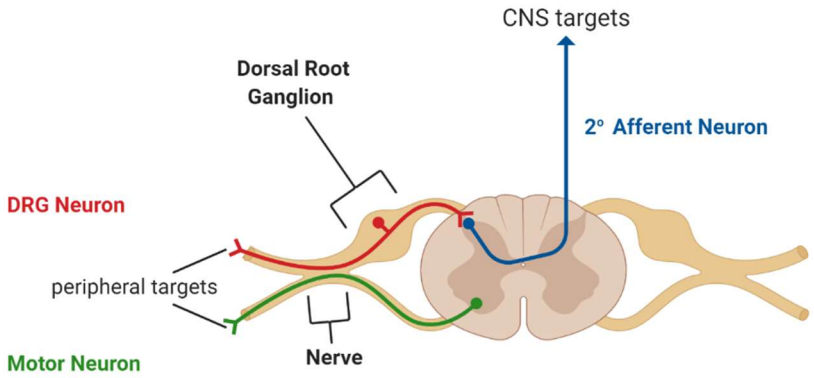

Figure 1. Basic Anatomy of Peripheral Somatic Neurons. Transverse diagram of spinal column and peripheral somatic neurons. Lower motor neurons (green) have soma within the ventral horn of the spinal column and have efferent projections out to peripheral targets (motor fibers). DRG neuron (red) soma are in the Dorsal Root Ganglion adjacent to the dorsal horn of the spinal column, where they have one afferent axon branch which synapse with secondary afferent neurons projecting to CNS somatosensory targets. A second axonal branch transmits sensory information from peripheral tissue. For brevity, a reflex arc/circuit, where DRG neurons form a localized circuit with motor neurons and interneurons in the spinal cord, have been omitted. Abbreviations are as follows, CNS, Central Nervous System; 2°, secondary, DRG; Dorsal Root Ganglion. This and all other illustrative figures herein were created with BioRender.com

The neurons of the PNS can be roughly divided into two distinct groups. Autonomic neurons include the sympathetic, parasympathetic, and enteric neuron populations. While somatic neurons comprise efferent lower motor neurons and afferent somatosensory neurons (Basso et al., 2019) (Fig. 1). Both motor and somatosensory neurons are highly susceptible to damage in acquired and inherited peripheral neuropathies (Azhary et al., 2010). However, lower motor neurons have their cell bodies in the ventral horn of the spinal cord, or cranial nerve nuclei, with axonal projections to distal muscle fiber targets, and thus cannot be considered solely in the context of the PNS environment, unlike primary, or first-order, somatosensory neurons (Felten, O'Banion and Maida, 2016b, 2016a).

Primary somatosensory neurons are responsible for conveying sensory information from the periphery to secondary CNS afferent neurons in a relay system ending at the central somatosensory system. Additionally, some somatosensory neurons are part of localized reflex arc/circuits in the spinal cord along with motor neurons and spinal interneurons, which mediate reflex responses(Akinrodoye and Lui, 2020). Primary somatosensory neurons have their cell body (soma) located in a series of small ovoid organs adjacent to the spinal cord called the Dorsal Root Ganglia (DRG) and are, therefore, collectively known as DRG neurons. DRG neurons relay an extensive array of stimulus information, from proprioception and touch to temperature and pain (nociception)(Cesmebasi, 2015). Consequently, DRG neurons vary largely in size, receptor properties, biomarkers, and conduction speed (Nascimento, Mar and Sousa, 2018).

However, while DRG neurons are an extremely heterogeneous population, they all share a unique pseudounipolar structure. Lacking dendrites, DRG neurons instead have a single stem like axonal projection which bifurcates. One branch extends along the dorsal root, traveling medially to synapse with neurons located in the spinal cord. The other branch exits the DRG distally and merges with motor neuron projections in the diverging nerves of the peripheral nervous system before innervating peripheral tissue. As DRG are somas are closely adjacent to the spinal cord and have extended axonal projections to all distal tissues, they are exceptionally reliant on close interactions with

PNS glia cells for trophic support, both during and after development (Cesmebasi, 2015; Nascimento, Mar and Sousa, 2018).

Gila

While the CNS has a diverse retinue of glia cells, the glia cells of the PNS are traditionally limited to satellite glia cells (SGC) and Schwann cells (SCs). Although, there are several disputed candidates which are also instrumental in nerve structure. For instance recent evidence suggests many, if not all, perineurial cells are glia of CNS origin residing in the PNS, rather than as previously believed, fibroblasts (Kucenas, 2015). SGCs reside exclusively within PNS ganglia, including the DRGs, sympathetic and parasympathetic ganglia, where they form extremely close (20nm) associations with neuron cells bodies. They also form both tight and gap junctions with other SGCs surrounding the same DRGs, producing what amounts to a structured pocket engulfing DRG soma. Although SGC function is far from fully understood, many investigators propose SGCs have a functional role analogous to CNS astrocytes, including glutamate and potassium buffering, electrical coupling, and trophic signaling (Kastriti and Adameyko, 2017; Hanani and Spray, 2020). Interestingly, although SGCs are functionally distinct from SCs *in vivo* it has also been proposed that satellite glia are actually a subpopulation of early Schwann cell precursors, arrested in development by soma contact signaling (George, Ahrens and Lambert, 2018). This is supported by their ability to function as Schwann cell progenitors and, more controversially, neuron progenitors, after injury (Arora et al., 2007; Li, Say and Zhou, 2007; Muratori et al., 2015). Also, when cultured from DRGs, satellite glia cells are capable of myelination and take on morphology and expression profiles currently indistinguishable from comparably cultured Schwann cells derived from distal nerves (George, Ahrens and Lambert, 2018). Experimentally, this is important to note in the context of in vitro experiments, which often utilize dorsal root ganglion and nerve derived glia interchangeably.

What the PNS may lack in overall glia diversity, Schwann cells make up for in a diversity of roles. As previously mentioned, Schwann cells are primarily known as the

myelinating cell of the PNS. A large subset of Schwann cells, also known as myelinating Schwann cells, form a one-to-one relationship with medium-to-large caliber axons (≥1 micron in diameter), which they then myelinate. However, peripheral nerves also contain non-myelinating Schwann cells that closely associate with many small caliber axons concurrently to form loosely enveloped axon collectives called Remak bundles. Both myelinating, and non-myelinating Schwann cells are considered instrumental to conduction and axonal trophic support (Griffin and Thompson, 2008). Additionally, several Schwann cell subtypes exist with far less elucidated functions, such as terminal Schwann cells, found in association with synapses at the neuromuscular junctions, and inter organal Schwann cells, located within distinct tissue niches such as pancreatic islets (Sunami et al., 2001; Kang et al., 2014).

A Timeline of Nerve Development

Neurogenesis and Gliogenesis

Almost all peripheral glia cells and neurons (autonomic and somatosensory) originate from neural crest cell progenitors and DRG neurons begin development as clear forerunners. Between E8.5 and E10 in the mouse, neural crest cells located in the dorsal region of the neural tube after neurulation begin to migrate ventrally and form the nascent dorsal root ganglia (Kasemeir-Kulesa, Kulesa and Lefcort, 2005; Nascimento, Mar and Sousa, 2018) (Fig 2.). Directly after this migration, the majority of DRG neurons are generated and immediately begin target seeking in two distinct but overlapping waves from E9.5 to E11.5 (Lawson and Biscoe, 1979)(Marmigère and Carroll, 2014). A third smaller wave occurs after E12 from a divergent population, called the boundary cap cells, which also give rise to small population of Schwann cells (Marol et al., 2004). Schwann cells precursors, separated from their neural crest progenitors by expression of unique markers such as cadherin-19, do not infiltrate the peripheral nerve until around E12-13 (Takahashi and Osumi, 2005; Jessen and Mirsky, 2019). Glia cell populations remaining within the DRG after migration, and associated with somata rather than axons, become

satellite glia cells(Le Douarin and Dupin, 1993; Hanani and Spray, 2020)(Hanani and Spray, 2020) . Once present in the nerve, Schwann cell precursors are reliant on axonal signals for migration guidance, continued proliferation, and survival signaling as they migrate in association with pioneering target-seeking axonal projections from DRG neurons (Mirsky et al., 2008).

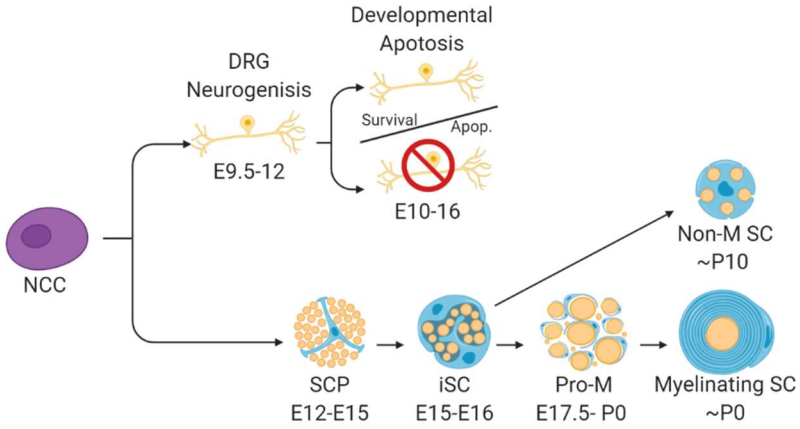

Figure 2. Diagram of Schwann cell and DRG neuron development. This timeline is based on mouse peripheral nerve development (rat development is approximately 1 day delayed). Neural crest cell progenitors give rise to both the DRG sensory neurons and Schwann cells during embryonic development. DRG neurons undergo a period of programed cell death, or naturally occurring neuronal death, soon after neurogenesis and axonal outgrowth towards target tissues. Schwann cells undergo several transitionary stages during development before differentiating into either a Remak bundle forming non-myelinating Schwann cell, or a myelin forming myelinating Schwann cell. Abbreviations are as follows, NCC, neural crest cell; DRG, dorsal root ganglion neuron; Apop., apoptosis; SCP, Schwann cell precursor, iSC; intermediate Schwann cell, Pro-M; pro-myelinating Schwann cell (late state radial sorting); Non-M SC, non-myelinating Schwann cell; E, embryonic day; P, post natal day (P0= day of birth).

Programed Cell Death and the Neurotrophin Family

While DRG neurons are not dependent on Schwann cells for survival immediately after neurogenesis, they are immediately beholden to external factors that determine their cell fate. As in the CNS, neurogenesis in the PNS produces a surplus of most neuronal subtypes, many more than necessary, or even optimal, for signaling. Consequently, an

estimated half of all neurons in PNS development undergo apoptosis in a period of programed cell death (PCD), also termed Naturally Occurring Neuronal Death (NOND). In the DRG, NOND transpires concurrently with neurogenesis and axonal outgrowth, ending shortly after target innervation is fully established, and is thought to be regulated primarily by target derived neurotrophic factor signaling (Oppenheim, 1991; Lossi, Castagna and Merighi, 2015b).

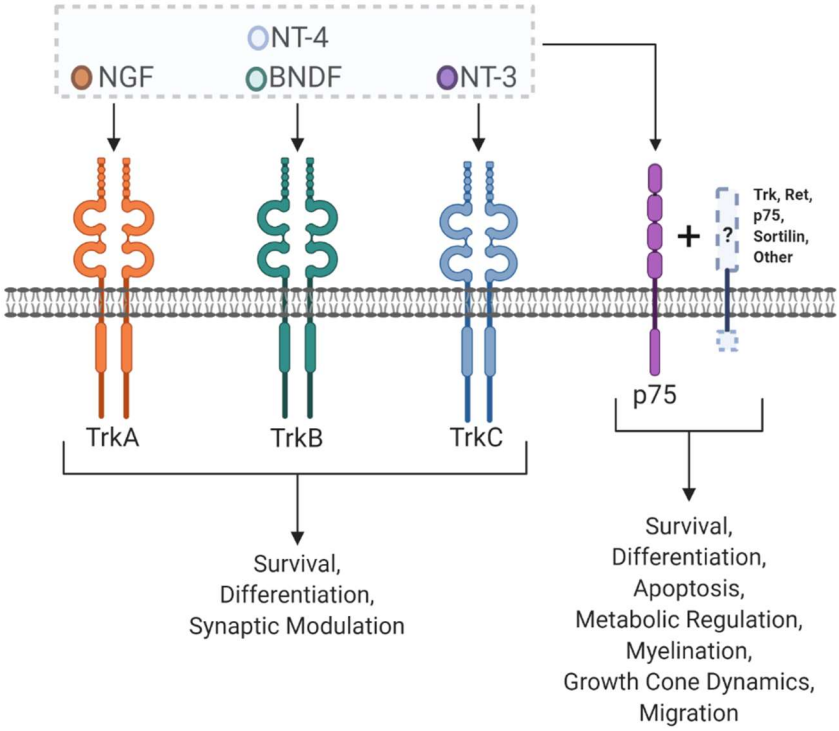

Figure 3. Simplified overview of neurotrophin binding and signaling pathways. Neurotrophin receptors are depicted as dimers, as neurotrophin signaling typically results in the dimerization of neurotrophin receptors. Neurotrophins are specific ligands to Trk receptors, but all bind to p75. P75 has several potential receptor signaling partners, which alter both neurotrophin binding affinity and downstream signaling. It should be noted these partners include the Trk family receptors themselves, which can form a high affinity receptor complex. Abbreviations are as follows, Trk A-C; Tropomyosin Receptor Kinase A-C; p75, p75 neurotrophin receptor; NGF, Nerve Growth Factor; NT-3/4, Neurotrophin-3/4; Ret, Ret Receptor.

The most significant neurotrophic factors for DRG survival during development belong to the neurotrophin family which, in mammalians, is comprised of Nerve Growth

Factor (NGF), Brain Derived Neurotrophic Factor (BNDF), Neurotrophin-3, and Neurotrophin-4/5 (NT-3, NT-4/5) (Fig. 3). Neurotrophins are small highly conserved polypeptides, which are secreted as either cleaved mature neurotrophins or as pro-neurotrophin precursors. All sensory neurons are thought to express at least one major neurotrophin receptor belonging to one of two receptor families, the tyrosine receptor kinases of the tropomyosin-related kinase (Trk) family (TrkA, TrkB,TrC), or p75 (also known as the nerve growth factor receptor (NGFR)) a member of the tumor necrosis factor receptor family (TNFR) (Marmigère and Carroll, 2014; Skaper, 2018). Upon binding to their mature neurotrophin ligands Trk receptors activate pro-growth and survival pathways in developing neurons. However, while capable of contributing to neuron survival signaling, p75 signaling is significantly more diverse than that of Trk receptors. P75 can bind all of the mature neurotrophins with similar affinity and, through association with a corresponding Trk receptor, promote neuronal survival (Chao, 2003). In addition, p75 can interact with a variety of other receptors, which expands its repertoire of ligands and subsequent signaling. For example, p75 forms a complex with the receptor Sortilin to bind the pro-neurotrophins and promote apoptosis (Nykjaer *et al.*, 2004; Meeker and Williams, 2014, 2015). Consequently, p75 signaling has been found to regulate not only survival signaling, but also apoptosis, metabolic regulation, growth cone collapse, proliferation, myelination, axonal degeneration and migration, depending on context (Chao, 2003; Meeker and Williams, 2015).

According to the Neurotrophic hypothesis, the rate limiting step in neuron survival during NOND is the availability of neurotrophins. Released primarily from target tissues, neurotrophins are thought to be secreted in amounts sufficient to promote survival signaling in only a fraction of the total developing neuronal population. The resulting lack of survival signaling to out of range, or less target established, axons is thought to shift cell signaling in those surplus neurons towards apoptosis (Levi-Montalcini, 1966; Hamburger, 1992; Ichim, Tauszig-Delamasure and Mehlen, 2012). In support of this hypothesis, deletion, or alteration of either neurotrophins or neurotrophin receptors, significantly alters the survival of corresponding DRG populations. In mice, deletion of TrkA or its ligand NGF, results a significant reduction in small and medium DRGs, which function as thermo- and nociceptors, and are predominantly TrkA positive (Crowley et

al., 1994; Smeyne et al., 1994). While disruption of either TrkB or BDNF signaling resulted in a reduction of larger caliber myelinated DRGs, which predominately express TrkB (Klein *et al.*, 1993; Jones *et al.*, 1994a).

Radial Sorting and Myelination

Around E15-16, Schwann cell precursors (SCPs) in the nerve, responding to persistent axonal signaling, including Neruregulin I (NRG1) type III signaling through the ErbB (erb-b receptor tyrosine kinase) 2/3 receptor complex, begin transcriptional remodeling. This prompts their transition into autocrine competent, basal lamina secreting immature Schwann (iSCs) cells (Jessen and Mirsky, 2019). Beginning perinatally, these iSCs begin to sort and subdivide axons into organized bundles, or fascicles, segregating large and small caliber axons in a multi-stage process called radial sorting. Those iSCs that are associated in a 1:1 relationship with medium and large caliber axons during the later stages of radial sorting, then begin differentiating into pro-myelinating SCs (Feltri, Poitelon and Previtali, 2015). Pro-myelinating SCs have upregulated levels of transcription factors, such as Krox20, which shift their metabolism towards manufacturing the wide array membrane components needed for myelination. Myelin begins after birth, concurrent with the last stages of radial sorting, and continues until approximately the third week of life (Mirsky et al., 2008) (Fig. 2).

It should be noted that while early embryonic DRG neurons are not dependent on Schwann cells for survival, neuron-Schwann cell interactions become increasingly important to neuron vitality. ErbB3-/- deficient mice, which fail to retain SCPs population due to the loss of Neuregulin signaling, demonstrate normal DRG formation and axon growth. However, by E14.5 ErbB3 deficient DRG neurons display signs of advanced apoptosis/neuronal loss, and are ultimately reduced by 82% compared to WT at E18.5 (Riethmacher et al., 1997). Likewise, deficits in both early and late stages of radial sorting are noted to cause neuropathy in humans as well as animal models. For example, disruption the LAMA2 gene encoding the Laminin alpha-2 subunit alters basal lamina formation in iSCs. Consequently this results in a form of dysmyelinating neuropathy and

muscular dystrophy, Mersin-deficient Congenital Muscular Dystrophy, characterized by a preferential loss of large diameter sensory and motor fibers (Di Muzio et al., 2003). Furthermore, primary de-/dysmyelination in SCs prompting secondary axonal degeneration is a common feature of many inherited and acquired neuropathies, suggesting Schwann cell and myelin function is necessary for peripheral neuron function throughout adulthood (Azhary et al., 2010).

Lipid Metabolism in the Developing Nerve

While myelin is integral to the development and maintenance of the peripheral nervous system, its generation comes at a tremendous metabolic expense to Schwann cells. In addition to producing a host of myelin-specific, or myelin-enriched, membrane proteins, myelinating cells undergo an immense metabolic reorganization and increase in lipid biosynthesis. It estimated that the plasma membrane of Schwann cells expands 6500 fold during myelination (Webster, 1971). Additionally, myelin has a much larger ratio of lipids to proteins than average cell membranes, with lipids constituting 70-80% of compact myelin by weight, relative to 50% in other cells (Poitelon, Kopec and Belin, 2020). Myelin also has a very specialized lipid composition. While there are no myelin specific lipids, several classes of lipids are highly enriched in peripheral nerves including cholesterol (~26% of myelin), glycolipids (~31%, most notably galactosylceramide), and sphingomyelin phospholipids (~10-35%) (Garbay et al., 2000; Chrast Roman et al., 2011).

Furthermore, while lipid uptake from the bloodstream, especially in the case of cholesterol, often reduces metabolic demands on many cells, the lipids of myelin membranes are theorized to be primarily synthesized de novo in Schwann cells (Fu et al., 1998; Jurevics et al., 1998). Multiple studies have shown that reducing or altering cholesterol, or fatty acid, synthesis in developing Schwann cells results in pronounced peripheral myelin deficits, including early postnatal lipid depletion and hypomyelination. These abnormalities can only be partially rectified by upregulation of external uptake later in development (Saher et al., 2005; Verheijen et al., 2009; Montani et al., 2018). Additionally, the low density lipoprotein receptor (LDLR), which is most associated with

exogenous cholesterol uptake, is dispensable for both myelin generation and repair in the peripheral nerve (Goodrum et al., 1994, 2000), suggesting that, as with oligodendrocytes in the CNS, Schwann cells are not primarily reliant on hemodynamically circulated lipids.

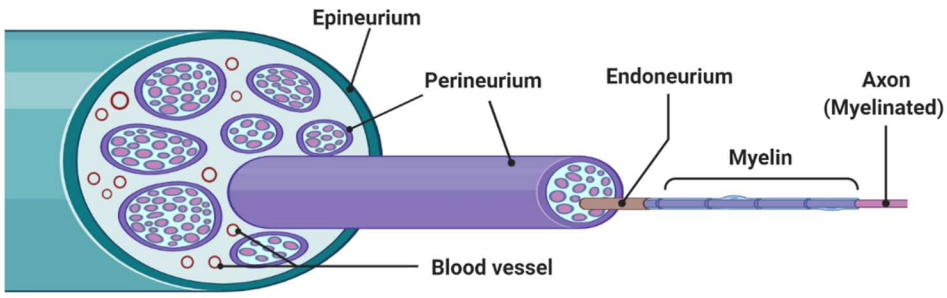

Figure 4. Anatomy of the peripheral nerve. Myelinated and unmyelinated axons are encircled by endoneurium which contains endoneurial fluid, secreted basal lamina, endothelial cells, and endoneurial vessels (small caliber arterioles, capillaries, and venules). Large bundles of axons are arranged in fascicles which are encircled by thick cell layers forming the perineurium. Outside the blood-nerve-barrier, formed by the endoneurium and perineurium, are larger caliber blood vessels and a nerve encompassing epineurium.

This endogenous lipid production may be necessary due to the presence of the blood-nerve barrier (BNB), a system analogous to the more famous blood-brain barrier (BBB) of the CNS. The BNB consists of the perineurium, a multilayered structure surrounding bundles of axons, or fascicles, and the vessels of the endoneurium which are sealed by tight junction expressing endothelial cells and pericytes at endoneurial capillaries (Reinhold and Rittner, 2020) (Fig. 4). While the barrier function of the BNB is not as robust as that of the BBB, the BNB is impermeable to many lipids and other large molecules. It is likely, therefore, that the BNB both limits the rate and efficiency of exogenous lipid uptake for Schwann cells from peripheral circulation, and as noted with the BBB in the CNS, reduces the rate of exchange lipids between the nerve and peripheral circulation. In the CNS, this renders the brain and spinal cord uniquely susceptible imbalances in lipid metabolism, or trafficking, leading to neurotoxic lipid accumulation in neurodegenerative diseases such as Alzheimer's Disease, Parkinson's Disease, Multiple

Sclerosis, and inherited leukodystrophies (Corraliza-Gomez, Sanchez and Ganfornina, 2019). However, lipid permeability of the blood-nerve-barrier during development and myelination are not well characterized. Although it has been noted that endoneurial tight junctions are less robust at birth (Reinhold and Rittner, 2020). Additionally, DRGs, as well as their dorsal roots, are excluded from the BNB, making it difficult to determine the true extent of DRG neuron and Schwann cell isolation from hemodynamic metabolites (Cesmebasi, 2015).

Even though endogenous lipid biosynthesis is a key component of myelinating Schwann cell development, our understanding of the modulators of lipid metabolism in the PNS is very limited. There is some evidence that the timing of lipid biosynthesis during myelination, as with myelin proteins, is regulated primarily by Schwann cell-axonal signaling in the PNS. Neuregulin 1 has been linked to the transcription of 3-hydroxy-3-methylglutaryl-coenzyme-A (HMG-CoA) reductase, an early rate limiting enzyme of cholesterol biosynthesis, and the regulation the of broadly focused metabolism-governing kinases mitogen-activated protein (Maf) and mechanistic target of rapamycin (mTOR) (Pertusa *et al.*, 2007a; Kim *et al.*, 2018; Poitelon, Kopec and Belin, 2020). Additionally, Krox20, a transcription factor instrumental in the upregulation of myelin protein synthesis, is also thought to influence SREBP (sterol-responsive element binding protein) regulation. SREBPs are a family of transcription factors instrumental in the upregulation of lipid and sterol biosynthesis during myelination (LeBlanc et al., 2005). However, there are many elements of lipid biosynthesis and metabolic maintenance that have yet to be elucidated in Schwann cells.

Our lack of knowledge on the regulation lipid metabolism in the Schwann cells extends to a lack of clarity on the lipid metabolic dynamics between Schwann cells and neurons within the peripheral nerve. In the CNS it has been demonstrated that a robust exchange of lipids, and other large energy metabolites, occurs between astrocytes, oligodendrocytes, and neurons during development and as well as in the adult (Jha and Morrison, 2018; Tracey *et al.*, 2018; Barber and Raben, 2019). Additionally, astrocytes are thought to be a key factor in the mitigation of oxidative stress in neurons, through their ability to uptake and breakdown peroxidated fatty acids bound to lipoproteins released by

neurons undergoing metabolic stress (Barber and Raben, 2019; Chamberlain and Sheng, 2019). In the PNS, Schwann cells are well known to augment neuronal metabolism. For example, Schwann cells initiate vesicular transfer of RNA, ribosomes, and proteins to axons after injury, and likely during development (Lopez-Verrilli and Court, 2012; Wei et al., 2019). Moreover, it is hypothesized that Schwann cells act as a diffusion barrier between axons and the hemodynamic environment, necessitating a Schwann cell-axon metabolic transport system to convey sufficient metabolites for axon maintenance and function (Weerasuriya and Mizisin, 2011; Jha and Morrison, 2018). However, it is not clear to what extent Schwann cells contribute to the peripheral neuron lipid composition, or metabolic establishment and maintenance.

Schwann Cell Lipid Dysregulation and Neuropathy

The importance of Schwann cell lipid metabolism to neuron viability and function is highlighted by recent research indicating that dysfunction of Schwann cell lipid biosynthesis and/or breakdown has widespread implications in the survival and function of peripheral neurons. These effects on neurons are not just due to loss of trophic support from Schwann cells or myelin impairment, but also due to the accumulation of toxic lipid species within the nerve, leading to axon degeneration/dysfunction. In the CNS, it has been well established that accumulation of neurotoxic lipids in the brain contributes to many neurodegenerative pathologies such as Alzheimer's Disease, Parkinson's Disease, Multiple Sclerosis, and several inherited leukodystrophies (Corraliza-Gomez, Sanchez and Ganfornina, 2019). Additionally, neurodegenerative diseases tied to dysfunctional regulation or disruption of lipid metabolism, especially those which involve lipid accumulation, heavily favor pathways that are highly enriched in myelinating cells (Garbay et al., 2000; Chrast Roman et al., 2011). In many of these disorders, accumulation of these neurotoxic lipid species has been noted not just within the brain, but also within peripheral nerves and tied to neuropathic symptomology (Dali et al., 2015; Dodge, 2017). Since it is theorized that accumulated lipids originate primarily from Schwann cells, this has led to the recent exploration of the contribution of Schwann cell

metabolic dysfunction to toxic gain-of-function pathology in a wide range of inherited and acquired neuropathies.

What Makes a Lipid Toxic? : Mechanisms of Neurotoxicity

Lipids exhibit extreme structural and function diversity, serving as molecules of energy storage, structural components, and dynamic signaling factors. As a result, there is not a single mechanism of lipid toxicity in neuropathy, but many, often acting concurrently or in a cascade. Additionally, an imbalance in one area of lipid synthesis can often lead to large shifts in cellular lipid metabolism and/or the accumulation of secondary lipid species. Primarily, due to the complex, interdependent nature of lipid synthesis, the reactivity of many lipid intermediates, and multi-faceted mechanisms of lipid feedback regulation (Tracey et al., 2018). Due to these complications, the precise pathological processes in many disorders involving lipid induced neurotoxicity/axonopathy are still under investigation. However, there are several conventional mechanisms of neurotoxicity that neurotoxic lipids have consistently been found to perpetuate.

Destabilization of Membrane Function

Lipids constitute the vast majority of both axon and Schwann cell membranes, as a result many neurotoxic lipids are theorized to disrupt neuron/Schwann cell membrane flexibility, electrical dynamics, and signal transduction (M. C. Perez-Matos, Morales-Alvarez and Mendivil, 2017). In neurons, the disruption of membrane dynamics can reduce the ability of axons to propagate action potentials, leading to deficient conduction, or mediate pathological excitotoxicity (Taso et al., 2019a). Furthermore, altered membrane dynamics in Schwann cells can cause de-/dysmyelination and disruption of trophic support/intercellular signaling to axons, prompting secondary axonopathy (Schmitt, Cantuti Castelvetri and Simons, 2015a). Lipid rafts, major membrane structures enriched in phospholipids, cholesterol, and sphingolipids, which serve instrumental organizing centers for proteins and signaling receptors, are thought to be particularly sensitive to lipid modifications (Tracey et al., 2018). Pathological alterations of lipid raft

domain function driven by toxic lipid accumulation has been theorized to result either from the direct incorporation of accumulated lipid species, or from imbalances in lipid synthesis and transport resulting in a non-optimal ratio of lipid membrane components (Bonetto and Di Scala, 2019; Campomanes, Zoni and Vanni, 2019). Additionally, lipid peroxidation has been demonstrated to alter the composition lipid rafts (Zhai et al., 2009). As lipid rafts have been implicated in a wide range of processes including receptor localization/trafficking, neurotransmitter transport, cytoskeletal rearrangement, exocytosis, and metabolic signaling, their disruption has widespread effects on neuronal health and survival (Allen, Halverson-Tamboli and Rasenick, 2007).

Oxidative Stress and Lipid Peroxidation

Many neurotoxic lipid species have been found to contribute to the initiation or amplification of oxidative stress. Oxidative stress occurs when the accumulation reactive oxygen species (ROS) in the form of oxidants or free radicals, molecular species containing at least one unpaired electron, are not mitigated by cellular antioxidants. ROS are highly volatile and cause widespread modifications to other lipids, proteins, and nucleic acids, leading to the disruption of organelle function. Mitochondria and the Endoplasmic Reticulum (ER) are especially prone to damage from oxidative stress due to their management of high levels of ROS intermediates, leading to further metabolic imbalance (Singh et al., 2019). Additionally, a process called lipid peroxidation occurs when ROS modify the polyunsaturated fatty acids (PUFAs) of cellular membranes, leading to membrane disruption and the generation of highly reactive aldehyde species including 4-hydroxy-2-noneal (HNE) and malondialdehyde (MDA). Once formed, these aldehydes bind covalently to amino acids, a process termed Michael adduction, to form protein adducts, which can cause DNA damage, further organelle collapse, and the initiation of apoptotic signaling (Taso et al., 2019b). Thus, several noted cytotoxic lipids are ROS, and are either themselves unstable lipid metabolic intermediates or generated from intermediate oxidation (Komen et al., 2007; Korade et al., 2010; Nagai, 2015; Pfeffer et al., 2016).

Disruption of Energy Metabolism

While large scale disruption of mitochondrial and ER function prompted by lipid peroxidation is a major factor in metabolic disruption, accumulated lipid species are often themselves tied to large shifts in cellular metabolism. For example, high levels of free fatty acids in diabetic neuropathy are thought to perpetuate insulin resistance through inducing the formation of diacylglycerols (DAG) and ceramides that in turn lead to activation of the PKC (protein kinase C)-theta and PKC-delta kinases. PKX then increases insulin receptor substrate (IRS) phosphorylation, further compromising insulin signaling and cellular glucose metabolism (M C Perez-Matos, Morales-Alvarez and Mendivil, 2017). Furthermore, many key regulators of cell metabolism are regulated by lipids. For instance, Liver X Receptors (LXRs) mediate cholesterol, fatty acid, glucose, and oxidative homeostasis and are, in turn, regulated by oxysterol ligands, formed by the oxidation of cholesterol or its precursors (Hichor et al., 2018; Sundaram, Massaad and Grenier, 2019). Therefore, accumulation of one metabolite can alter many pathways involved in energy homeostasis, potentially contributing to neural pathology.

Biological Activity/Altered Signaling

While lipids were once considered largely structural molecules, it has become clear that many lipids are dynamic regulators of key cellular pathways. They serve as receptor ligands, scaffolding substrates, and secondary messengers in an expansive range of cellular processes, including neurotransmitter release, channel regulation, proliferation, apoptosis, inflammatory signaling, and metabolism (Schmitt, Cantuti Castelvetri and Simons, 2015a; M C Perez-Matos, Morales-Alvarez and Mendivil, 2017; Tracey *et al.*, 2018). Consequently, alterations in either lipid species concentrations, or signaling, can lead to cytotoxicity. For example, ceramides are potent regulators of inflammatory signaling factors and, when accumulated, have been shown to propagate apoptotic signaling in DRGs through NFκB (nuclear factor kappa-light-chain-enhancer of activated B cells) activation (Gill and Windebank, 1998, 2000). Additionally, lipid species belonging to the same class can have diametrically opposing cell functions. For instance, some

species of PUFAs, including many omega-3 fatty acids, are known for having anti-inflammatory signaling, while omega-6 fatty acids are distinctly pro-inflammatory (Tracey et al., 2018). Thus, even seemingly small-scale biogenic imbalances within lipid classes can initiate substantial cellular pathway disruption, potentially leading to neurotoxicity.

Disruption of Axonal Transport

Both motor neurons and DRG sensory neurons feature long axonal projections, containing a disproportionately large cell volume relative to their soma. This results in PNS neurons having a tremendous reliance on cellular transport machinery, both retrograde and anterograde, to support their energetic and biosynthetic requirements. To the extent that if either retrograde or anterograde transport is disrupted, axonal degeneration and cell death can result (Coleman, 2005; Cashman and Höke, 2015a; Stavrou et al., 2020). Neurotoxic lipids have been shown to alter axon transport due to direct interactions with motor proteins, destabilization of cytoskeletal dynamics, or interference with vesicle transport machinery (Cantuti Castelvetri et al., 2013; Spassieva and Bieberich, 2016).

Channel Dysregulation

All cells are reliant on efficient intracellular and extracellular ion channel function to maintain membrane potentials. However, neurons are especially sensitive to channel dysregulation as ion channels are fundamental components of neuronal conduction and signaling (Kim, 2014). Altered sodium (Na^+) or potassium (K^+) channel function can result in either excitotoxic signaling, or reduced conduction, while impaired intracellular channel regulation can initiate or amplify of cell stress and organelle dysfunction (Cashman and Höke, 2015b). Neurotoxic lipids have been shown to be involved in the dysfunctional regulation of intracellular Ca^{2+} channels through mis-localization, altered membrane dynamics, or altered cell signaling (Choi et al., 2015; Wilson et al., 2018). Additionally, some neurotoxic lipids, are thought to affect axonal Na^+ or K^+ ion channel localization and sensitization (Kleinecke et al., 2017; Bonetto and Di Scala, 2019).

Overview of Diseases Linked to Neurotoxic Lipid Accumulation in the PNS

As previously stated, the brain and spinal cord are uniquely susceptible to disorders of lipid transport and biosynthesis, due to the BBB and their high energetic and lipid requirements (Corraliza-Gomez, Sanchez and Ganfornina, 2019). Therefore, many disorders involving lipid toxicity in the nervous system have severe, quality of life affecting symptomology in the CNS and are thus more characterized in that context. However, it has long been noted that several primary CNS disorders with toxic lipid accumulation also can result in peripheral neuropathy (Chrast Roman et al., 2011; Spassieva and Bieberich, 2016). Additionally, there are several neuropathies involving toxic lipid accumulation that are exclusive to the PNS (Atkinson et al., 2017; Schwartzlow and Kazamel, 2019). Exploration of the pathology of these diseases has the potential to inform out understanding of how lipid mediated toxic gain-of-function affects peripheral neurons, as well as the role of Schwann cells in their progression. Therefore, the following is an overview of disorders that have been theorized to involve lipid derived toxic gain-of-function pathology within the context of the peripheral nervous system.

Sphingolipidoses

The largest group of disorders associated with toxic lipid accumulation in both the CNS and PNS are sphingolipidoses, a class of lysosomal storage diseases that result from deficiencies or dysfunction in sphingolipid metabolism and degradation (Fig. 5). Sphingolipids are a class of lipids containing sphingolipid backbones, including glycosphingolipids (e.g., cerebrosides and gangliosides), ceramides, and sphingomyelin, all of which are greatly enriched in myelin (Fig. 6). Accordingly, sphingolipid depositions are found in both central and peripheral nervous tissue in many sphingolipidoses, leading to a broad range of peripheral nervous system anomalies including de-/dysmyelination and both primary and secondary axonopathy (Castelvetri et al., 2011; Alaamery et al., 2020).

Once thought to primarily function as structural elements of the plasma membrane, sphingolipids have come to be known as highly biologically active molecules. Thus, they have been shown to be involved in diverse signaling pathways in the nervous system including proliferation, metabolic regulation, maturation, and apoptotic pathways (Posse de Chaves, 2006; Schmitt, Cantuti Castelvetri and Simons, 2014; Spassieva and Bieberich, 2016). The diversity of nerve abnormalities noted in sphingolipidoses, as well as the disparate biological roles of sphingolipids, suggest there are likely multiple etiologic mechanisms of sphingolipid neurotoxicity.

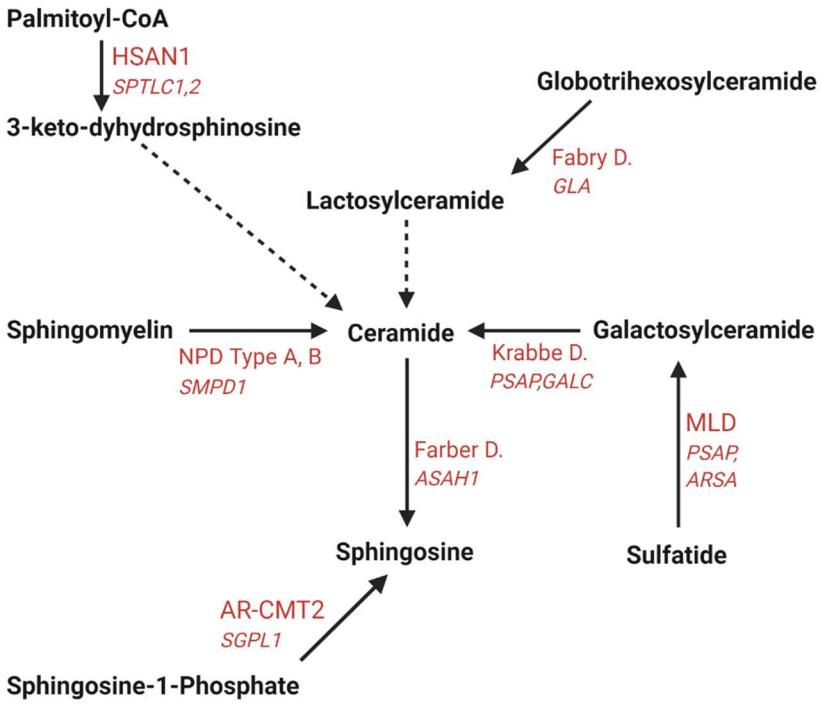

Figure 5. Summary of metabolic pathways associated with Sphingolipidoses. Solid arrows represent a direct link between two steps. Dashed arrows indicate there are intermediates that have been omitted. Disease names are listed in red next to the step in the metabolic pathway where deficient/aberrant enzymatic function has been noted. Directionality of the arrows indicates the most interrupted primary process observed in each disease, omitting other possible substrates/products for brevity. Specific gene/s known to be modified in each disease are indicated in red italics. Abbreviations are as follows, D., Disease; HSAN1; Hereditary Sensory and Autonomic Neuropathy 1; NPD, Niemann-Pick Disease, MLD; Metachromatic Leukodystrophy, AR-CMT2; Autosomal Recessive Charcot-Marie-Tooth Disease 2 (axonal).

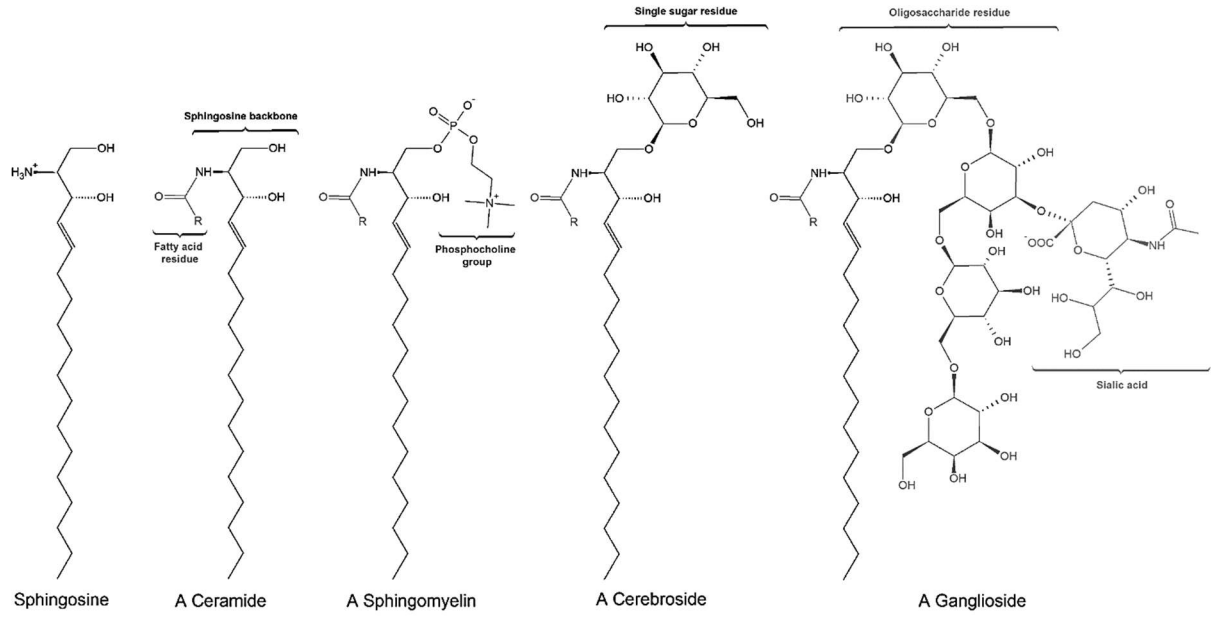

Figure 6. Diagram of Basic Sphingolipid Structure. Sphingolipids contain a sphingoid base (long chain amino alcohols) and often have a fatty acid residue amide-linked to the backbone. Ceramides have a hydrogen head group only. The addition of a phosphocholine or phosphoethanolamine headgroup to ceramide yields a sphingomyelin. Alternately, the addition of a sugar residue produces a cerebroside and multiple sugar residues combined with salic acid/s yield a ganglioside. Image modified from graphic by LHcheM distributed under a CC-BY-SA 3.0 license.

Krabbe Disease

However, a one common pathological element in several sphingolipidoses is the secondary accumulation of toxic lysosphingolipids, metabolic byproducts of impaired sphingolipid degradation (Spassieva and Bieberich, 2016). The most well-known example of which is observed in Krabbe disease. Krabbe disease is caused by either a defect in β-galactosylceramidase or Saposin A, which results in accumulation of galactosylceramide in peripheral nerves. However, galactosylceramide itself is not thought to be a mediator of neurotoxicity in Krabbe disease, instead its accumulation leads to the buildup of the lysosphingolipid psychosine (galactosylsphingosine).

Psychosine is highly bioactive, and can disrupt membrane dynamics and impair vesicular transport, leading to cytotoxicity in both glia and neurons (Spassieva and Bieberich, 2016).

The precise mechanisms of psychosine toxicity are still under investigation. However, psychosine is readily incorporated into lipid rafts where it is theorized to inhibit PKC, a major cell regulator, and promote membrane destabilization. Additionally, it can inhibit fast axonal transport through the activation of axonal protein phosphatase 1 (PP1) and glycogen synthase kinase-3 (GSK3β), promoting aberrant phosphorylation of kinesin motor protein light chains (Cantuti Castelvetri et al., 2013; Spassieva and Bieberich, 2016). A model of Krabbe disease, the Twitcher mouse, carries a recessive, naturally occurring mutation of Galactosylceramidase leading to dysfunction. Twitcher mice exhibit primary axonopathy, characterized by axonal degeneration in advance of later neuronal apoptosis. The axonopathy is followed by a demyelinating phenotype in the peripheral nervous system, suggesting neurons are impacted before Schwann cell phenotypes arise (Suzuki and Suzuki, 1995; Castelvetri et al., 2011). Neurons do not synthesize significant quantities of galactosylceramide, but this lipid and its derivative, sulfatide, account for one-third of the lipid content in myelin. Therefore, psychosine is hypothesized to be transported from Schwann cells to neurons in the PNS, although the mechanism of that transfer has not been elucidated (Dodge, 2017). A recent report revealed that the pathology of Krabbe disease is further complicated by the fact that macrophages, which get recruited to degenerating and demyelinating nerves, also contribute to the pathology. In degenerating nerves, macrophages phagocytose the myelin debris and utilize galactosylceramidase to breakdown the lipids. However, if the macrophages are deficient in the enzyme, they also produce sphingosine, exacerbating the degeneration (Nadav et al., 2020).

Metachromatic Leukodystrophy

Lysosphingolipid accumulation also occurs in Metachromatic Leukodystrophy (MLD) (Toda *et al.*, 1989; Spassieva and Bieberich, 2016). The accumulation of sulfatides and the secondary accumulation of lysosulfatides in MLD arises due to insufficiency of

either arylsufatase A or Saponin B. The buildup of these lipids results in improper myelin formation and myelin breakdown in both the CNS and PNS, eventually leading to neuron dysfunction and degeneration. In the PNS, both neurons and Schwann derived lipids are thought to contribute to the pathology(Baba and Ishibashi, 2019). In Schwann cells, sulfatides regulate the initiation of myelin, while in neurons they are instrumental for proper development of nodes of Ranvier(Bosio, Binczek and Stoffel, 2002; Baba and Ishibashi, 2019). Moreover, sulfatide enriched lipid rafts are highly localized to myelin paranodes, highly structured domains adjacent to the nodes of Ranvier (Bonetto and Di Scala, 2019). Thus, their aberrant accumulation is theorized to cause pathology through myelin membrane disruption and altered axon structural arrangement. Additionally, excess sulfatides are thought to activate inflammatory cytokines, potentially contributing to apoptosis (Van Rappard, Boelens and Wolf, 2015). The role of the lysosulfatide accumulation in MLD pathology is less well established. However, in late infantile MLD, a form of MLD where peripheral neuropathy often precedes CNS manifestations, Dali et al. (2015) reported that the degree of lysosulfatide accumulation correlated with the scale of sensory loss and neuropathy. Interestingly, CNS symptom severity did not correlate with lysosulfatide levels in the same patients, indicating that lysosulfatide accumulation may have divergent pathology in Schwann cells and peripheral neurons(Dali *et al.*, 2015).

Fabry Disease

Fabry disease, caused by the deficiency of α-galactosidase A, is associated with dysfunction in many cell types, including a systemic vasculopathy associated with the primary deposition of globotriaosylceramide in peripheral tissues. Additionally, patients with Fabry disease exhibit accumulation of the lysophingolipid lysoglobotriaosylceramide/globotriaosylsphingosine (lysoGb3), a deacylated form of globotriaosylceramide, in plasma and peripheral tissues (Aerts *et al.*, 2008; Rombach *et al.*, 2010). However, while many organ systems are affected, patients with Fabry disease often present first with neuropathic pain caused by the onset of small-fiber neuropathy (SFN), a form of neuropathy characterized by progressive length dependent axonopathy of sensory, but not motor, neurons (Biegstraaten *et al.*, 2012). The mechanisms behind

SFN in Fabry disease remain elusive. However, a high level of lipid accumulation in the soma of DRG neurons, as well as Schwann cells, is thought to play a role. Foot pad injection of lysoGb3 in mice was found to induce mechanical allodynia through the upregulation of voltage-dependent Ca^{2+} channels in DRG nociceptive neurons, suggesting that neural death may occur due to excitotoxicity (Choi *et al.*, 2015). Additionally, patients with Fabry disease have pronounced DRG enlargement, and decreased blood-DRG permeability, thus neurotoxic effects could also be mediated by decreased neuronal blood supply/nutrient availability (Godel *et al.*, 2017). Interestingly, echoing MLD findings, levels of lysoGb3 have been shown to be proportionate with the severity of temperature sensation deficits in patients with Fabry disease (Biegstraaten *et al.*, 2012).

Niemann Pick type A and B

Niemann Pick disease type A and B are a spectrum disorders sharing deficiencies of the same enzyme, acid sphingomyelinase (ASM), which converts sphingomyelin into phosphocholine and ceramide (Schuchman and Desnick, 2017; Breiden and Sandhoff, 2020). Niemann Pick Type A is characterized by early onset severe CNS and PNS pathology with hepatosplenomegaly, while Type B has later onset, and generally milder symptoms. In both cases, absent or reduced ASM activity results in the formation large multilayer inclusions, containing sphingomyelin and lysophingomyelin, in both peripheral Schwann cells and neurons. The appearance of which are often associated with pronounced segmental demyelination and axonopathy (Gumbinas, Larsen and Liu, 1975; Landrieu and Saïd, 1984; Schuchman and Desnick, 2017).

There are several lipid mediated mechanisms theorized to contribute to NPD type A and B pathology. Sphingomyelin has been shown to inhibit lysosomal sphingolipid and cholesterol catabolism, which is thought to prompt the secondary accumulation of cholesterol, lysophingolipids, and several types of phospholipids and glycolipids in affected cells (Breiden and Sandhoff, 2020). Additionally, in response to various stressors, ASM translocates from lysosomes to the plasma membrane to facilitate lipid

raft reorganization/remodeling. Therefore, ASM deficiency can disrupt this cellular stress response, resulting in modified lipid raft signaling due to altered lipid composition (Charruyer *et al.*, 2005; Schuchman and Desnick, 2017). Interestingly, a mouse model for Niemann Pick type A and B, the ASM knockout mouse, demonstrates elevated rather than reduced ceramide levels due to breakdown of aberrantly accumulated sphingomyelin by other sphingomyelinases. As a consequence, ceramide, which can be neurotoxic, accumulation has also been proposed as a source of pathogenesis (Schuchman and Desnick, 2017).

Farber Disease

Accumulation of ceramides is also found in Farber disease, a rare Sphingolipidosis of diverse presentation categorized by a deficiency of Acid Ceramidase. This enzyme catalyzes the hydrolysis of ceramide into sphingosine and a free fatty acid, during the terminal step in glycosphingolipid breakdown (Cozma *et al.*, 2017)(Yu *et al.*, 2018). Consequently, Farber Disease is associated with robust ceramide accumulation, leading to large membrane-bound inclusions in peripheral nervous tissues, most notably in Schwann cells (Zappatini-Tommasi *et al.*, 1992). These inclusions have been linked to the development of neuropathic symptoms in Type 5, or classical Farber disease. However, it has not been elucidated whether aberrant ceramide signaling, disruption in lipid metabolism resulting from lack of ceramide processing, or dysfunction relating to the large inclusion bodies, the primary driver of Farber nerve pathology (Yu *et al.*, 2018).

Hereditary Sensory and Autonomic Neuropathy

While inherited sphingolipidoses are most associated with broad and severe symptomology in both the CNS and PNS, it has recently been revealed that alterations in sphingolipid metabolism can cause some forms of PNS exclusive inherited neuropathy. Hereditary Sensory and Autonomic Neuropathy (HSAN) is a heterogenous group of disorders characterized by progressive sensory and autonomic deficits. The most

common form, HSAN1, is caused by missense mutations of the SPTLC1 and SPLC2 genes, which encode the enzyme serine palmitoyltransferase. Rather than causing loss of function, these mutations increase the enzyme reactivity to alternate substrates, resulting in atypical sphingolipid production and accumulation of the 1-deoxysphingolipids (deoxysphinganine (doxSA) and deoxymethylsphinganine (doxmethSA)). Both accumulated species are neurotoxic to DRG neurons, and correlate to symptom severity in patients. They are, therefore, recognized as a primary instigator of HSAN1 neuropathy (Penno *et al.*, 2010; Garofalo *et al.*, 2011; Schwartzlow and Kazamel, 2019). Although the pathological mechanism of 1-deoxysphingolipid neurotoxicity is still being investigated, *in vitro* experiments suggest that exposure to doxmethSA and doxSA disrupts Ca^{2+} channels in the ER and mitochondria, leading to loss of mitochondria membrane potential and dysfunction (Wilson *et al.*, 2018).

Charcot-Marie-Tooth

Additionally, an autosomal recessive form of Charcot-Marie-Tooth (CMT) disease has also been tied to sphingolipid metabolism. CMT, as with HSAN, is a heterozygous group of inherited disorders, but is distinguished from HSAN1 by the common addition of motor neuron pathology (Fridman and Reilly, 2015). Atkinson et al. (2017) identified heterozygous mutations in the *SGPL1* gene, encoding sphingosine 1-phosphate lyase (SPL), as the causative mutation in rare form of axonal CMT (AR-CMT2) distinguished by acute/subacute onset and mononeuropathy. The mutations result in deficiency of SPL and the accumulation of sphingosine-1-phosphate (S1P) as well as an abnormal ratio of sphingosine/sphingoalanine species in the blood and PNS (Atkinson *et al.*, 2017). S1P functions intracellularly as a versatile second messenger as well as serving an extracellular ligand for S1P receptors. These receptors are a family G-protein coupled receptors that have been implicated in TRPV1-dependent nociceptor sensitization and inflammatory pain. Additionally, Hagen et al. (2011) reported that accumulation of S1P in SPL deficient cerebellar neurons induces apoptosis through calpain induced ER stress, leading to activation of a caspase cascade and aberrant activation of cyclin-dependent

kinase 5 (CDK5). Although, it is not yet known if this mechanism contributes to pathology in DRG neurons (Ueda, 2020).

Disorders of Fatty Acid Catabolism

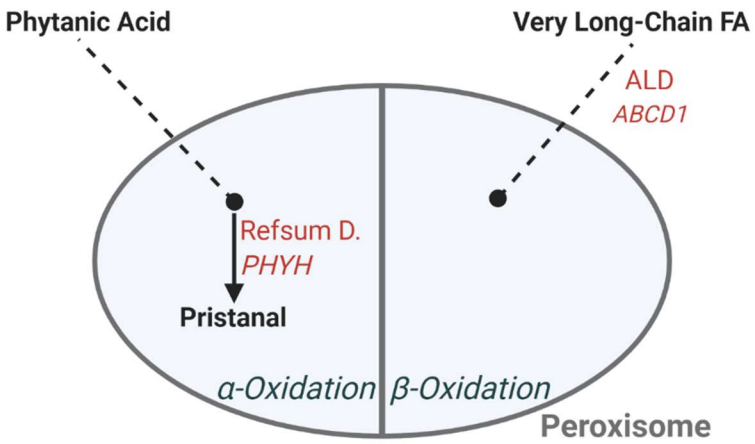

Figure 7. Summary of metabolic pathways associated with fatty acid catabolism featuring the accumulation of toxic lipid species in peripheral nervous system tissues. Grey oval represents steps occurring within the peroxisome, either associated with alpha, or beta- oxidation. Solid arrows represent a direct link between two steps. Dashed arrows indicate transport of indicated species into the peroxisome. Disease names are listed in red next to the step in the metabolic pathway where deficient/aberrant protein function has been noted. Directionality of the arrows indicates the most interrupted primary process observed in each disease, omitting other possible substrates/products for brevity. Specific gene/s known to be modified in each disease are indicated in red italics. Abbreviations are as follows, D., Disease; ALD, X-linked Adrenoleukodystrophy, FA; Fatty acids

X-linked Adrenoleukodystrophy

The accumulation fatty acids can also lead to forms of neuropathy (Fig. 7). For example, in X-linked Adrenoleukodystrophy (X-ALD) mutations in the gene encoding the ATP-binding cassette transporter (ABCD1) results in deficient transport of fatty acid-CoA-esters into peroxisomes, where they would normally undergo degradation through beta-oxidation. Consequently, Very Long-Chain Fatty Acids (VLCFAs) accumulate in CNS and PNS tissue, predominantly esterified with cholesterol and glycerophospholipids.

Especially in late onset ALD, also known as adrenomyeloneuropathy (AMN), this accumulation is tied to progressive spinal and peripheral nerve degeneration (Kemp, Berger and Aubourg, 2012). Axonal degeneration is noted in almost all men, due to the X-linked nature of the disease, and 80% of women with AMN(Court *et al.*, 2008; Huffnagel *et al.*, 2019; Turk *et al.*, 2020). Interestingly, DRG neurons of patients with AMN have notable lipid inclusions in their mitochondria, indicating possible lipid induced dysfunction(Powers *et al.*, 2001). Additionally, Demyelination as a result of inflammatory and oxidative signaling is thought to be a large component of VLCFA pathophysiology in all myelinating cells (Turk *et al.*, 2020). However, Kleinecke et al. (2017) reported that a Schwann cell specific Pex5 (peroxisome biogenesis factor peroxin 5) knock out mouse, which displays similar altered peroxisomal processing to ABCD1 deficient models, exhibited increased VLCFA accumulation and incorporation in gangliosides of lipid rafts. This incorporation resulted in altered axonal $K_V1.1$ channel localization, and the development of age dependent peripheral axonopathy. These findings suggest that VLCFA accumulation in Schwann cells may be a significant driver of axonopathy in AMN (Kleinecke *et al.*, 2017).

Refsum Disease

Abnormal fatty acid accumulation is also a hallmark of Refsum disease (RD). In RD, mutation of the gene encoding the peroxisomal enzyme phytanoyl-CoA hydroxylase leads to the accumulation of phytanic acid in plasma and tissues. Phytanic acid is a dietary derived fatty acid that normally undergoes alpha oxidation by phytanoyl-CoA hydroxylase and subsequent peroxisomal degradation(Komen *et al.*, 2007). In RD, patients develop advanced polyneuropathy attributed to accumulation of phytanic acid in Schwann cells through an unknown depository mechanism (Jansen *et al.*, 1997). The etiology of the neuropathy in RD is unknown, however *in vitro* experiments on astrocytes, fibroblasts and Neuro2A cells have shown that application of phytanic acid leads to cell death through oxidative stress, mitochondrial impairment from decreased membrane

potential, NADPH depletion, and histone deacetylase activation (Komen *et al.*, 2007; Nagai, 2015).

Disorders of Sterol Metabolism and Trafficking

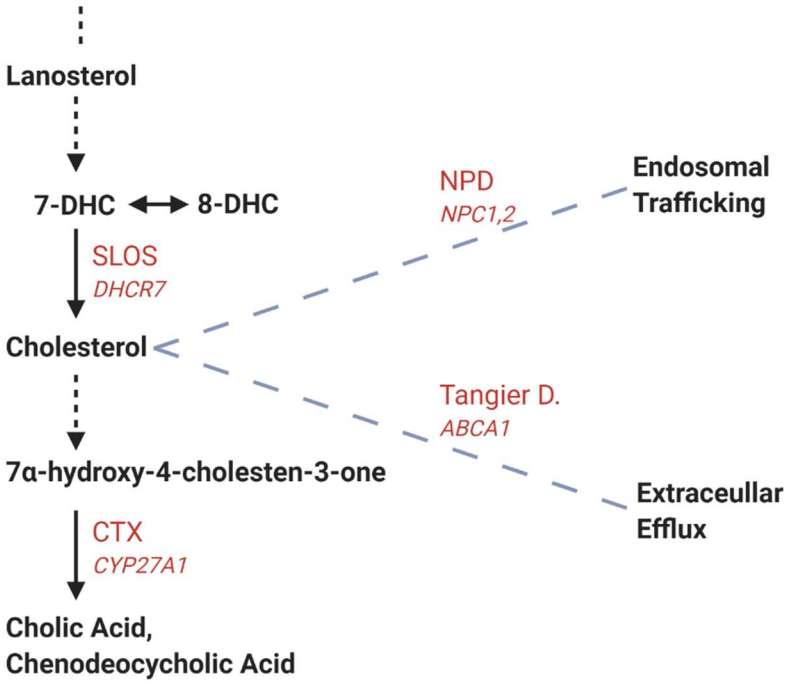

Figure 8. Summary of metabolic pathways associated with cholesterol biogenesis and trafficking. Solid arrows represent a direct link between two steps. Black dashed arrows indicate there are intermediates that have been omitted. Grey dashed lines indicate altered proteins are associated with transport of species within in the specified trafficking process. Disease names are listed in red next to the step in the metabolic pathway where deficient/aberrant protein function has been noted. Directionality of the arrows indicates the most interrupted primary process observed in each disease, omitting other possible substrates/products for brevity. Specific gene/s known to be modified in each disease are indicated in red italics. Abbreviations are as follows, D., Disease; SLOS, Smith-Lemli-Opitz Syndrome; NPD; Niemann-Pick Disease Type C and D, CTX; Cerebrotendinous xanthomatosis.

Niemann-Pick Type C and D

Cholesterol is not only a large component of cell membranes. Its precursors and metabolites have diverse functions in cellular signaling and the regulation of lipid biogenesis. Therefore, many neuropathies caused by cholesterol metabolic pathway disruption are thought to involve not only cholesterol deficiency, but also have been tied to cytopathic effects of disrupted cell metabolism and accumulated lipid species (Fig. 8). For instance, in Niemann-Pick Type C and D, mutations in *NPC1* or *NPC2* genes result in impaired intracellular processing of low-density lipoprotein (LDL) derived cholesterol. This results in not only the primary accumulation of cholesterol, but secondary accumulation of oxysterols, gangliosides, and sphingolipids (Sitarska and Ługowska, 2019). The primary mechanism of neuropathy in Niemann-Pick Type C and D is thought to be due to hypomyelination from cholesterol deficiency. However, several of the secondary lipid species that accumulate in the disease, such as sphingomyelin, have been suggested to contribute to pathology through toxic-gain of function mechanisms (Erickson, 2013; Breiden and Sandhoff, 2020).

Cerebrotendinous xanthomatosis

Sterol accumulation is found also found in Cerebrotendinous xanthomatosis (CTX), an autosomal-recessive disease caused by loss-of-function mutations in the *CYP27A1* gene, encoding sterol 27-hydroxylase. The loss of sterol 27-hydroxylase function leads to upregulation of *CYP7A*, a gene encoding cholesterol-7-alpha-hydroxylase, which catalyzes the conversion of cholesterol to cholestanol (Crestani *et al.*, 1998). The resulting accumulation of cholestanol is thought to be neurotoxic, as cholestanol has been shown to induce apoptosis in cerebellar neurons. Moreover, a majority of patients with CTX display peripheral nerve abnormalities (Mignarri *et al.*, 2016). However, the presentation of neuropathy in CTX varies widely, with some studies suggesting de-/dysmyelination precedes neural involvement, and others observing only

primary axonal degeneration, suggesting multiple pathomechanisms may be present (Ginanneschi *et al.*, 2013; Nie *et al.*, 2014).

Tangier Disease

Tangier disease (TD) is caused by mutations in the gene-encoding ATP-binding cassette transporter 1 (ABCA-1). Reduced ABCA-1 function results in the accumulation of cholesterol esters in peripheral cells due to disrupted HDL cholesterol efflux. Around 50 percent of patients with TD experience neuropathy; however, there are two divergent subtypes of neuropathy associated with TD(Zyss *et al.*, 2012; Mercan *et al.*, 2018). One mimics the presentation of syringomyelia, a rare disorder where cysts form in the spinal cord(Leclerc, Matveeff and Emery, 2020). TD patients who present thusly are said to have syringomyelia-like neuropathy, characterized by upper-extremity muscle weakness and loss of small fiber mediated pain and temperature sensation. The other subtype is a multi-focal mono-or polyneuropathy that presents with recurrent and remitting motor and sensory deficits. Therefore, it has been suggested they may have divergent etiology (Mercan *et al.*, 2018). In the multi-focal subtype, cholesterol ester accumulation is theorized to prompt neuropathy because of tomacula, areas of focal myelin swelling/ altered compaction, formation and cyclical demyelination. Primarily due to structural abnormalizes tied to cholesterol ester localization in paranodal regions of myelinated Schwann cells (Cai *et al.*, 2006). While in the syringomyelia-like neuropathy subtype, the early loss of small, non-myelinated fibers precedes demyelination, indicating a neuronal etiology. Accumulation of cholesterol esters in the DRG soma has been noted, but the mechanism leading to neuron loss is not known (Zuchner, 2003; Zyss *et al.*, 2012).

Smith-Lemli-Opitz

Smith-Lemli-Opitz syndrome (SLOS) is another example of cholesterol pathway disruption leading to neurological dysfunction. Although peripheral neuropathy in SLOS is much rarer than in TD, polyneuropathy with demyelinating features has been noted in several patients with SLOS (Starck *et al.*, 2007; Ballout *et al.*, 2020). Unlike the previously listed sterol disorders, SLOS results not from impaired sterol trafficking but a defective cholesterol biosynthetic pathway. In SLOS, mutations affect the gene, *dhcr7,* encoding the enzyme 7-dehydrocholesterol (7-DHC) reductase, which mediates the conversion of 7-DHC to cholesterol in the terminal step of the Kandutsch-Russel pathway of cholesterol biosynthesis. Deficiency of 7-DHC reductase function results in accumulation of 7-DHC and its isomer 8-DHC in central and peripheral tissues as well as plasma (Porter, 2008; Porter and Herman, 2011; Griffiths *et al.*, 2017). Additionally, 7-DHC is prone to free radical oxidation, prompting the secondary accumulation of 7-DHC oxidative derivatives in rodent models as well as patients with SLOS (Griffiths *et al.*, 2017). The primary mechanisms of pathophysiology are still under debate; however, one hypothesis is that central and peripheral neurological deficits primarily result from cholesterol deficiency. This theory is supported by the fact that treating patients with supplemental dietary cholesterol lessens the peripheral symptom severity (Starck *et al.*, 2007). However, 7-DHC and several 7-DHC/8-DHC derivatives are highly bioactive *in vitro* and in rodent models affect diverse pathways involved in membrane dynamics, oxidative stress, lipid metabolic regulation, proliferation, and apoptotic signaling. These effects suggest they may contribute to SLOS pathology through toxic gain-of-function mechanisms (Keller, Arnold and Fliesler, 2004; Korade *et al.*, 2010; Xu *et al.*, 2012a; Pfeffer *et al.*, 2016; Fliesler and Xu, 2018).

Acquired Neuropathy

Chemotherapy-induced Peripheral Neuropathy

Chemotherapeutic agents are a common cause of acquired neuropathy, a phenomenon termed chemotherapy-induced peripheral neuropathy (CIPN). CIPN occurs in 30-70% of patients treated with chemotherapeutic agents associated and can have long term effects after treatment cessation. Patients with CIPN exhibit primarily small fiber associated symptoms including neuropathic pain, burning, tingling, loss of temperature, but can also experience muscle weakness, and mechanical allodynia (Fukuda, Li and Segal, 2017). Intriguingly, Kramer et al. (2015) reported that breast cancer patients treated with paclitaxel, a chemotherapeutic agent that inhibits microtubule depolymerization, had elevated 1-deoxysphingolipid plasma levels (Fukuda, Li and Segal, 2017). The levels of this lipid correlated with the severity of CIPN neuropathic symptoms (Kramer, Bielawski, Kistner-Griffin, *et al.*, 2015; Fukuda, Li and Segal, 2017). Additionally, one species of sphingosine-1-phosphate (S1P), d16:1, was found to disproportionately accumulate in patients treated with oxaliplatin, a CIPN-associated platinum based chemotherapeutic agent. In a cisplatin-induced CIPN mouse model D16:1 S1P accumulation was also shown to promote pro-inflammatory $S1P_1$ receptor signaling and neuropathic symptoms, suggesting CIPN may be, in part, facilitated by lipid accumulation and cytotoxic signaling (W. Wang *et al.*, 2020).

Diabetic Neuropathy

As previously mentioned, Diabetes type 2 is the most common cause of acquired peripheral neuropathy (Hicks and Selvin, 2019). Although, it should be noted that diabetic neuropathy also occurs as a complication of Type 1 diabetes. Patients with diabetic neuropathy (DN) have varied presentation, exhibiting small fiber, autonomic, and polyneuropathies with both primary and secondary axonopathy (Gonçalves, Vægter and Pallesen, 2018). Diabetes type 2 is metabolic disorder caused by disruption of glucose metabolism leading to the onset of hyperglycemia. Historically, hyperglycemic conditions,

and/or ischemic and hypoxic conditions from vascular modifications were accepted as the most probable cause of axonal degeneration in DN. However, clinical trials have found glycemic control is not sufficient to prevent DN from occurring, suggesting that progression of DN is also mediated by other factors (M. C. Perez-Matos, Morales-Alvarez and Mendivil, 2017; Gonçalves, Yan, *et al.*, 2020).

Several lipid-associated mechanisms have been proposed to contribute to DN pathophysiology. Patients with diabetes who have elevated plasma lipid levels, including triglycerides and LDL cholesterol, are at higher risk for developing DN(Tesfaye *et al.*, 2005; Wiggin *et al.*, 2009; Smith and Singleton, 2013). Hyperglycemia is associated with an overall increase in hemodynamic and tissue oxidation from many metabolic insults, including depletion of NAPDH after activation of a polyol pathway to metabolize excess glucose, increased mitochondrial dysfunction, and ROS formation mediated by advanced glycosylation end products(Vincent *et al.*, 2004). This is thought to promote the oxidation of circulating LDLs to form oxyLDLs (Njajou *et al.*, 2009; Vincent, Hayes, *et al.*, 2009). In a high fat diet mouse model, which mimics the development of DN, mice generated high levels of oxyLDLs, which activates the oxyLDL receptor, lectin-like oxyLDL receptor (LOX-1) (Vincent, Hayes, *et al.*, 2009). The LOX-1 activation amplified oxidative stress in DRG neurons through activation of NADPH oxidase, leading to NADPH depletion/oxidation, increasing mitochondrial superoxide levels, and caspase 3 activation (Vincent, Hayes, *et al.*, 2009).

Additionally, accumulation of free fatty acids (FFA) are proposed increase diacylglycerol (DAG) and ceramide levels in peripheral neurons leading to DN progression through cellular metabolic disruption and inflammatory signaling (M. C. Perez-Matos, Morales-Alvarez and Mendivil, 2017). The role of Schwann cell derived lipids in these neurotoxic mechanisms is still unclear. However, morphological and metabolic changes in Schwann cells have been found to precede axonal pathology (Gonçalves, Vægter and Pallesen, 2018). Moreover, exposure of Schwann cells to long chain fatty acids, which have been implicated in type 2 DN, induce mitochondrial dysfunction and oxidative stress (Hinder *et al.*, 2014). Mitochondrial dysregulation is a hallmark of DN, and it has been demonstrated that disruption of Schwann cell

mitochondrial function through deletion of a mitochondrial transcription factor (Tfam), can cause neurotoxicity, leading to small fiber neuropathy that is remarkably similar to that seen in DN. The neurodegeneration was caused by the release of neurotoxic acylcarnitine species from the Schwann cells (Viader, 2012; Viader *et al.*, 2013). Taken together, these studies suggest that metabolic lipid imbalances are a key driver of neurotoxic pathology in diabetes mellitus, although the full scope of the changes are still under investigation.

Implications in Other Disease Pathologies

A common feature in many neuropathies, inherited or acquired, is phenotypic variation. As previously noted in this work, diabetes is the known progenitor of diabetic neuropathy, but only 20- 40% of patients with diabetes acquire diabetic neuropathy and both the severity and form of the disease vary greatly in those individuals (M C Perez-Matos, Morales-Alvarez and Mendivil, 2017). Additionally, patients with the most common form of CMT, CMT1A, resulting from nearly identical duplications of a chromosomal segment containing the gene encoding peripheral myelin protein 22 (PMP22), have greatly varied phenotypic presentation and progression (Visigalli *et al.*, 2020). This variation suggests that unknown factors, either environmental or genetic, act as modulators in these disorders. It is possible that variations in lipid metabolism, and consequently varied susceptibility to maladaptive lipid accumulation, could be a significant modulator of the progression and severity of neuropathic manifestation. Especially considering, as previously mentioned, that altered circulating lipid levels are a key risk factor for the development of diabetic neuropathy (M C Perez-Matos, Morales-Alvarez and Mendivil, 2017). Moreover, CMT1A models have recently been shown to have significantly altered lipid metabolism, with widely dysregulated sphingolipid and glycerophospholipid metabolism including aberrant species accumulation (Visigalli *et al.*, 2020).

However, as detailed in this introduction, our understanding of the regulation of lipid metabolism both in peripheral nerve development and as a potential element of nerve

pathology is still nascent, even when compared with our knowledge of lipid dynamics in the CNS. Most of the disorders described here are inherited and have known mutations in either lipid biosynthetic enzymes, or lipid transporters, resulting in sometimes extreme but, also, somewhat predictable disruptions in lipid metabolism. However, there are many neuropathies where the etiology is either unknown, or, as in diabetic neuropathy, may involve irregularities in many intertwined and poorly elucidated lipid-mediated cell processes. Thus, a better understanding the complex pathways governing lipid metabolism in both normal development and in cases of maladaptation, is needed to inform our inquiries into the etiology, and potential treatment, of neuropathies.

Project Aims

The following chapters detail my effort to determine the function of the p75 neurotrophin receptor in Schwann cells and neurons during PNS nerve development. Mice lacking p75 have a sensory deficiency due to loss of ~50% of the DRG neurons (Lee *et al.*, 1992; Lee, Davies and Jaenisch, 1994; Murray, Bartlett and Cheema, 1999). This has long been thought to be the result of reduced survival signaling due to the loss of the p75-Trk high affinity neurotrophin binding complex. In addition, the $p75^{KO}$ mice exhibit hypomyelination with thinner myelin and fewer myelinated fibers(Cosgaya, Chan and Shooter, 2002). However, understanding these phenotypes is complicated by the fact that p75 is expressed by both sensory neurons and Schwann cells. I hypothesized, based on the phenotypic presentation of mice lacking p75, that selective Schwann cell p75 disruption would primarily impact myelin formation, while deletion in PNS neurons would result in reduced neuronal survival consequent to embryonic programmed cell death. To our surprise I discovered that loss of p75 in Schwann cells leads to a significant reduction in DRG neuron survival, while deletion of p75 in neurons had insignificant effects on DRG numbers. Moreover, loss of p75 in either cell type did not significantly affect myelin. After adjusting my aims towards elucidating the cause of this surprising result on neuron survival, I discovered that cholesterol biosynthesis is disrupted in p75 deficient Schwann cells, resulting in the accumulation of neurotoxic 7-DHC in developing nerves. Therefore, I theorize that p75 plays a key role in the regulation of cholesterol biosynthetic metabolism

in developing Schwann cells, and the alteration of that metabolism in p75 null Schwann cells contributes to peripheral neurodegeneration. Thus, this project adds to the growing body of work reviewed above that suggests dysregulation of Schwann cell lipid metabolism, leading to accumulation of toxic lipids may be a common factor in the etiology of neuropathy.

Disease	OMIM	Pathway	Gene	Protein Affected	Lipids Accumulated
Fabry disease	301500	Sphingolipid	*GLA*	α-Galactosidase A	Globotriasylceramide, Globotriasylsphingosine
Metachromatic leukodystrophy, PSAP variant	249900	Sphingolipid	*PSAP*	Saposin B	Sulphatide, Lysosulfatide
Metachromatic leukodystrophy	250100	Sphingolipid	*ARSA*	Arylsulphatase A	Sulphatide, Lysosulfatide
Krabbe disease, atypical	611722	Sphingolipid	*PSAP*	Saposin A	Galactosylceramide, Psychosine
Krabbe Disease	245200	Sphingolipid	*GALC*	β-Galactosylceramidase	Galactosylceramide, Psychosine
Niemann-Pick (type A, B)	257200, 607616	Sphingolipid	*SMPD1*	Sphingomyelinase	Sphingomyelin
HSAN, type 1A	162400	Sphingolipid	*SPTLC1, SPTLC2*	Serine palmitoyl transferase	Deoxysphinganine, Deoxymethylsphinganine
Farber disease	228000	Sphingolipid	*ASAH1*	Acid ceramidase	Ceramide
AR-CMT2	N/A	Sphingolipid	*SGPL1*	Sphingosine 1-phosphate lyase	Sphingosine 1-phosphate
Adrenoleukodystrophy	300100	Fatty acid Catabolism	*ABCD1*	Adrenoleukodystrophy protein	Very long-chain fatty acids
Refsum disease	266500	Fatty acid Catabolism	*PHYH*	Phytanoyl-CoA hydroxylase	Phytanic acid
Cerebrotendinous xanthomatosis	213700	Sterol	*CYP27A1*	Sterol 27-hydroxylase	Cholestanol
Niemann-Pick (type C, type D)	257220, 607625	Sterol	*NPC1, NPC2*	NPC-1 and NPC-2	Cholesterol, various sphingolipids
Tangier disease	205400	Sterol	*ABCA1*	ATP-binding cassette transporter	Cholesterol esters
Smith-Lemli-Opitz	222100, 125853	Sterol	*DHCR7*	*7-Dehydrocholesterol reductase*	7-Dehydrocholesterol, 8-Dehydrocholesterol, various oxysterol metabolites
Diabetes Mellitus	270400	Assorted		Assorted	Assorted

Table 1. Diseases associated with toxic lipid accumulation.

Chapter II

Deletion of p75 in Schwann Cells Leads to Uniform DRG Neuron Loss and Hypoalgesia

Introduction

In addition to its assumed role in mediating developmental apoptosis/survival in neurons, the neurotrophin receptor, p75, has long been proposed to play a role in the regulation of Schwann cell myelination. P75 is highly expressed in Schwann cells both during early development and after injury, contemporaneous with many known regulators of myelination(Jessen *et al.*, 2016)(Lemke and Chao, 1988). Additionally, mice lacking p75, $p75^{KO}$, exhibit a marked hypomyelination phenotype (Cosgaya, Chan and Shooter, 2002). However, deciphering the role of p75 in Schwann cell myelination has been challenging due to its concurrent expression in DRG sensory neurons during development. In fact, decreased neurotrophin signaling during embryonic development in neurons has been primarily credited as the basis for a ~50% reduction in DRG neurons and pronounced sensory deficits in $p75^{KO}$ mice, a severe phenotype potentially obscuring the complete role of p75 in Schwann cell development (Lee *et al.*, 1992; Lee, Davies and Jaenisch, 1994; Murray, Bartlett and Cheema, 1999).

Therefore, to investigate the hypothesis that neuronal p75 is a primary regulator of DRG survival/death during development while p75 in Schwann cells is involved in the regulation of myelin formation, we generated two mouse models. Thy1-$p75^{\Delta}$ and Dhh-$p75^{\Delta}$ feature the mid-embryonic deletion of p75 specifically in neurons and Schwann cells, respectively. Interestingly, loss of p75 in either neurons or Schwann cells did not significantly affect myelin formation. However, to our surprise, we found that p75 deletion in Schwann cells, but not neurons, lead to significant loss of DRG neurons during development. As a result, we adopted the secondary aim of defining the neuronal populations diminished in mice with Schwann cell p75 deletion. We discovered that the loss of DRG neurons in Dhh-$p75^{\Delta}$ was not confined to one identifiable subtype, but

appears uniform in the DRG, indicating both myelinated and Remak bundle associated DRG neurons are affected by loss of p75 signaling in Schwann cells during development.

Methods

Mouse Husbandry and Experimental Design

All experimental designs and procedures involving animals followed the guidelines of the Institutional Animal Care and Use Committee at Ohio State University and Vanderbilt University. Global p75 knockout mice ($p75^{KO}$, RRID:IMSR_JAX:002213) have been described previously (Lee *et al.*, 1992) and P75-floxed ($p75^{fl/fl}$) mice have been described by Bogenmann et al (2011) (Bogenmann *et al.*, 2011) To conditionally delete p75 from sensory neurons and Schwann cells, $p75^{fl/fl}$ mice were first crossed with Thy1-cre (RRID:IMSR_JAX:006143) (Dewachter et al., 2002), and Dhh-cre (RRID:IMSR_JAX:012929)(Jaegle *et al.*, 2003), respectively. The resulting Thy1-$cre^{+/-}$: $p75^{fl/-}$ mice were crossed with Thy1-$cre^{-/-}$: $p75^{fl/wt}$ mice to obtain Thy1-$cre^{+/-}$: $p75^{fl/fl}$ (Thy1-$p75^{\Delta}$) and Thy1-$cre^{+/-}$: $p75^{wt/wt}$ (Thy1-$p75^{C}$) mice. The same breeding strategy was used for Dhh- $p75^{\Delta}$ and Dhh-$p75^{C}$ mice. Thy1-$p75^{C}$,Dhh-$p75^{C}$, or when appropriate, C57BL/6J (WT, RRID:IMSR_JAX:000664) mice were utilized as controls.

Thermal hyperalgesia Analysis

Thermal hyperalgesia was evaluated using a modified Hargreaves Apparatus from Ugo Basile using infrared as a heat source at 50°C as we have previously published (Tep *et al.*, 2013)

Dorsal Root Ganglion (DRG) Morphological Analysis

L4-6 DRGs were isolated from adult (P28) and juvenile (P5-7) mice and fixed in 4% paraformaldehyde (Sigma-Aldrich Cat#P6148) or 10% neutral buffered formalin. Once

imbedded in paraffin, whole DRGs were sectioned at 5 μm using a Leitz 1512 microtome. After deparaffinization and rehydration, sections were stained with toluidine blue (Sigma-Aldrich Cat#89640, 10 min), rinsed briefly in H_20, 95% ETOH, and 100% ETOH sequentially before mounted with DPX (Electron Microscopy Solutions Cat#13512). For embryonic DRG analysis, intact lumbar spine sections were processed to prevent DRG damage during isolation. DRGs were imaged in brightfield on a Nikon Eclipse Ti scope with DS-Qi2 camera (Nikon) and NIS-Elements (https://www.microscope.healthcare.nikon.com/products/software/nis-elements) at 20x magnification by a blinded individual. The first section imaged was randomly selected from sections 1-12, and subsequently every 12^{th} section was imaged. Images were then imported into FIJI (https://fiji.sc/) and stitched together to form whole DRG images. To determine DRG number, every neuron with a defined nuclear profile was counted using the empirical method as described in (Coggeshall *et al.*, 1984) To determine soma diameter, each neuron included in the previous counts was outlined manually in FIJI, the area in an ROI encompassing the soma was measured, and the diameter was derived from $A=2\pi r^2$.

Electron Microscopy

Sciatic nerves were prepared for transmission electron microscopy according to Kim et al. (2003). (Kim *et al.*, 2003) Sciatic nerve thin sections were then imaged in a randomized fashion on a Philips/FEI T-12 TEM (Phillips) electron microscope with a side mounted 2k x 2k AMT CCD camera (AMT http://www.amtimaging.com) system at 2700X magnification. For g-ratio analysis 20 images per sample were randomly selected by a blinded evaluator and, in FIJI, images were manually thresholded to clarify myelin profiles. Then, using the ROI selection wand the area of myelinated nerve fiber cross sections and axons were calculated. The diameters of axons and myelinated fibers were derived from collected areas ($A=2\pi r^2$) and the g-ratio (diameter of axon/diameter the myelinated fiber) was determined. To access Remak bundles, the number of distinct axons per bundle and the total number of Remak bundles per image were counted manually by a blinded observer.

RNAScope

L4-6 DRGs were isolated form P28 Dhh-p75$^{\Delta}$ and Dhh-p75^{C} mice, fixed in 4% paraformaldehyde, paraffin embedded, and sectioned at 5 µm. DRG sections with at least 150 neurons were selected from each sample for analysis, and deparaffinized as described above. As a control, sections with fewer than 50 neurons were also analyzed and were found to be consistent in distribution with the larger sections. Single-molecule fluorescence in situ hybridization was preformed using a RNAscope® Multiplex Fluorescent Reagent Kit v2 (ACDbio Cat#323100) and the TSA® Plus Cyanine 3 (Cy3) detection kit (Perkin Elmer Cat#NEL744001KT) according to the manufacturer's instructions with the following RNA Scopes probes. Fluorescent images were captured at 20x (Nikon) and analyzed in FIJI. Neurons were manually counted and ranked as being high, medium, or low expressing by a blinded observer according to a scale developed prior to analysis.

Quantification and Statistical Analysis

Quantitative data are presented as mean ± SEM. All experiments were independently repeated and evaluated at least 3 times by a blinded individual. Prism 6/7 (Graphpad Software http://www.graphpad.com/scientific-software/prism/) was used to determine statistical significance between groups using one-way analysis of variance (ANOVA) with Tukey's post hoc test (for experiments with more than 2 groups), or Student's t-test.

Results

Selective deletion of p75 in Schwann cells leads to minor effects on myelination

To generate the conditional mouse models, Dhh-p75$^{\Delta}$ and Thy1-p75$^{\Delta}$, we utilized a conditional p75$^{fl/fl}$ line, which carry an allele with LoxP flanking exons 4-6 of the gene encoding p75. As a result, all transmembrane and cytoplasmic domains of p75 are

eliminated after Cre recombination in targeted cells (Bogenmann *et al.*, 2011). P75 was selectively deleted in Schwan cells by crossing $p75^{fl/fl}$ mice with Desert Hedgehog-Cre transgenic mice, which express Cre recombinase in the Schwann cell lineage beginning at embryonic day 12 (E12) (Jaegle *et al.*, 2003). This resulted in the generation of experimental, Dhh-cre+/-: $p75^{fl/fl}$ (Dhh-$p75^{\Delta}$) and control, Dhh-cre+/-: $p75^{wt/wt}$ (Dhh-$p75^{C}$) mice. Second, p75 was selectively deleted in neurons by crossing $p75^{fl/fl}$ mice with the Thy-1 Cell Surface Antigen (Thy1)-Cre transgenic mice, which drives Cre recombinase expression in both central and a majority of sensory neurons of the periphery by E12.5 (Feng *et al.*, 2000; Dewachter *et al.*, 2002; Alić *et al.*, 2016) generating Thy1-cre+/-: $p75^{fl/fl}$ (Thy1-$p75^{\Delta}$) and control, Thy1-cre+/-: $p75^{wt/wt}$ (Thy1-$p75^{C}$) mice. Immunofluorescence staining for p75 in adult sciatic nerve sections showed, as expected, greatly decreased p75 in non-myelinating Schwann cells (only non-myelinating Schwann cells retain p75 expression after early development) in Dhh-$p75^{\Delta}$ and $p75^{KO}$ mice relative to a wildtype (WT) control (Lemke and Chao, 1988; Jessen *et al.*, 2016). Conversely, Thy1-$p75^{\Delta}$ and $p75^{KO}$, exhibited reduced p75 signal in only DRG neurons relative to WT controls (Fig. 9).

As we expected that p75 primarily regulates myelin formation in Schwann cells during development, we first examined the myelin profiles of sciatic nerves extracted from Dhh-$p75^{\Delta}$, Thy1-$p75^{\Delta}$ and their respective controls, Dhh-$P75^{C}$ and Thy1-$P75^{C}$. We collected g-ratios and surveyed myelinated axons for gross morphological abnormalities at P0 (post-natal day 0), P5, P15 (during the normal myelination period) and P25 (once myelination is complete) using transmission electron microscopy. To our surprise, none of the models exhibited a gross myelin deficit at any age, and only a transient, mild, but not significant, hypomyelination was observed in P15 Dhh-$p75^{\Delta}$ mice compared to control (Fig. 10 A-C). Since $p75^{KO}$ mice show an advanced hypomyelination phenotype, these results suggest that p75 signaling in both neurons and Schwann cells must be lost to meaningfully compromise adult myelin formation.

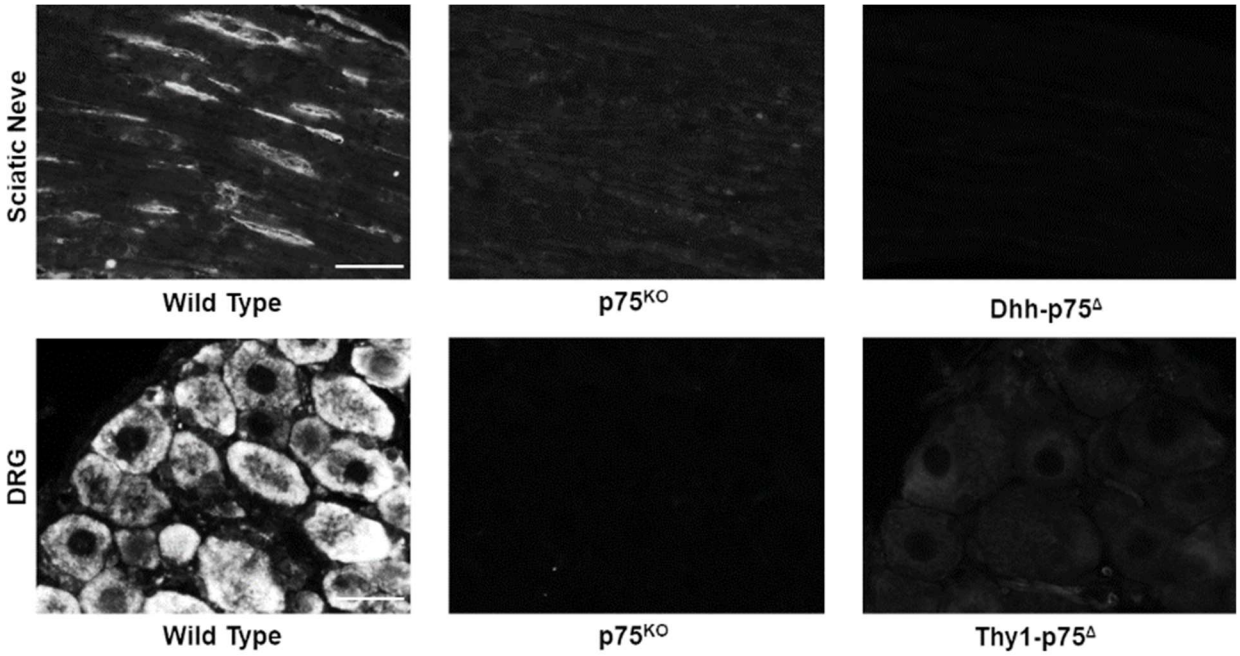

Figure 9. Selective loss of p75 in Dhh-P75$^{\Delta}$ and Thy1-P75$^{\Delta}$ mice. (A) Adult sciatic nerves from the wild type, p75^{KO}, and Dhh-p75$^{\Delta}$ mice were stained for p75. Scale bar, 25 μm. (B) Adult DRG from the wild type, p75^{KO}, and Thy1-p75$^{\Delta}$ mice and stained for p75. Scale bar, 25 μm. It should be noted that while the majority of adult DRGs are expected to retain p75 expression in adulthood, only non-myelinating SCs retain p75 expression in adult nerves.

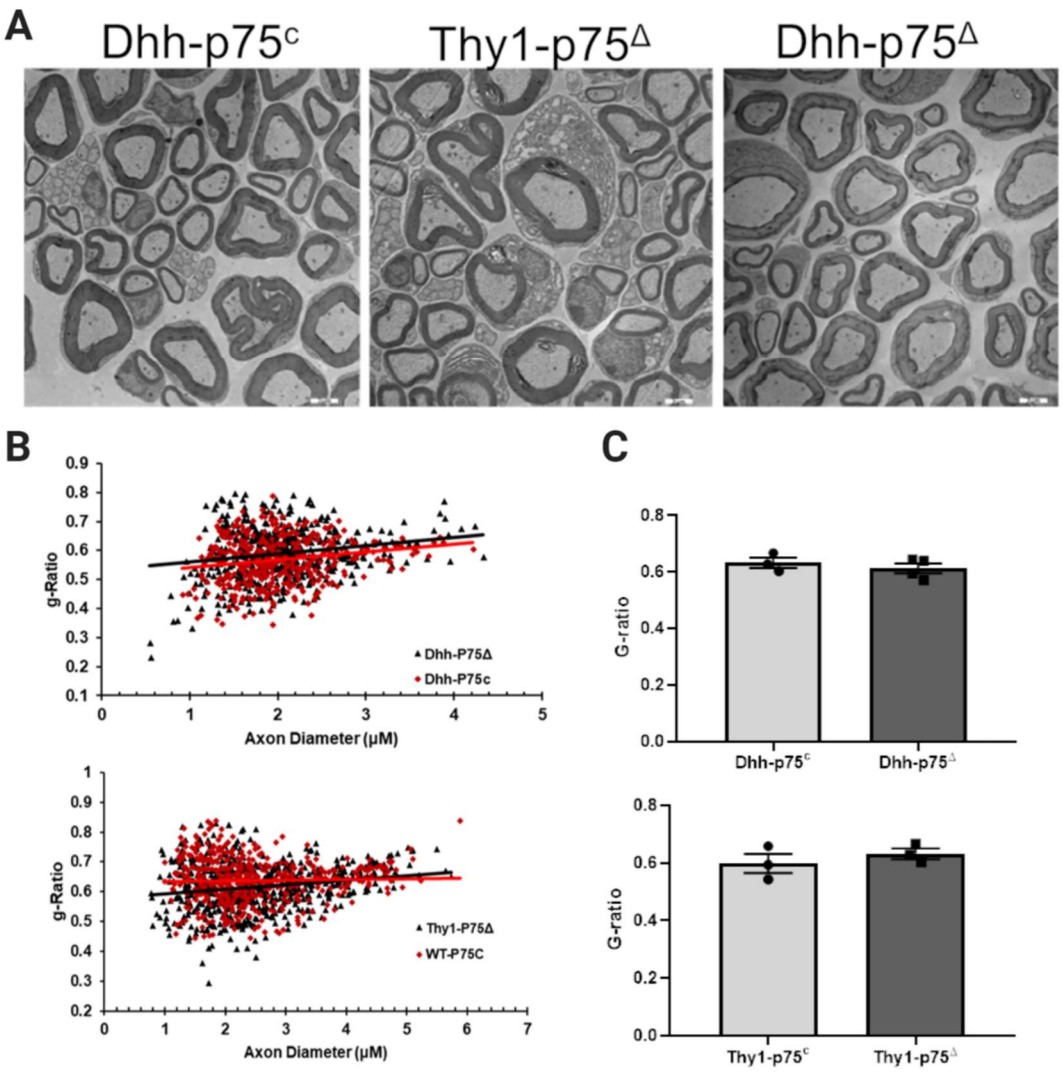

Figure 10. Deletion of p75 in Schwann cells or neurons has no significant effect on myelination. (A) Representative electron micrographs of P25 sciatic nerve cross sections from Dhh-p75$^{\Delta}$, Thy1-p75$^{\Delta}$ and their respective controls, Dhh-P75^{C} and Thy1-P75^{C}. Both Schwann cell and neuron conditional p75 knockout models exhibited grossly normal myelin and Remak morphology. Scale bar, 2 μm. (B) G-ratios plotted as a function of axon diameter (left) and average g-ratio (right) from P15 Dhh-p75$^{\Delta}$ and control sciatic nerves (N=3). (C) G-ratios plotted as a function of axon diameter (left) and average g-ratio (right) from P25 Thy1-p75$^{\Delta}$ and control sciatic nerves (N=3).

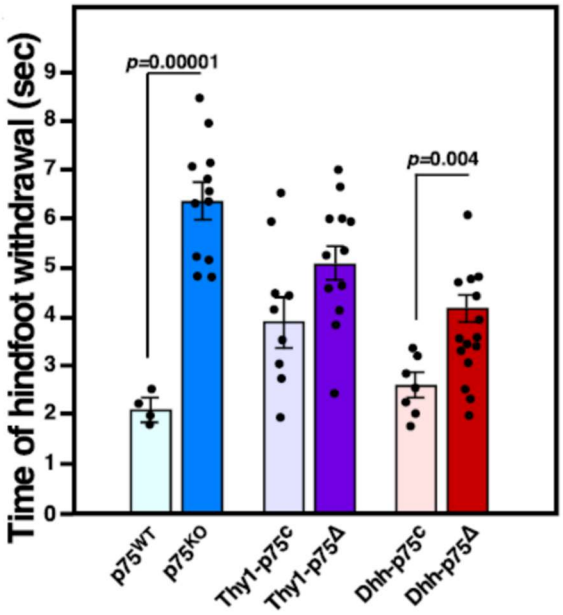

Figure 11. Deletion of p75 from Schwann cells results in thermal hypoalgesia. Mice were examined for thermal hyperalgesia utilizing a modified Hargreaves Apparatus at 50°C. Student's t-test, unpaired one-way, was used for statistics

Selective deletion of p75 in Schwann cells results in reduced thermal sensitivity and DRG neuron loss.

P75^{KO} mice have also been noted to exhibit thermal hypoalgesia, a sensory deficit attributed to the loss of sensory neurons during development. The decrease in sensory neurons was attributed to reduced survival signaling during the period of embryonic programed cell death, also known as naturally occurring neuronal death (NOND), as result of neurons lacking p75 trophic contributions (Lee *et al.*, 1992; Stucky and Koltzenburg, 1997; Vaegter *et al.*, 2011). This interpretation was also supported by a 2-3 fold decrease in NGF sensitivity of p75^{KO} sensory neurons, when cultured in isolation without Schwann cells (Lee, Davies and Jaenisch, 1994). We, therefore, examined whether our models, absent of myelin deficits, display a thermal hypoalgesia phenotype. In agreement with previous results, P75^{KO} mice exhibited a significantly delayed response to thermal stimulation (Lee *et al.*, 1992). Unexpectedly, however, Thy1-p75$^{\Delta}$ mice failed to display a significant difference from control, while Dhh-p75$^{\Delta}$ mice showed significant hypoalgesia (Fig. 11).

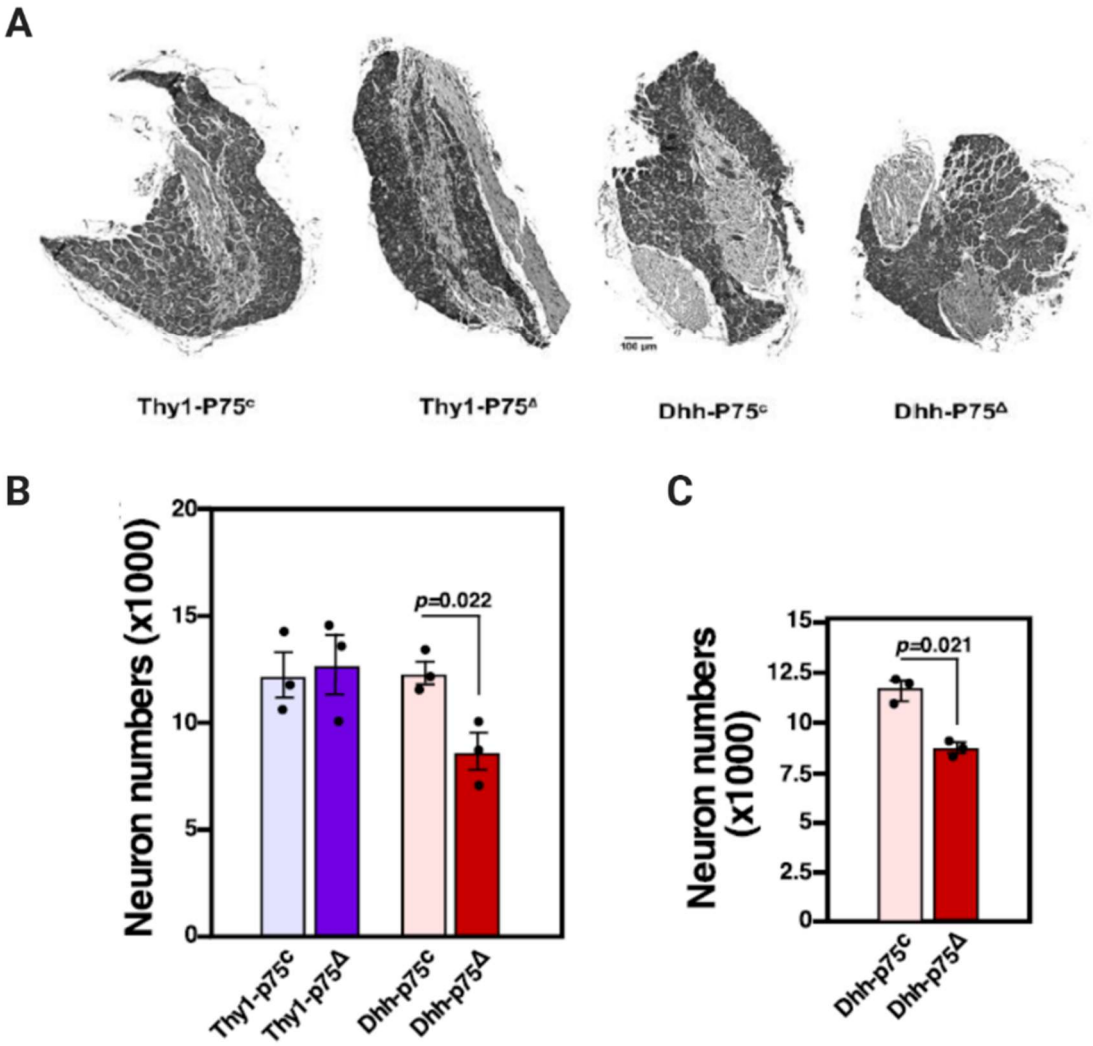

Figure 12. Selective deletion of p75 in Schwann cells results DRG neuron loss. (A) Representative images of DRG sections at P25 from Thy1-p75$^{\Delta}$, Dhh-p75$^{\Delta}$ and their respective controls. Scale bar, 100 µm. (B) Quantification of DRG neurons at P25 from Thy1-p75$^{\Delta}$, Dhh-p75$^{\Delta}$ and their respective controls. (C) Quantification of DRG neurons in Dhh-P75$^{\Delta}$ and control mice at P5, before myelination is complete.

Because the thermal hypoalgesia previously noted in $p75^{KO}$ mice has been attributed primarily to their reduced sensory neuron number, we next quantified the number of L4-6 DRG sensory neurons at P25 in our conditional knockout models. In agreement with the thermal sensitivity results, there was no reduction in the number of lumbar DRG neurons in Thy1-$p75^{\Delta}$ mice; however, Dhh-$p75^{\Delta}$ mice had 30% fewer DRG neurons compared to control (Fig. 12 A,B). Given that the neuronal loss in Dhh-$p75^{\Delta}$ mice was already present at P25, which is after the termination myelination formation, we reasoned that the neuronal loss may occur during active Schwann cell myelination, when metabolic activity is highly up regulated to accommodate myelination. Indeed, we found a 25% decrease in the number of neurons already at P5 in Dhh-$p75^{\Delta}$ mice compared to the control (Fig. 12C), concurrent with large scale myelination (Jessen, Mirsky and Lloyd, 2015). Taken together, these data suggest that neuronal p75 does not play a significant role in sensory neuron survival in conditions of unchallenged development. Instead, DRG neuronal survival is in large part dependent on p75 function in developing Schwann cells.

If neuron survival is not dependent on neuronal p75 mediated survival signaling during embryonic development, we reasoned that there should be equal number of neurons in $p75^{KO}$ mice at E17.5, since that is after normal developmental apoptosis is complete in DRGs (Fariñas *et al.*, 1996; White *et al.*, 1996) but before the initiation of myelination(Jessen, Mirsky and Lloyd, 2015). Indeed, we found that there was no deficit in the number of DRG neurons in $p75^{KO}$ mice at E17.5, although at P28 there was a 50% reduction (Fig. 13A-B). This result suggests that reduced neurotrophic signaling through neuronal p75 during PCD is not the primary cause of the 50% reduction in DRG neurons in $p75^{KO}$ mice. Based on our data from Thy1-$p75^{\Delta}$ and Dhh-$p75^{\Delta}$ mice, we surmise that sensory neuron loss in $p75^{KO}$ mice is therefore primarily due to the absence of p75 signaling in Schwann cells.

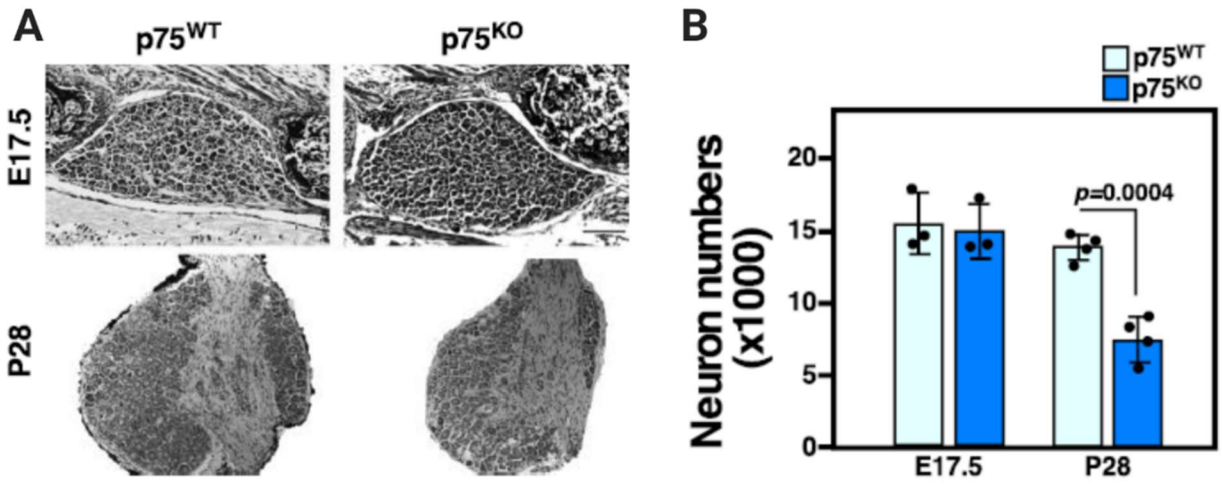

Figure 13. Deletion of p75 does not cause DRG neuron loss during middle embryonic development. (A) Representative images of DRG sections from wild type and $p75^{KO}$ at E17.5 and P28. Scale bar, 100 μm. (B) Quantification of DRG neurons from the wildtype and $p75^{KO}$ mice.

The loss of DRG neurons in Dhh-$p75^{\Delta}$ mice is not specific to a particular neuronal subtype.

Given the large diversity of neuronal subtypes present in DRGs, we next sought to determine if any specific group of neurons were preferentially affected in Dhh-$p75^{\Delta}$ mice. Because p75 continues to be highly expressed in non-myelinating Remak Schwann cells throughout adulthood, and these Schwann cells enfold the unmyelinated c-fibers that respond to thermal stimuli (Murinson and Griffin, 2004), we first quantified the number of axons ensheathed per Remak bundle (Fig. 14 A), but found no differences. Additionally, there were no discernable organizational differences in Remak bundles (Fig. 10A). As there is a general correlation between the soma size of sensory neurons and their functional subtypes, we also analyzed the distribution of soma sizes within the DRGs of Dhh-$p75^{\Delta}$ mice, but again found no significant differences(de Moraes, Kushmerick and Naves, 2017) (Fig. 14 B). This data suggests that there is a general reduction in all types of DRG neurons in the Dhh-$p75^{\Delta}$ mice.

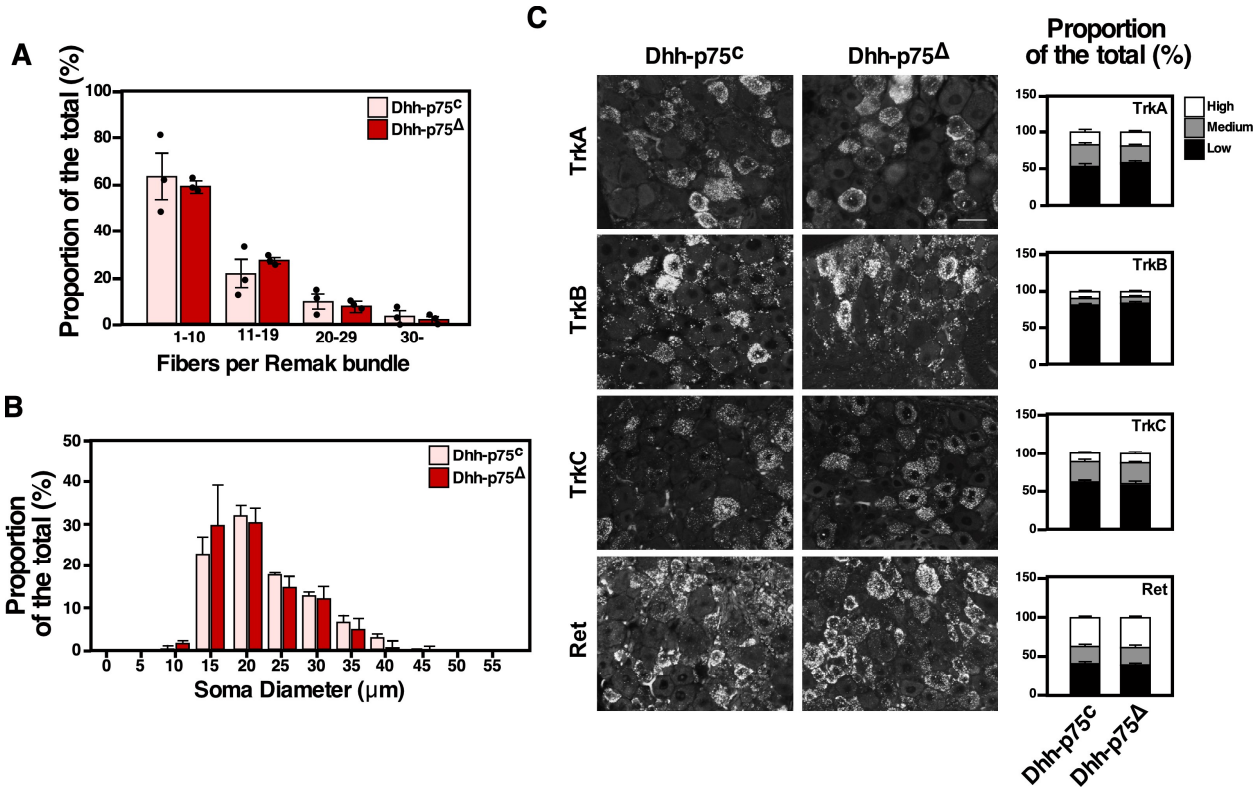

Figure 14. The loss of DRG neurons in Dhh-p75$^{\Delta}$ mice is not specific to any neuronal subtype. (A) Size distribution of Remak bundles in sciatic nerves of P25 Dhh-p75$^{\Delta}$ and control mice. There was no significant difference between genotypes (one-way ANOVA). (B) Soma size distribution of L4-6 DRGs of P25 Dhh-p75$^{\Delta}$ and control mice (N=3). No significant difference was found in neuronal soma size (one-way ANOVA) (C) RNA scope with probes specific to TrkA, TrkB, TrkC, and Ret receptor mRNA. Representative images and quantification of L4-6 DRG sections from P25 Dhh-p75$^{\Delta}$ and control mice. Scale bar, 25 μm. Cells were evaluated as having no/low, medium, or high quantities of puncta (N=4). No significant difference was found for any subtype (student's t-test)

Our conclusion was further supported when we analyzed the adult proportion of different DRG subtypes neurons, using RNAscope assays, based on subtype-specific markers, namely; TrkA for Aβ nociceptors and peptidergic nociceptors, TrkB for mechanoreceptors, TrkC for proprioceptors, or Ret for non-peptidergic nociceptors (Marmigère and Carroll, 2014). Corroborating our previous results, we found no changes in Dhh-p75$^{\Delta}$ DRGs relative to controls (Fig. 14 C). It should be noted, these results are similar to published examinations of p75^{KO} mouse DRGs, where neuron loss was found to be uniform across all sensory subtypes (Bergmann *et al.*, 1997, 1998; Murray, Bartlett

and Cheema, 1999). Together these data indicate that deletion of p75 in Schwann cells results in a global reduction in all DRG neurons, regardless of the subtype and their association with myelinating or Remak Schwann cells. We thus hypothesize the underlying mechanism of neuronal loss is likely to involve a defect in Schwann cell function capable of affecting widespread sensory neuron subtypes, rather than more localized disruption of intercellular signaling affecting only closely associated neurons.

Discussion

P75 has long been proposed to be a regulator of myelination formation in myelinating Schwann cells, and mediate survival signaling in embryonic DRG neurons during developmental apoptosis (Lee, Davies and Jaenisch, 1994; Cosgaya, Chan and Shooter, 2002). Our data counters both these suppositions. The lack of persistent hypomyelination phenotype in Dhh-p75$^{\Delta}$ does not exclude a potential role of p75 in myelination, as compensatory pathways might have been activated, but it does suggest Schwann cell p75 is not as essential to myelin regulation as previously believed. More surprising was our finding that deleting p75 from neurons did not result in DRG neuron loss, and there was also no decrease in sensory neurons in p75^{KO} mice at E17.5, a time point well after normal developmental apoptosis is complete in DRGs (Fariñas *et al.*, 1996; White *et al.*, 1996). In contrast, deletion of p75 in Schwann cells resulted in a 30% reduction in DRG neurons.

However, recent studies have also presented data that conflict with the prevailing hypothesis of p75 regulation of embryonic DRG apoptosis. For instance, a recent report, utilizing another neuron specific promoter, neurofilament-light chain-Cre, also failed to find any changes in sensory neuron survival (Qin *et al.*, 2020). Similarly, Chen al. (2017) noted only a 20% reduction among the IB4^{+}/peripherin^{+}/Ret^{+} class of nonpeptidergic nociceptors occurring between P14 and adulthood when p75 was deleted in the DRG beginning at E12.5 in Islet1-p75$^{\Delta}$ mice(Chen *et al.*, 2017). As in Qin et al (2020), we failed to detect any significant loss in total adult DRG neurons in Thy1-p75$^{\Delta}$ mice. Additionally, we observed no change in the frequency of DRGs with small diameter soma in adult

Dhh-p75$^{\Delta,}$, a popultion that would be highly likely to overlap with the majority of Ret^{+} nociceptors (data not shown). However, it should be noted that we found that approximately 5.7% of DRG neurons still expressed p75 in these mice (data not shown). The incomplete deletion of p75 in the Thy1-p75$^{\Delta}$ mice could account for both the difference between the 50% loss of neurons in the total knock out compared to 30% loss in the Schwann cell-specific deletion of p75 and the lack of early adolescent sensory nociceptive loss.

Still, there are other equally plausible explanations for the difference in neruonal loss between p75^{KO} and Dhh-p75$^{\Delta}$ mice. One explanation is that the additional neuronal loss occurs from loss of p75 signalling in other non-neuronal cell types. For instance, our model does not delete p75 in satellite glia, which are themselves key mediators of DRG neuron health and survival (Hanani and Spray, 2020). Alternatively, deletion in both neurons and glia could have additive repercussions from the loss of concurrent, or coordinated, p75 signaling between axons and Schwann cells. It has been shown that p75^{KO} mice exhibit delayed/abnormal axon outgrowth and Schwann cell precursor migration between E11.5-E14.5 (Bentley and Lee, 2018). At that time point Schwann cell precursors are reliant on axonal guidance for migration and survival, and axons, in turn, are reliant on efficient target acquisition to survive (Mirsky *et al.*, 2008). Therefore, p75 may have a role in the coordination of axon-SC interactions, with mutual deletion producing significantly more deleterious effects.

That the nature of the sensory loss is universal accross all subtypes was also suprising, although not without precedent, as p75^{KO} mice have been reported to have proportional sensory neuron loss across all identifiable subtypes (Stucky and Koltzenburg, 1997). However this model of uniform sensory loss makes much more intrinsic sense in a paradigm where a universal loss of p75 mediated neurotrophic support is the perpetuating factor of neuronal death. In a scenario involving p75 deletion in Schwann cells leading to neuronal loss, we expected there might be preferential loss of either unmyelinated fibers or myelinated fibers. Especially, due to the vastly different roles of non-myelinating and myelinating SCs in axonal function. This premise is

supported by the fact that in neuropathies tied to Schwann cell dysfunction, axon degeration/loss is often highly subtype specific, at least in early stages (Fridman and Reilly, 2015). That this was not the case suggests the loss of neurons may not be due to a mechanism of direct cell-cell signalling, but through an indirect mechanism that has the potential to affect neuronal populations as a whole within the nerve. Additionally, that the loss of neurons occurs perinatally, a timpoint where the process of myelientionis the dominating metabolic process occurring in the nerve, suggests that the loss occurs as a result of disordered regulation of myelin formation.

Taken together, these results indicate that reduced neurotrophic signaling, at least as it relates to normal developmental apoptosis, is not the main cause of DRG neuron loss in p75 deficient models. Instead, our study indicates that neuronal survival is affected most substantially by the loss of p75 in Schwann cells.

Chapter III

Deletion of p75 leads to the Accumulation of Neurotoxic 7-DHC, Resulting in Neuronal Loss During Development

Introduction

In preparation for myelination, perinatal myelinating Schwann cells undergo an immense metabolic reorganization and shift towards lipid biosynthesis. It estimated that the plasma membrane of Schwann cells expands 6500 fold during myelin (Webster, 1971). Additionally, myelin has a much larger ratio of lipids to proteins than average cell membranes, with a lipid/protein ratio of 186:1(Schmitt, Cantuti Castelvetri and Simons, 2015b). Previous studies have proposed that p75 signaling can regulate some aspects of lipid metabolism, including the expression levels of cholesterol biosynthetic enzymes in several cell types, and ceramide levels in Schwann cells (H Hirata *et al.*, 2001; Korade *et al.*, 2007). This suggests that a reduction in p75 signaling may result in dysregulation of lipid biosynthetic pathways in myelinating Schwann cells.

Additionally, it has repeatedly been demonstrated that alterations in lipid metabolism can cause neurotoxicity through the accumulation of neurotoxic lipids (for a full review see Chapter 1). For instance, Viader et al. (2013), demonstrated that the disruption of fatty acid biosynthesis by deletion of the mitochondrial transcription factor, Tfam, in Schwann cells led to the production and accumulation of neurotoxic acylcarnitines resulting in induced sensory neuron degeneration without any effect on Schwann cell viability. These findings are remarkably reminiscent of our observation of sensory neuron loss without overt myelin changes in Dhh-p75$^{\Delta}$ mice. Therefore, we hypothesized that Schwann cells lacking p75 have altered lipid metabolic regulation, potentially contributing to the etiology of neuron loss in p75^{KO} and Dhh-p75$^{\Delta}$ models. Indeed, we found that both p75^{KO} and Dhh-p75$^{\Delta}$ models exhibited altered regulation of cholesterol biosynthesis pathways, resulting in the aberrant accumulation of a highly neurotoxic cholesterol precursor, 7-dehydrocholesterol (7-DHC). Furthermore, lenti-viral

induced upregulation of *dhcr7* , the gene encoding 7-DHCR, in p75 null Schwann cells within the sciatic nerve is sufficient to significantly rescue the sensory neuron deficit observed in p75 null mice, suggesting that 7-DHC accumulation is a causative factor in the observed neuron loss.

Methods

Lipid Extraction and LC-MS/MS (SRM) Analysis

Sciatic nerve lipid extraction- Whole sciatic nerves were isolated and immediately frozen in liquid N_2 and stored at -80^{o}C until the day of lipid extraction. Prior to extraction, nerves were ground to the consistency of a powder on dry ice with a plastic pestle to increase buffer permeability. Ice-cold NP40 lysis buffer (120 mM NaCl, 50 mM HEPES, 1% Igepal) was added to samples and incubated for 15 minutes before being spun down at 15000 rpm for 20 min. Total protein content was measured using a BCA assay (Pierce Cat#23225) and recorded for subsequent normalization. After lysis, lipids were extracted and derivatized with PTAD as described previously(Genaro-Mattos *et al.*, 2018, 2019).

^{13}C-Glucose labeling in mouse Schwann cells -Primary mouse Schwann cells were cultured as below, plated in 96 well plates, and kept in culture for 7 days prior to treatment. C^{13}-glucose (Cambridge Isotope Lab Cat#CLM-1396-0) labeled DMEM media (10 mM $^{13}C_6$-glucose, 1 mM L-glutamine, 10% delipidated fetal bovine serum) was then added and changed every 2-3 days for a total of 9 days. Live cells were then incubated with 40 ng/µL Hoechst 33258 (Molecular Probes Cat#H-3569) for 20 minutes at 37^{o}C and imaged under 10X magnification using ImageExpress XL (Molecular Devices) with 4 images collected per well. Cell number was determined by automated nuclear counting on MetaXpress® 4 (https://www.moleculardevices.com/products/cellular-imaging-systems/acquisition-and-analysis-software/metaxpress#gref) for the purpose of normalization. Cells were then rinsed twice with PBS and lipids were extracted and analyzed as previously described(Genaro-Mattos *et al.*, 2019).

Sterol Analysis-Samples were placed in an Acquity UPLC system equipped with ANSI-compliant well plate holder coupled to a Thermo Scientific TSQ Quantum mass spectrometer equipped with an APCI source. Then 10 µL was injected onto the column (Phenomenex Luna Omega C18, 1.6 µm, 100 Å, 2.1 mm × 50 mm) with 100% MeOH (0.1% v/v acetic acid) mobile phase for 1.0 min runtime at a flow rate of 500 µL/min. Natural sterols were analyzed by selective reaction monitoring (SRM) using the following transitions: Chol 369 → 369, 7-DHC 560 → 365, desmosterol 592 → 560, lanosterol 634 → 602, with retention times of 0.7, 0.4, 0.3 and 0.3 min, respectively. SRMs for the internal standards were set to: d7-Chol 376 → 376, d7-7-DHC 567 → 372, 13C3-desmosterol 595 → 563, 13C3-lanosterol 637 → 605. Final sterol numbers are reported as nmol/mg of protein.

Acylcarnitine Analysis– The acylcarnitine profile was assessed by LC-MS/MS as described previously(Brittain *et al.*, 2016) Briefly, samples were spiked with a known amount of d_3-palmitoylcarnitine as the internal standard and the lipid was extracted. After extraction, acylcarnitines were injected onto the column (Phenomenex Luna Omega C18, 1.6 µm, 100 Å, 2.1 mm × 100 mm) with 100% acetonitrile (0.1% v/v formic acid) (solvent B) and water/acetonitrile (90:10 v/v, 0.1% v/v formic acid and 10 mM ammonium formate) (solvent A) for 5 min runtime at a flow rate of 500 µL/min. Individual acylcarnitines were analyzed by SRM using transitions of the precursor ion (as M+H) to the respective product ions with 85 *m/z* ratio.

Primary Schwann Cell Culture

Rat-Primary rat Schwann cells were isolated from P2-P3 rats according to Chan et al. (Chan *et al.*, 2004) and maintained on collagen coated (1:20 collagen/H_20, Sigma-Aldrich Cat#C3867D) plates with high glucose DMEM (Gibco Cat#11995-065) with 10% FBS (Omega Cat#FB-01) and 2 µM Forskolin (Sigma-Aldrich Cat#F6886-10MG) at 37°C, 5% CO_2.

Mouse- Mouse sciatic nerves were harvested from P4-P6 C57/B6J or $P75^{KO}$ mice and chilled in 1:1 DMEM/PBS on ice. After collection, nerves were digested at 37°C with 0.3%

collagenase (Sigma-Aldrich Cat#C5894-50MG) for 15 minutes, after which 0.4% trypsin (Worthington Cat#LS003708) was added for subsequent 15 minutes. 1ml DMEM was added to the reaction, and nerves were rinsed twice with PBS before being manually triturated and plated to the desired density on Poly-d-lysine (Fisher Scientific Cat# 215017525) coated plates. Cells were maintained in DMEM with 10% FBS (Hyclone Cat#SH30088.03) and 50 ng/ml GGF (R&D Systems Cat#396-HB) at 37°C, 5% CO_2.

Primary Neuron Culture

DRGs were isolated from P4-P6 rat pups and chilled in 1:1 DMEM/PBS on ice and subjected to digestion with 0.08% collagenase (Sigma-Aldrich) and 500 K.U. DNase I (Sigma-Aldrich Cat #D5025) for 30 minutes at 37°C, which was followed by 10 minute digestion with 0.01% trypsin (Worthington). Digestion was quenched with the addition of 1ml DMEM with 10% FBS (Hyclone) and washed in fresh DMEM before resuspension in DMEM (10% Hyclone FBS, 25ng/ml NGF, 1% NG2, 2% B27 (Gibco Cat#17504-044)). Neurons were then plated on poly-d-lysine and laminin (Fisher Scientific) coated plates/coverslips.

7-DHC Treatment

Schwann cells- rat Schwann cells were plated at 10,000 per well in 96-well plates. The next day, they were treated 7-DHC/ETOH (Sigma-Aldrich Cat#30800-5G-F) or ETOH. The media with 7-DHC was refreshed daily, due to its oxidizable nature, until the end of the 72 hr treatment period, after which the cells were stained with 40 ng/µL Hoechst (Molecular Probes) for 10 minutes at 37°C and live imaged at 10X using the Image Express Micro XL (Molecular Devices). Four images were taken per well, which were imported into FIJI and Hoechst positive nuclei exhibiting normal morphology were counted manually by a blinded individual.

Immunofluorescence

Samples were rinsed in PBS and permeabilized for 10 min with 0.1% Triton-X (Sigma-Aldrich Cat#T8787). They were then blocked with 5% Normal Goat Serum (Gibco Cat# 16210064) for 1hr at RT and placed in primary antibody overnight. Slides were rinsed three times with PBS and incubated in secondary antibody for 1 hr at RT before being rinsed three times with PBS and mounted with Prolong anti-fade reagent with DAPI (Life Technologies Cat#P36931). For paraffin embedded DRGs, 5 µm slide mounted sections were first deparaffinized and rehydrated as above, then slides were placed in a pressure cooker for 15 min (GoWise USA) within a copulin jar filled with citrate buffer antigen retrieval solution (10mM Citric Acid, 0.05% Tween 20, pH 6.0). After cooling to RT, sections were permeabilized and stained in the same manner as detailed above. Antibodies used were: Anti-NGFR p75 (RRID:AB_784824), Anti-Neurofilament (RRID:AB_91201), Anti-p75 ECD 9650 Serum (Palmada *et al.*, 2002), 596-Alexa Flour Goat anti-Mouse (RRID:AB_141369), and 647-Alexa Flour Donkey anti-rabbit (RRID:AB_2536183).

Injection of Lentivirus into Neonate Mice

Lentivirus Generation- To generate lentivirus, 293T cells were transfected with Lipofectamine 2000 (Thermo-Fisher Sci. Cat# 11668030) with an empty pLX304 vector (addgene #25890), or a pLX304 vector harboring a DHCR7 construct (ccsbBroad304_06097 from the CCSB-Broad Lentiviral Expression Collection) and psPax2 (addgene # 12260) and pMD2.G (addgene # 12259) constructs. 48h and 72h after transfection, virus-containing media was harvested, passed through a 0.45 µm syringe filter, and combined. To concentrate the virus, the collected media was run through 100kDa Amicon® Ultra-15 Centrifugal Filter Units (Millipore-Sigma Cat# UFC910024) columns following manufacturer's directions.

Injections- 2-3 µl of concentrated lentivirus solution was injected, using a 6mm 31GG fixed insulin needle (BD) penetrating through the outer skin, into the distal thigh of post-natal day 0 neonate, Care was taken to target the intermuscular area adjoining the sciatic

nerve, to avoid potential nerve damage. At postnatal day 5, the sciatic nerves were harvested and stained as described in the following methods for the presence of a V5 epitope tag to confirm infection. DRGs were extracted and counting as detailed previously.

Quantification and Statistical Analysis

Quantitative data are presented as mean ± SEM. All experiments were independently repeated and evaluated at least 3 times by a blinded individual. Prism 6/7 (GraphPad Software http://www.graphpad.com/scientific-software/prism/) was used to determine statistical significance between groups using one-way analysis of variance (ANOVA) with Tukey's post hoc test (for experiments with more than 2 groups), or Student's t-test.

Results

Loss of p75 in Schwann cells does not result in large scale disruption of acylcarnitine metabolism.

To determine whether p75 deletion in Schwann cells results in sensory neuron loss through the production of toxic lipid species, we first assessed whether loss of p75 contributes to acylcarnitine dysregulation, as observed in Tfam deficient mice (Viader *et al.*, 2013). Total lipids were extracted from sciatic nerves harvested from adult $p75^{KO}$, wild type, Dhh-$p75^{\Delta}$ and Dhh-$p75^{C}$ mice. Then acylcarnitine species were quantified by liquid chromatography-mass spectrometry (LC-MS). We detected no differences in the distribution of acylcarnitine species between the four genotypes. Additionally, while there was a very mild, but significant increase in the total levels of acylcarnitines in $p75^{KO}$ mice relative to control, no such increase was observed in Dhh-$p75^{\Delta}$ mice, indicating the increase may not be due to reduction of Schwann cell p75 signaling (Fig. 15A,B).

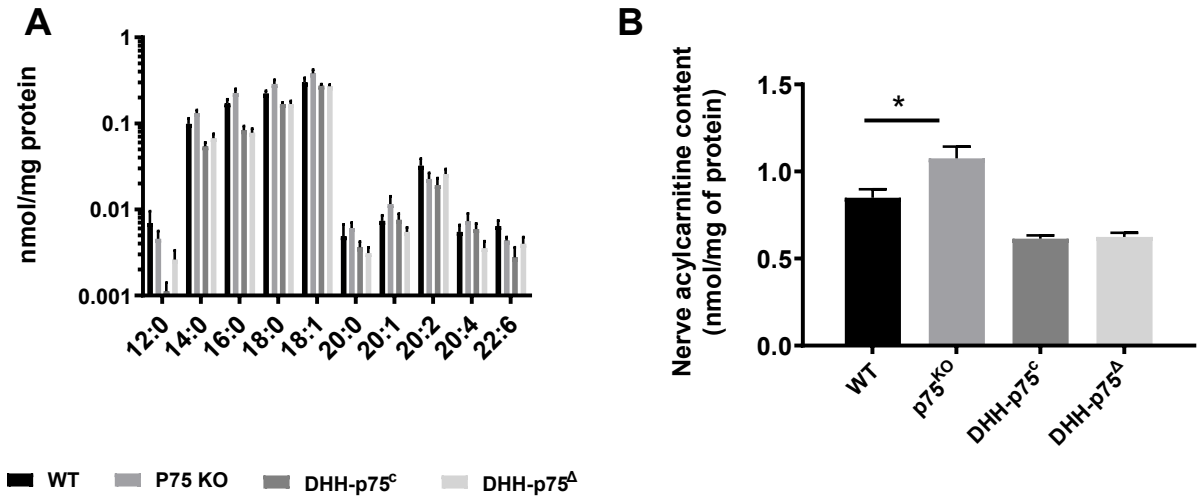

Figure 15. P75 deletion in Schwann cells does not alter acylcarnitine species levels. (A) LC-MS analysis showed no significant changes in the sciatic nerve acylcarnitine profile of $p75^{KO}$ or Dhh-$p75^{\Delta}$ mice relative to control at P25. (B) Total sciatic nerve acylcarnitine species were mildly increased in $p75^{KO}$ mice relative to control, but not in Dhh-$p75^{\Delta}$ nerves.

Loss of p75 in Schwann cells results in disrupted cholesterol biosynthesis and accumulation of 7-DHC

Previous studies have proposed that p75 also plays a role in cholesterol metabolism in several cell types(Dobrowsky *et al.*, 1994; Korade *et al.*, 2007; Pham *et al.*, 2016). Therefore, we analyzed cholesterol metabolites in sciatic nerves isolated from adult $p75^{KO}$, wild type, Dhh-$p75^{\Delta}$ and Dhh-$p75^{C}$ mice (Fig. 16). Intriguingly, although there was no significant change between genotypes in the absolute levels of cholesterol, or the cholesterol precursors desmosterol or lanosterol (Table 2), there was a significant increase in the ratio of 7-DHC to total cholesterol in both $p75^{KO}$ and Dhh-$p75^{\Delta}$ mice compared to respective controls (Fig. 17A). The accumulation of 7-DHC is noteworthy because this sterol is highly susceptible to free radical chain oxidation, producing a variety of oxysterols, including those that exert a toxic effect in Neuro2a cells and cortical neurons(Xu *et al.*, 2009, 2012b; Korade *et al.*, 2010) Additionally, accumulation of 7-DHC is associated with the neurodegenerative disease Smith-Lemli-Opitz Syndrome (SLOS) (Porter and Herman, 2011).

If the increase we see in 7-DHC relative to cholesterol indicates a production of toxic lipid species sufficient to affect DRG neurons, we should then detect an increase in its ratio around the time DRG neurons loss is observed in $p75^{KO}$ mice, that is, by postnatal day 6. This is also an age when Schwann cells are actively myelinating axons and lipid biosynthesis is highly up regulated. Indeed, the ratio of 7-DHC to cholesterol was nearly 3-fold higher at P6 relative to adult in wild type nerve (Fig. 17 A,B). Importantly, the 7-DHC to cholesterol ratio was substantially increased in the P6 $p75^{KO}$ mice compared to control, reaching 4-fold (Fig. 17B), a finding reflected in a significant enrichment of absolute levels of 7-DHC and 8-DHC in P6 myelinating nerves (Table 2). These results suggest that in the absence of p75 in Schwann cells cholesterol biosynthesis is disrupted and, specifically, biased towards 7-DHC accumulation over efficient conversion to cholesterol.

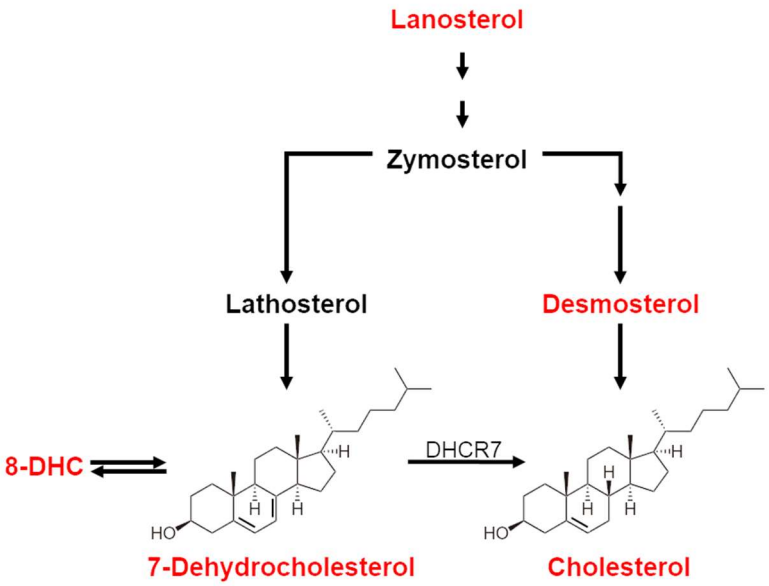

Figure 16. Simple schematic of late-stage cholesterol synthesis. The cholesterol precursor Zymosterol can be diverted into either the Kandutsch-Russell (Left) or Bloch (Right) pathways. 7-dehydrocholesterol reductase (7DHCR/DHCR7) catalyzes the terminal step of the Kandutsch-Russell pathway, the conversion of 7-dehydrocholesterol to cholesterol. Interrupted arrows represent the expulsion of intermediates. Intermediates profiled in this study are depicted in red.

to cholesterol ratio was substantially increased in the P6 $p75^{KO}$ mice compared to control, reaching 4-fold (Fig. 17B), a finding reflected in a significant enrichment of absolute levels of 7-DHC and 8-DHC in P6 myelinating nerves (Table 2). These results suggest that in the absence of p75 in Schwann cells cholesterol biosynthesis is disrupted and, specifically, biased towards 7-DHC accumulation over efficient conversion to cholesterol.

The analyses of cholesterol were performed using sciatic nerves, which contain axons and Schwann cells as well as various other cell types. Therefore, we repeated the same cholesterol measurements in isolated Schwann cell cultures. Mouse Schwann cells from wild type and $p75^{KO}$ mice were cultured for 7 days in the presence of delipidated serum to maximize cholesterol production. The newly synthesized sterols were then labeled with ^{13}C-glucose supplements for 9 additional days, and analyzed for sterols by LC-MS. While the amount of total ^{13}C-cholesterol was not significantly different between Schwann cells from the wild type and $p75^{KO}$ mice (Fig. 17C, Table 3), the amount of ^{13}C-7-DHC was significantly higher in $p75^{KO}$ Schwann cells compared to controls (Fig. 17D), as well as the ratio of 7-DHC to cholesterol, which was like that found in the P6 nerve (Fig. 17E). These results suggest that the increased 7-DHC to cholesterol ratio observed in $P75^{KO}$ and Dhh-$P75^{\Delta}$ sciatic nerve samples is mostly likely due to alterations specifically in Schwann cells.

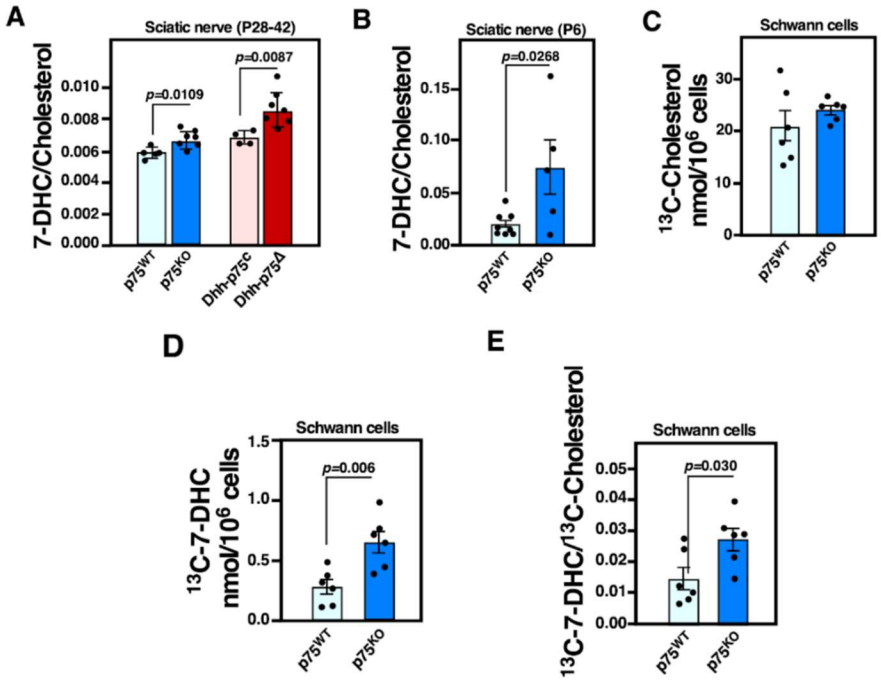

Figure 17. Deletion of p75 from Schwann cells results in elevated levels of 7-dehydrocholesterol (7-DHC), a reactive cholesterol precursor. (A) LC-MS/MS analysis of adult sciatic nerves from $P75^{KO}$ and Dhh-$p75^{\Delta}$ compared to their respective controls. (B) 7-DHC/Cholesterol ratios from P6 sciatic nerve from $P75^{WT}$ and $P75^{KO}$. (C) ^{13}C-cholesterol generated from mouse primary Schwann cultures from $P75^{KO}$ and $P75^{WT}$ mice at P3-6 and treated with ^{13}C-glucose in lipid depleted conditions. Lipid yield was normalized to total number cells from two independent experiments. (D) ^{13}C- 7-DHC levels from ^{13}C-glucose treated cells from $P75^{KO}$ mice compared to controls. (E) 7-DHC/Cholesterol ratio from ^{13}C-glucose treated $P75^{KO}$ and $P75^{WT}$ mouse Schwann cells.

7-DHC is toxic to DRG neurons but not to Schwann cells in culture

As previously detailed, the accumulation of 7-DHC has been heavily implicated in the neurodegeneration associated with Smith-Lemli-Opitz Syndrome (SLOS), which is caused by deficiency of 7-DHCR, an enzyme which reduces 7-DHC to cholesterol (Fig.16) (Porter and Herman, 2011). 7-DHC, and several 7-DHC oxysterol derivatives, are highly bioactive *in vitro* and in rodent models, affecting diverse pathways involved in membrane dynamics, oxidative stress, lipid metabolic regulation, proliferation, and apoptotic signaling. Thus, it has been suggested accumulation of 7-DHC, and 7-DHC derived oxysterols, may contribute to SLOS pathology through toxic gain-of-function mechanisms (Keller, Arnold and Fliesler, 2004; Korade *et al.*, 2010; Xu *et al.*, 2012a; Pfeffer *et al.*, 2016; Fliesler and Xu, 2018). Accordingly, 7-DHC derived oxysterols have been shown to be highly cytotoxic to both Neuro2a cells and cortical neurons, (Xu et al., 2012b).

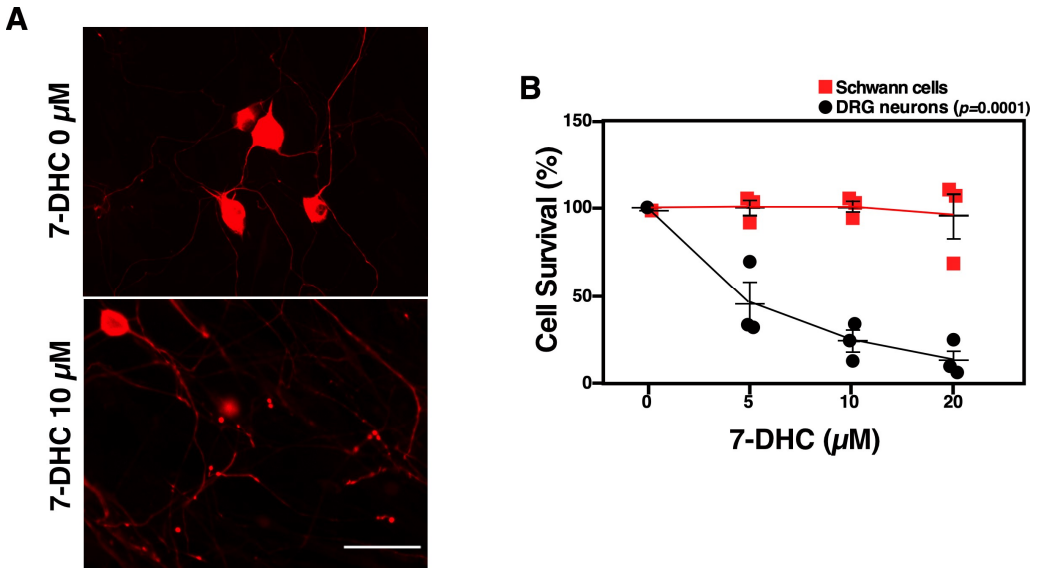

Figure 18. 7-dehydrocholesterol is toxic to sensory neurons, but not Schwann cells. (A) Primary rat DRG neurons or Schwann cells were treated with varied concentrations of 7-DHC for 72 hrs. Representative images of DRG neuron cultures stained for neurofilament. Scale bar, 50 μm (B) Quantification of DRG neurons and Schwann cells after 7-DHC treatment, $p<0.001$, one-way ANOVA, with Tukey's post hoc test.

However, while peripheral neuropathy has been noted in several patients with SLOS (Starck *et al.*, 2007; Ballout *et al.*, 2020), the effects 7-DHC on peripheral sensory neurons to our knowledge have never been examined. Therefore, we treated cultured rat DRG neurons were with 7-DHC and the number of live neurofilament^{+} neurons were quantified after 3 days. We found that 7-DHC was, indeed, toxic to DRG neurons, reducing the number of live neurons in a dose-dependent manner (Fig. 18A,B). It should be noted that DRG neurons appear to be quite sensitive to 7-DHC, which reduced the cell survival by 54% at 5 μM, a similar dose to the 1 μM 7-DHC oxysterol mixture that was required to reduce cell survival of cortical neurons by 60%. On the other hand, it required 50 μM of 7-DHC to reduce cell survival by 75% in Neuro2a cell lines (Korade *et al.*, 2010; Xu *et al.*, 2012b). Unlike DRG neurons, however, rat Schwann cells were completely resistant to 7-DHC, even at the highest dose of 20 μM (Fig. 18B). These results support the hypothesis that aberrant accumulation of 7-DHC, while not reducing Schwann cell viability, may lead to sensory neuron loss.

Increasing DHCR7 levels in p75 deficient Schwann cells during early postnatal nerve development reduces sensory neuron loss

To test the hypothesis that the reduction in 7-DHCR in Schwann cells is an underlying cause of the sensory neuron loss we noted in p75 deficient mice, we augmented 7-DHCR levels in p75^{KO} early postnatal nerves and assessed the effect on sensory neuron survival. We thus injected a lentivirus expressing V5-DHCR7 into the mouse sciatic nerves at P0, the onset of myelination in mice (Jessen, Mirsky and Lloyd, 2015) and quantified the number of DRG neurons at P5 . As published (Gonzalez *et al.*, 2014), the lentivirus infected Schwann cells in the nerve efficiently based on robust V5 tag expression (Fig. 19A) but not DRG neurons (Fig. 19B). When analyzed at P5, the number of DRG neurons were significantly increased, averaging ~35% more in lenti-DHCR7 injected p75^{KO} mice relative to those injected with a control lentivirus (Fig. 20 A, B). While not a complete rescue, these results indicate that increasing 7DHCR levels in p75 null Schwann cells is sufficient to significantly reduce the sensory neuron deficit observed in p75^{KO} mice.

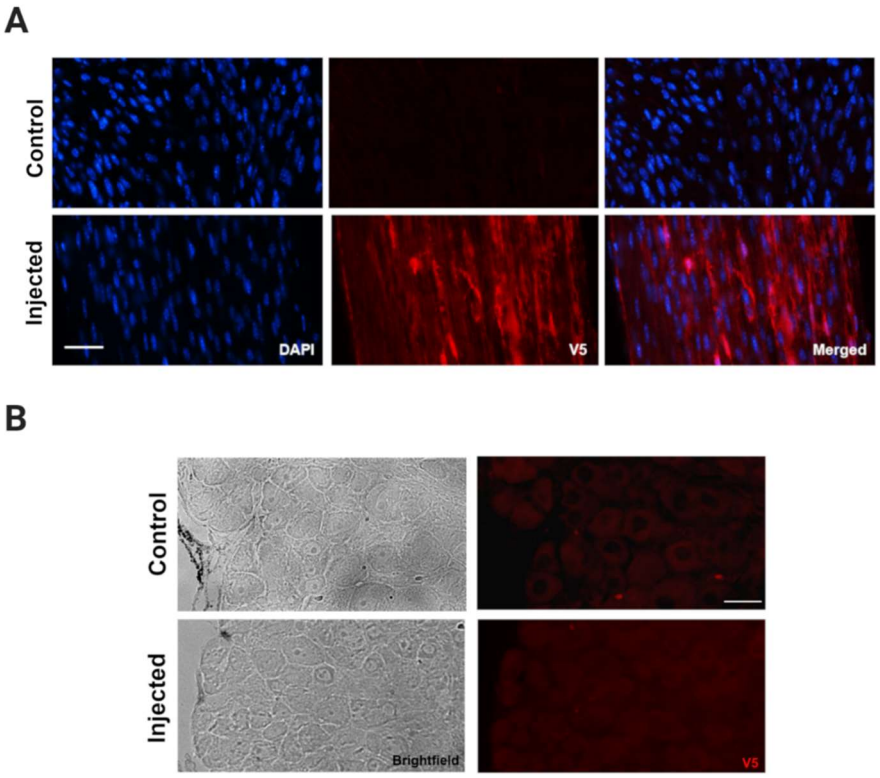

Figure 19. Injection of a DHCR7 expressing lentivirus into perinatal p75 deficient sciatic nerves results in Schwann cell, but not sensory neuron, infection. (A) Staining of injected and uninjected P5 sciatic nerves for the presence of a DHCR7 fused V5 epitope tag. Scale bar, 25μm. (B) V5 epitope tag staining was not observed in P5 DRGs harvested from control and injected $p75^{KO}$ mice. Scale bar, 25 μm.

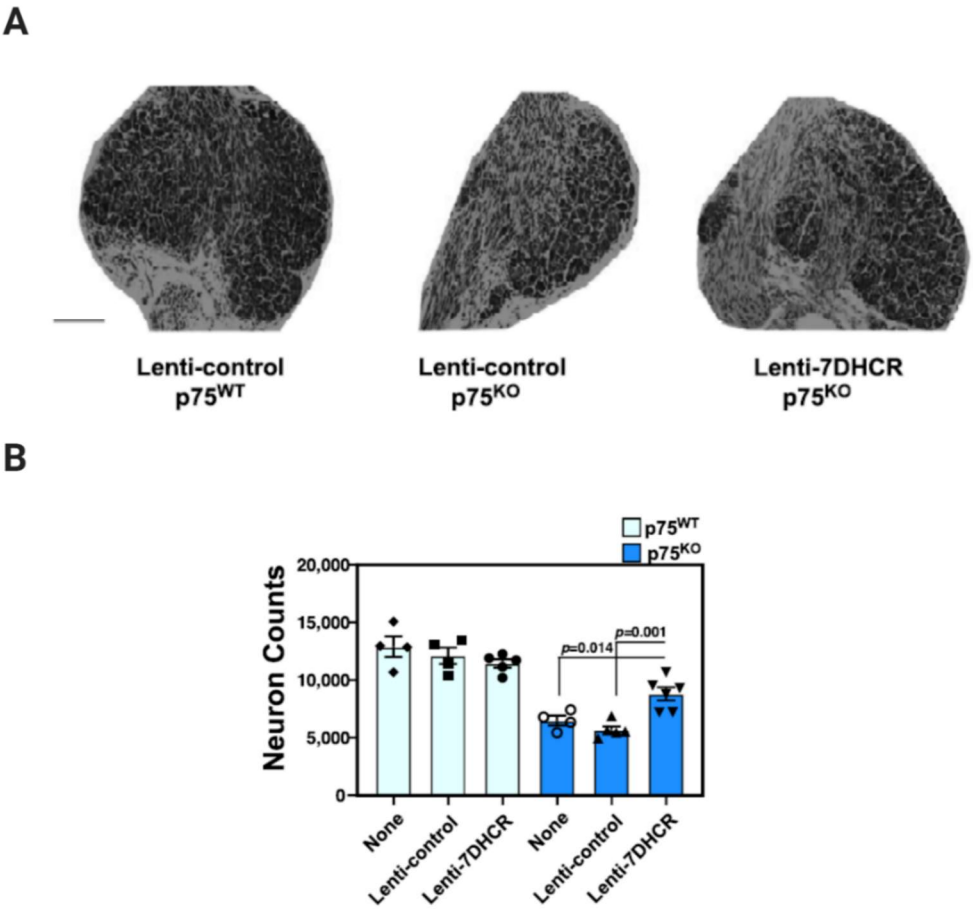

Figure 20. Increasing DHCR7 in p75 deficient Schwann cells during early postnatal nerve development rescues sensory neurons (A) Representative images of DRG sections harvested from injected and control mice. Scale bar, 100μm (B) Quantification of DRG neurons in wild type ($p75^{WT}$) or $p75^{KO}$ mice that were uninjected (Control), or injected at P0 with a lentivirus expressing V5-DHCR7 (Lenti-7DHCR), or injected with a lentivirus expressing only the V5 epitope (Lenti-Control) (p= 0.0010, one-way ANOVA, with Tukey's post hoc test) (N>3) .

	Lanosterol	Desmosterol	7- DHC	8-DHC	Cholesterol
P6 Sciatic Nerve					
WT (N=8)	0.40 ± 0.12	0.52 ± 0.19	1.2 ± 0.16	1.3 ± 0.23	74.48 ± 17.74
$P75^{KO}$ (N=5)	0.81 ± 0.21	0.61 ± 0.20	3.9 ± 1.5	2.2 ± 0.27	72.06 ± 20.04
P Value	0.09	0.74	****P<0.0001	*0.03	0.94
Adult Sciatic Nerve					
WT (N=5)	0.63 ± 0.046	0.74 ± 0.068	0.97 ± 0.10	1.1 ± 0.13	166.9 ± 19.04
$P75^{KO}$ (N=8)	0.62 ± 0.049	0.85 ± 0.18	1.6 ± 0.20	1.4 ± 0.19	217.7 ± 28.31
P Value	0.82	0.64	0.10	0.29	0.22
Adult Sciatic Nerve					
Dhh-$P75^{c}$ (N=4)	0.35 ± 0.049	0.46 ± 0.052	0.78 ± 0.064	0.80 ± 0.095	113.9 ± 10.19
Dhh-$P75^{\Delta}$ (N=7)	0.41 ± 0.014	0.59± 0.052	0.89 ± 0.065	0.87 ± 0.070	103 ± 5.633
P Value	0.17	0.16	0.32	0.56	0.33

Table 2. Quantification (nmol/mg protein) of cholesterol and cholesterol precursor levels. Sterol levels in the sciatic nerves of $P75^{KO}$ and Dhh-$p75^{\Delta}$ mice compared to their respective controls, $P75^{WT}$ and Dhh-$p75^{C}$, using LC-MS/MS analysis. Levels are displayed as mean +/- SEM. One-way student's t-test was used to determine significance.

	C13-Desmosterol	C13-7-DHC	C13-Cholesterol
WT (N=6)	13.6 ± 0.896	0.28 ± 0.057	21.1 ± 2.95
$P75^{KO}$ (N=6)	18.1 ± 2.17	0.67 ± 0.089	24.1 ± 0.856
P Value	0.07	**0.006	0.34

Table 3. 7-DHC production is elevated in p75 null Schwann cells. Levels (nmol/total cell) of ^{13}C-Desmosterol, ^{13}C-7-DHC, and ^{13}C-cholesterol generated by cultured mouse primary Schwann cells harvested from $P75^{KO}$ and $p75^{WT}$ mice at P3-6. Lipid yield was normalized to total cells in culture, N=6 from two experiments. Levels are displayed as mean +/- SEM. One-way student's t-test was used to determine significance.

Discussion

Our findings support the hypothesis that Schwann cells lacking p75 have altered lipid metabolic regulation. While we did not find large scale alterations in Schwann cell acylcarnitine levels, we did find pronounced alterations in cholesterol biosynthesis. Specifically, we found that the conversion of 7-DHC to cholesterol was compromised, resulting in the accumulation of 7-DHC both in $p75^{KO}$ and Dhh-$p75^{\Delta}$ sciatic nerves and isolated p75 deficient Schwann cells.

Additionally, the timeline of the 7-DHC/cholesterol imbalance does agree with myelin formation being the primary window of 7-DHC accumulation in nerves. We noted a higher ratio of 7-DHC/cholesterol in the first week of life, while adult mice had much reduced but still significantly elevated ratios of 7-DHC/cholesterol. This finding is very consistent with data from a compound heterozygote mouse model of SLOS. Compound heterozygous mice carry one allele expressing a knock in amino acid substitution of methionine for threonine (T93M), mimicking a mutation found in human patients, and a second alle expressing a null mutation of the *dhcr7* gene. In these mice, the ratio of 7-DHC/cholesterol was highly elevated in the brain at post-natal day 1 and increased

through early developmental time points but was reduced to much lower levels in adult mice around 1 month of age, a reduction that continued throughout adulthood. Therefore, as in our $p75^{KO}$ and Dhh-$p75^{\Delta}$ models, the youngest animals had the most severe imbalance with the ratio of 7-DHC/cholesterol tending to normalize over time (Marcos *et al.*, 2007).

One explanation for this is temporal variation could be the elevated cholesterol biosynthesis occurring during myelination in the nervous system, combined with the much greater stability of cholesterol over time relative to 7-DHC. While myelination in the brain does not exactly follow the timeline of PNS myelination, both begin perinatally and extend into early adulthood. Thus, cholesterol concentrations, and cholesterol intermediate levels, increase the most within the first four weeks of life in the brain, as well as the peripheral nerve (Czuba *et al.*, 2017). However, once generated, cholesterol is very stable in myelin membranes, with an estimated half-life of over 5 years in the CNS(Björkhem, et al. 1998). Although, it should be noted that the half-life of cholesterol in PNS myelin membranes has not been well established. PNS nerves have a marked reduction in SREBP2 (a key regulator of cholesterol biosynthesis) expression after P10, implying much lower cholesterol production after initial myelination (de Moraes, Kushmerick and Naves, 2017). In contrast, 7-DHC is highly reactive, more than 200 times as reactive to radical chain oxidation as cholesterol, prompting rapid conversion into of a variety of oxysterol derivatives in cells and tissues (Xu, Davis and Porter, 2009). Thus, 7-DHC/Cholesterol ratios could normalize over time due to the combined effects of 7-DHC decline from oxidation and reduced 7-DHC production after myelination is complete.

Also, consistent with the SLOS model, we found total cholesterol levels were not unduly affected in mice, or cultured Schwann cells. Cholesterol levels in compound heterozygous SLOS mice are reduced in embryonic and early adulthood but reach normal levels by 8 months. Whereas we did not find cholesterol levels were significantly reduced in either our mouse models, or p75 null cultured Schwann cells. This is somewhat puzzling in $p75^{KO}$ mice, which are expected to retain a hypomyelination phenotype, and even in consideration of the mild hypomyelination we noted early in Dhh-$p75^{\Delta}$ development(Cosgaya, Chan and Shooter, 2002). Further examination of the

composition of $p75^{KO}$ membranes may determine if there are other alterations in membrane composition to explain the divergence.

There are several plausible explanations for the lack of significant change in total cholesterol levels. One is that cholesterol synthesis continues, regardless of intermediate accumulation, until a sufficient cholesterol threshold for myelin is met within the cell. Another possibility is that, while exogenous cholesterol influx is not generally required for PNS myelination, there could be compensation measures to achieve sufficient exogenous cholesterol influx when synthesis is disrupted (de Moraes, Kushmerick and Naves, 2017). Interestingly, this metabolic switch might be mediated by 7-DHC accumulation itself, as 7-DHC and other oxysterols have been shown to inhibit the activity of HMG-CoA reductase, a rate limiting step of early cholesterol synthesis(Honda *et al.*, 1998). However, one point of evidence against this that we do not see any changes in cholesterol production within C-13 glucose treated Schwann cells cultured in sterol depleted conditions. Although their requirements for membrane cholesterol are likely much less than a myelinating Schwann cell, perhaps avoiding the threshold required for feedback inhibition of aberrant sterol synthesis.

Our results also indicate that 7-DHC is cytotoxic to DRG neurons. Additionally, we noted a striking lack of death in 7-DHC treated cultured Schwann cells compared to DRG neurons. This suggests Schwann cells are largely able mitigate the cytotoxic effects of 7-DHC. This resistance may be due to more robust antioxidant expression in Schwann cells, which due to their high sterol and lipid formation during myelination, require relatively high levels of compensatory mechanisms for the management of reactive species. For example, Schwann cells have been shown to have very high basal expression of nuclear factor eythroid 2 (NFE2)-related factor 2 (Nrf2), especially relative to DRG neurons. Nrf2 is a transcription factor which regulates a host of target genes instrumental in maintaining redox homeostasis, called antioxidant response elements (AREs) (Vincent, Kato, *et al.*, 2009; Lv *et al.*, 2018; Raghunath *et al.*, 2018). Additionally, when challenged by prooxidant treatments, such as H_20_2 or tert-butylhydroquinone, Schwann cells demonstrate both much faster and more robust Nrf2 upregulation than

observed DRG neurons, ultimately demonstrating much higher capacity to withstand prooxidant insult (Vincent, Kato, *et al.*, 2009).

Further evidence that 7-DHC accumulation is a causative element of neuronal loss after p75 deletion in Schwann cells is that increasing 7DHCR levels was sufficient to significantly decrease neuron loss in $p75^{KO}$ mice. That the rescue was not complete is likely due to incomplete infection of Schwann cells within the sciatic nerve, or the presence of other primary, or secondary pathological mechanisms.

Taken together our data suggests that deficiency of p75 in Schwann cells results in altered cholesterol metabolism, biasing it towards the generation of 7-DHC, resulting in the aberrant accumulation of 7-DHC in nerve tissue. Additionally, 7-DHC is toxic to peripheral sensory neurons and the reduction *dhcr7* expression, likely leading to 7-DHC accumulation, is a causative factor in the observed DRG neuron loss in mice lacking p75.

Chapter IV

P75 Regulates SC Cholesterol Biosynthesis in Coordination with the ErbB2 Receptor

Introduction

As previously outlined in chapter 1, surprisingly little is known about the regulation of cholesterol metabolism during myelination. However, one of the major factors governing lipid synthesis in myelinating Schwann cells is neuregulin signaling. During development, sensory axons express a transmembrane neuregulin family isoform, neuregulin 1 type III (NRG1/III), which serves as a ligand for the Schwann cell ErbB2/ErbB3 co-receptors. The level of NRG1/III expressed on axons, and thus amount of neuregulin signaling, dictate both the fate (myelinated or Remak bundle associated) of axons and the thickness of the myelin produced by myelinating Schwann cells (Michailov *et al.*, 2004; Taveggia *et al.*, 2005). Accordingly, neuregulin signaling, through ErbB2/ErbB3, has been tied to the metabolic regulation of both lipid metabolic factors such as HMG-CoA reductase, an early rate limiting enzyme of cholesterol biosynthesis, and numerous myelin proteins (Pertusa *et al.*, 2007b; Stassart *et al.*, 2013).

As p75 is known to interact with several partner receptors, and our previous data suggests p75 in Schwann cells regulates cholesterol metabolism, we hypothesized that p75 may regulate lipid synthesis in cooperation with neuregulin signaling during development (Chao, 2003). Surprisingly, we found that p75 signaling was collaborative with ErbB2, but not its customary co-receptor ErbB3, or neuregulin. Instead p75 and ErbB2, in response to the neurotrophin BDNF, prompted activation and increased expression of SREBP2, a transcription factor controlling expression levels of several enzymes involved in cholesterol and fatty acid metabolism, including 7-DHCR (Prabhu, Sharpe and Brown, 2014). Thus, loss of p75 results in downregulation of SREBP2 and lowered expression of *dhcr7*, leading to the previously noted accumulation of 7-DHC in $p75^{KO}$ and Dhh-$p75^{\Delta}$ nerves.

Methods

Injection of TrkB-Fc and IgG-Fc into Neonate Mice

TrkB-Fc and IgG-Fc were obtained from R&D Systems. Injection of Fc proteins into P0 mice sciatic nerves were performed as described (Tep *et al.*, 2012). Briefly, 3 ul of Fc solutions (1 µg/µl) was injected using 31G insulin syringe over the sciatic nerve midway between the knee and hip through the skin. Five days after the injection, sciatic nerves were isolated for protein extraction.

Western Blotting

Western blotting was performed as described by (Harrington, Kim and Yoon, 2002).

RNAi

The oligonucleotides containing the shRNA of the individual RNAi sequences were placed into pSIREN-RetroQ-ZsGreen1 vector (Clontech) using Bam HI and Xba I sites as directed by the vendor. Retroviruses were generated following transient transfection of the shRNA constructs in PlatE cells (Cell Biolabs) and the viral supernatants were concentrated by centrifugation at 20,000 rpm for 4 hrs at 15^{o}C using SW28 rotor (Beckman). The viral pellet was resuspended in small volume of media and frozen at 80^{o}C until use. For infection of Schwann cells in vitro and in vivo, a combined mixture of three different RNAi viruses were used for efficient knockdown.

Preparation of neuregulin 1 type III

Neuregulin 1 type III cDNA was transfected into 293T cells and the membranes were prepared according to (Taveggia *et al.*, 2005), and the membranes were added onto Schwann cell monolayers as described (Maurel and Salzer, 2000; Taveggia *et al.*, 2005) As a control, the membranes from untransfected 293T cells were prepared in parallel. To

add the membranes to Schwann cells, 8 μg of membrane preparations was placed onto the cells and spun for 3 min at 3000 rpm.

Gene Expression Analysis

Primary mouse Schwann cells were lysed after 7 days in culture with 400μl Trizol (Invitrogen Cat#15596026) and incubated for 5 min at room temperature (RT). 100μl Chloroform (Sigma-Aldrich Cat#270636) was added and samples were incubated for 2 min RT after mixing. The solution was spun down for 12000 x g for 15min (Sorvall-ST 16R) and the supernatant was transferred to a new tube with equal volume of 70% ETOH (Sigma-Aldrich). Total RNA was then isolated with the RNeasy Mini Kit (Qiagen Cat# 74104) with Qiagen DNase I following manufacturer's directions. To determine mRNA levels, 10μl of the total RNA collected was reverse transcribed using the High-Capacity cDNA Reverse Transcription Kit (Thermo Fischer Cat#4368814) following the manufacturer's directions. The mRNA levels of *dhcr7* and the control *Gapdh* were assessed using TaqMan (IDT) probes, assay numbers Mm00514571_m1 and Mm99999915_g1, respectively, in conjunction with Taqman Fast Advanced Master Mix (Invitrogen Cat#4444556) and the Biorad CFX96 apparatus according to the manufacturer's protocols.

Quantification and Statistical Analysis

Quantitative data are presented as mean ± SEM. All experiments were independently repeated and evaluated at least 3 times by a blinded individual. Prism 6/7 (GraphPad Software http://www.graphpad.com/scientific-software/prism/) was used to determine statistical significance between groups using one-way analysis of variance (ANOVA) with Tukey's post hoc test (for experiments with more than 2 groups), or Student's t-test.

Results

BDNF regulates SREBP2 via recruiting ErbB2 to the p75 signaling pathway

To determine if p75 influences neuregulin signaling during development, we first sought to ascertain if neuregulin signaling was altered in nerves lacking p75. We found that while at P5-P7 phospho-ErbB2 (activated) levels were unchanged in Thy1-p75$^{\Delta}$ sciatic nerves compared to control, they were significantly reduced in Dhh-p75$^{\Delta}$ (Fig. 21 A, B). This suggests there could be cooperative signaling between p75 and ErbB2 in Schwann cells.

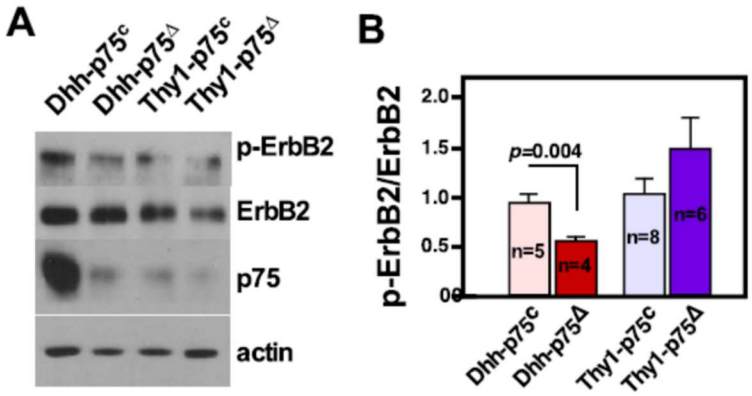

Figure 21. ErbB2 signaling is altered by the absence of Schwann cell derived p75. (A) ErbB2 tyrosine phosphorylation in P5-7 sciatic nerves was reduced in Dhh-p75$^{\Delta}$ compared to the control Dhh-p75^{C} mice. (B) Quantification of ErbB2 activation in P5-7 sciatic nerves.

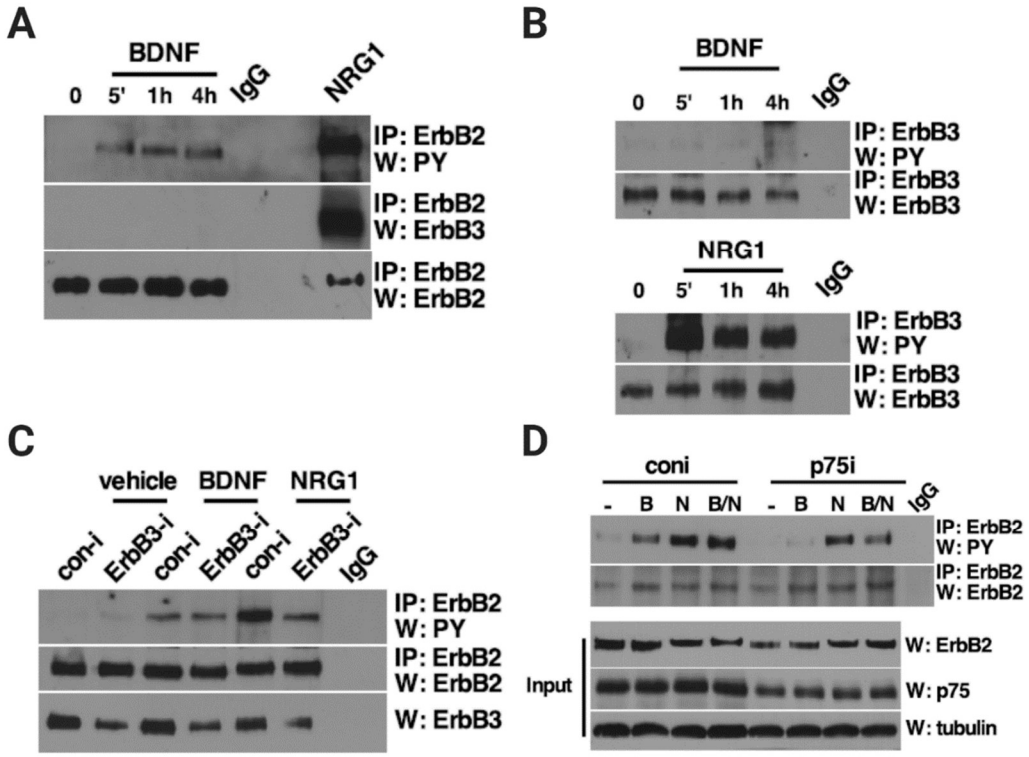

Figure 22. ErbB2, but not ErbB3, is recruited to p75 signaling pathway upon BDNF binding. A) BDNF induced tyrosine phosphorylation of ErbB2 in Schwann cells. ErbB2 was immunoprecipitated and blotted with phosphotyrosine antibodies. As a positive control, the lysates from Schwann cells that had been treated with NRG1 were subjected to the same immunoprecipitation. The blot was re-probed for ErbB2 and ErbB3. (B) BDNF did not activate ErbB3, while neuregulin did in Schwann cells. ErbB3 was immunoprecipitated and blotted with phosphotyrosine antibodies. The blot was re-probed for ErbB3. (C) Knock-down of ErbB3 inhibited ErbB2 activation by NRG1, but not by BDNF. ErbB2 was immunoprecipitated and blotted with phosphotyrosine antibodies. The blot was re-probed for ErbB2. The extent of ErbB3 knock down is shown in ErbB3 blot. (D) Knock-down of p75 in Schwann cells inhibited ErbB2 activation by BDNF, and BDNF with NRG1, but not by NRG1 alone. The extent of p75 knock down is shown in p75 blot. B, BDNF; N, neuregulin.

BDNF is released by sensory axons and has been shown to promote peripheral myelination during development and repair (Cosgaya, Chan and Shooter, 2002; Ng *et al.*, 2007) . Therefore, it is likely an endogenous ligand of Schwann cell p75 during myelination, especially as Schwann cells do not express the full length form of BDNF's alternate neurotrophin receptor, TrkB. (Funakoshi *et al.*, 1993). Therefore, we hypothesized that BDNF may be involved in p75-ErB2 signaling. Indeed, BDNF addition

to Schwann cells resulted in tyrosine phosphorylation, or activation, of ErbB2, albeit to a lesser extent than neuregulin (Fig. 22 A).

The ErbB2 receptor kinase does not interact with neuregulin directly, due to ErbB2 lacking an extracellular ligand binding domain. Instead ErbB2 forms a heterodimeric association with ErbB3, a receptor lacking an active kinase domain, after ErbB3 undergoes conformation change upon neuregulin binding (Citri, Skaria and Yarden, 2003; Ledonne and Mercuri, 2020). Surprisingly, ErbB3 was not associated with activated ErbB2 after treatment with BDNF, as shown by immunoprecipitation (Fig. 22 A). We thus asked whether ErbB3 is tyrosine phosphorylated by activated ErbB2 after BDNF treatment, as occurs after neuregulin binding prompts ErbB2 recruitment to ErbB3 (Ledonne and Mercuri, 2020). While neuregulin induced robust tyrosine phosphorylation of ErbB3, BDNF failed to do so in Schwann cells (Fig. 22 B). Similarly, knockdown of ErbB3 was effective in inhibiting tyrosine phosphorylation of ErbB2 by neuregulin, but not by BDNF (Fig. 22 C). In contrast, knockdown of p75 prevented ErbB2 phosphorylation in response to BDNF but not neuregulin (Fig.22 D). These results together suggest that BDNF binding to p75 leads to activation of ErbB2, independent of ErbB3 in Schwann cells.

P75 regulates cholesterol biosynthesis through activation of Sterol Regulatory Element Binding Protein 2 (SREBP2) in response to BDNF

In considering how BDNF provoked ErbB2-p75 signaling might be tied to cholesterol metabolism, one candidate we speculated could be involved was the transcription factor SREBP2. SREBP2 is a master regulator of the expression levels of many enzymes involved in cholesterol and fatty acid metabolism, including HMG-CoA reductase and 7-DHCR (Brown and Goldstein, 1997). Normally, SREBP2 is retained in the endoplasmic reticulum of cells; however, when sterol levels are low inside the cell, it is transported to the Golgi where it undergoes proteolytic cleavage followed by translocation to the nucleus (Horton, Goldstein and Brown, 2002). We thus hypothesized that p75-ErbB2 activates SREBP2. To test whether BDNF promotes SREBP2 activation, we treated Schwann cells for various times and measure the accumulation of the cleaved

product. Indeed, we saw increasing levels of activated SREBP2 with a peak at about 8 hours (Fig. 23 A, B). To determine if ErbB2 signaling is involved in the activation of SREBP2, we treated Schwann cells with BDNF in the presence of 10 μM PKI-166, an ErbB2/EGF receptor-specific inhibitor (Mellinghoff *et al.*, 2004; Tapinos, Ohnishi and Rambukkana, 2006). PKI-166 inhibited the increase in SREBP2 cleaved products (Fig. 23 A, B). Since the EGF receptor is not expressed in Schwann cells (DeClue *et al.*, 2000), the major target of PKI-166 is ErbB2 in these cells, indicating that BDNF induced SERBP2 cleavage is reliant on ErbB2, as well as p75, in Schwann cells.

Additionally, we found that SREBP2 activation is altered in Dhh-p75$^{\Delta}$ mice compared to controls at P5. Both the levels of SREBP2 precursor and active cleaved products were significantly reduced in Dhh-p75$^{\Delta}$ nerves, compared to those of control Dhh-p75^{C} mice (Fig. 23 C, D). To further explore whether BDNF may be contributing to SREBP2 activation *in vivo*, we injected the sciatic nerve of P2 rat pups with TrkB-Fc, which prevents it from signaling through p75 via scavenging endogenous BDNF. There was a significant reduction in activated SREBP2 in the animals injected with TrkB-Fc, relative to control pups that were injected with IgG-Fc (Fig. 23 E, F). These data indicate that p75 regulates cholesterol metabolism in developing Schwann cells through modulation of SREBP2 levels and activation.

During cholesterol biosynthesis, 7-DHC is converted to cholesterol by 7-dehydrocholesterol reductase, 7-DHCR (Fig. 16). Thus, 7-DHC accumulation could occurs either from altered 7-DHCR function, as seen in Smith-Lemli-Opitz Syndrome pathology, or aberrant downregulation (Porter and Herman, 2011). It was previously reported that p75 knockdown resulted in a transcriptional reduction of *dhcr7* in Neuro2a cells (Korade *et al.*, 2007). Similarly, we found that *dhcr7* transcript levels were significantly reduced in p75^{KO} Schwann cells relative to the wild type (Fig. 23 G). This result suggests that reduced p75 signaling in Schwann cells decreases transcription of the gene encoding 7-DHCR, likely through altered SREBP2 regulation, cueing the aberrant accumulation of its substrate, 7-DHC, in nerves.

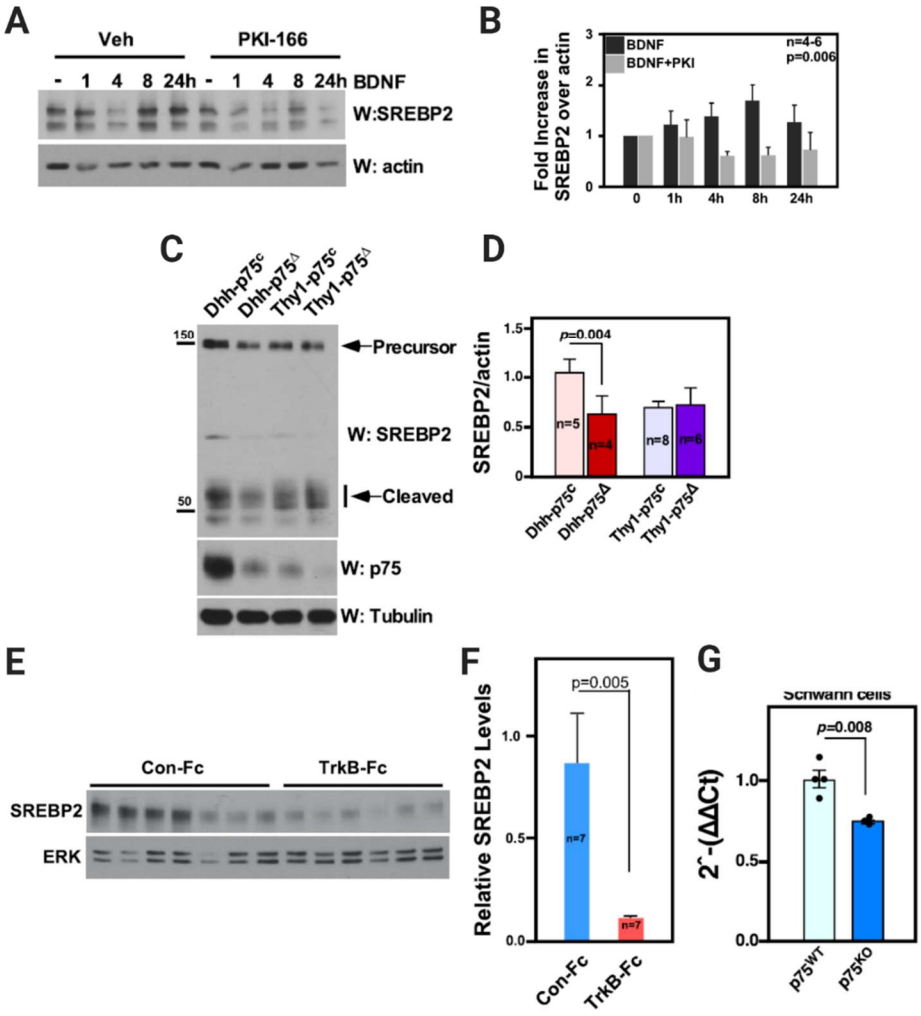

Figure 23. Loss of BDNF-p75 signaling in Schwann cells reduces *dhcr7* expression and SREBP2 activation. (A) BDNF treatment of Schwann cells resulted in the accumulation of activated SREBP2. ErbB2 activity was required for SREBP2 activation by BDNF in Schwann cells. PKI-166 at 10 μM inhibited the increase in SREBP2 cleaved products, while the vehicle (DMSO) did not. (B) Quantification of SREBP2 over actin controls. For statistics, one-way ANOVA was used. (C) Representative western blot of SREBP2 precursor and active cleaved product levels from Dhh-p75Δ, Thy1-p75Δ and respective control sciatic nerves. (D) Quantification of SREBP2 over tubulin control (student t-test). (E) Competitive binding of BDNF by TrkB-Fc injected into the sciatic nerve reduced SREBP2 expression levels. (F) Quantification of SREBP2 protein levels in. (G) qPCR analysis of *dhcr7* mRNA levels in primary mouse Schwann cells from P75WT and P75KO mice at P3-6.

Discussion

Our study details a novel pathway whereby BDNF modulates cholesterol biosynthesis through cooperative signaling of Schwann cell expressed p75 and ErbB2 receptors. Interestingly, BDNF null mice exhibit a 34% reduction in L4 DRG neurons at P15, as well as CNS deficits, but like $p75^{KO}$ mice, have no deficit of motor neurons(Jones *et al.*, 1994b). This is in contrast to TrkB knockout mice, which exhibit extensive motor neuron disruption as well as sensory loss, resulting in death by P1 (Klein *et al.*, 1993). Together this suggests that BDNF may influence sensory neuron survival, but not motor neuron survival, in part, through Schwann cell p75 signaling during development.

Additionally, we found that p75 regulates cholesterol biosynthesis through ErbB2-dependent regulation of SREBP2 in response to BDNF. While, to our knowledge, SREBP2 has never been directly connected to BDNF signaling, p75 has previously been shown to regulate SREBP2 cleavage in response to Nerve Growth Factor (NGF) in hepatocytes (Pham *et al.*, 2016). More surprising is the exclusion of ErbB3 and neuregulin from this pathway, due to their acknowledged roles as master regulators of myelin programing.

What then would be the purpose of BDNF-dependent activation of ErbB2 and SREBP2, independent of neuregulin/ErbB3 in Schwann cells during development? One possibility is that it allows for more temporally responsive or narrowly focused regulation cholesterol synthesis. This additive regulation could refine the broad developmental regulation of neuregulin. Neuregulin is instrumental to Schwann cells starting in SCPs and persisting into adulthood, while SREBP2 expression increases perinatally and peaks from P4-P10 in nerves before decreasing to low levels in adulthood (Verheijen *et al.*, 2003). Independent p75 signaling, which diminishes as myelinating Schwann cells mature, could assist in boosting SREBP2 expression/activity during peak preparation for myelination. Additionally, if Schwann cells, like astrocytes in the CNS, do supplement neuron sterol production, sensory neurons secreting BDNF could prompt a localized upregulation of sterol regulation in surrounding Schwann cells, without depending on neuregulin1 type III signaling, which requires direct cell-cell contact.

We also observed that the loss p75 affects *dhcr7* expression. SREBP2 is thought to bind to 2 SRE sites on the murine *dhcr7* promoter, which are conserved in humans(Prabhu, Sharpe and Brown, 2014). Therefore, that we observe modulation of *dchr7* expression coupled with decrease in expression/activity SREBP2 is not unexpected. However, why cholesterol biosynthesis is not more imbalanced by the reduction in SREBP2 expression/activation remains in question. It is possible that other factors affecting the regulation of cholesterol synthesis enzymes can compensate, in part, for the loss of p75 signaling.

These results suggest that altered p75 signaling in Schwann cells, affects transcriptional regulation of the gene encoding 7DHCR, likely through altered SREBP2 regulation.

Chapter V

Deletion of P75 Results in Significantly Altered Nerve Lipid Profiles

Introduction

As reviewed in Chapter 1, even small, localized alterations in lipid metabolism do not often remain isolated to one lipid pathway. Due to the complex diversity of lipid roles, the reactive nature of many lipid intermediates, and interdependent lipid biogenesis, small changes in lipid dynamics can lead to more large scale alterations in lipid homeostasis (Tracey *et al.*, 2018). For instance, SREBP2 does not only modulate cholesterol biosynthesis, but is also involved to some extent in regulating fatty acid biogenesis, raising the possibility that altered SREBP2 expression and activity could affect more than sterol biogenesis in p75 null Schwann cells (Camargo, Smit and Verheijen, 2009). Additionally, 7-DHC and its oxidative derivatives can initiate and propagate reactive oxygen stress, which leads to alterations in lipid metabolism from lipid peroxidation and altered organelle function.

Therefore, we hypothesized that deletion of p75 could result in wide-spread alterations in nerve lipid metabolism. We thus conducted a global, untargeted ultra-performance liquid chromatography coupled to mass spectrometry (UPLC-MS/MS)-based analysis to interrogate the lipid profiles of sciatic nerves from post-natal day 6 $p75^{KO}$ and wild type mice. Interestingly, we found substantial alterations in $p75^{KO}$ nerve lipid profiles, with the abundance of hundreds of lipid components significantly altered compared to wild type controls. The altered lipids were primarily composed of membrane glycerophospholipid, ceramide, and triacylglycerol/diacylglycerol species, suggesting that p75 deficiency results in dysfunctional regulation of several key lipid metabolic pathways in peripheral nerves.

Methods

Sample preparation

Sciatic nerves were extracted at post-natal day 6 from $p75^{KO}$ and WT mice and immediately frozen on dry ice. Due to the small size of the tissues, 3 sciatic nerve pairs extracted from same genotype littermates were pooled to constitute one N, for a total of 5 Ns per genotype. Sample were suspended in 300µL ice cold lysis buffer (1:1:2 MeOH: AcCN: Ambic buffer) and twice sonicated for 10 pulses at 50% power, on ice. Protein levels were quantified by BCA assay, and normalized to 100µg total protein. Lipid metabolites were extracted through liquid-liquid extraction by MTBE following a MeOH:H_20 80:20 protein precipitation.

UPLC-MS/MS analysis

Mass Spectrometry-UPLC-MS/MS analysis and initial data analysis was performed by the Vanderbilt Center for Innovative Technology as described in Gibson et al. (2018)(Gibson *et al.*, 2018). Briefly, lipid extracts were reconstituted in acetonitrile/water (80 : 20, v/v). Quality control (QC) samples were prepared by pooling equal volumes from each experimental sample and compared to Quality Control Reference Material to verify instrument performance and reproducibility. MS analyses were performed on Agilent 6450 QTOF mass spectrometer equipped with reverse phase lipid chromatography, which was preformed over a 30 min gradient using solvent A: 100 H20, 10mM AF, 0.1% FA and Solvent B 60:36:4 IPA/SCN/H20 with 10mM AF, 0.1% FA. Full MS analyses were acquired under an ESI positive profile mode and separately under an ESI negative profile mode.

Data analysis-UPLC-MS/MS raw data was processed and reviewed using Pyogenesis Q1 2.0 (Non-linear Dynamics, Newcastle, UK) as in Gibson et al. (2018). A one-way analysis of variance (ANOVA) test was to assess significance between WT and KO

groups for each lipid species (retention time_m/z descriptor) P-value ≤0.05 taken as significant, fold change was also calculated. Additionally, a principal components analysis was conducted determine ensure genotype dependent clustering was present. Pyogenesis and MetaboloAnalyst 4.0, and the LipidMatch and LipidAnnotator databases were utilized to assign punitive structural annotations/ candidate IDs for species. IDs, where available, were ranked according to level of confidence from Level 2, most confidant, to Level 3 a-b. Only candidates with Level 2 or 3a were further analyzed. To further examine pathway level alterations, compounds were then manually sorted into broader metabolic categories according to class structure and function.

Results

P75 null sciatic nerves display altered lipid composition

To determine if lipid profiles were altered in $p75^{KO}$ nerves during myelination, sciatic nerves were harvested from $p75^{KO}$ and wild type (WT) mice at P6, a time point when Schwann cells are very actively myelinating axons. Nerve extracts were subjected to a global, untargeted UPLC-MS/MS lipid analysis. Because many membrane and metabolic lipids are polarized, reverse-phase lipid chromatography-MS was used, and samples were run in both a positive and negative ionization mode to maximize compound detection. A one-way ANOVA was used to determine genotype dependent variation in abundance, with a p-value of ≤0.05 set as the threshold of significance. In the positive mode a total of 3583 distinct lipid compounds were detected, with 791 (329 with positive fold change, 462 negative fold change) compounds featuring significantly altered abundance compared to WT. (Fig. 24 A). In the negative mode 3714 total compounds were detected, with 549 (237 with positive fold change, 312 with negative fold change) compounds significantly altered in abundance compared to WT (Fig.24 B).

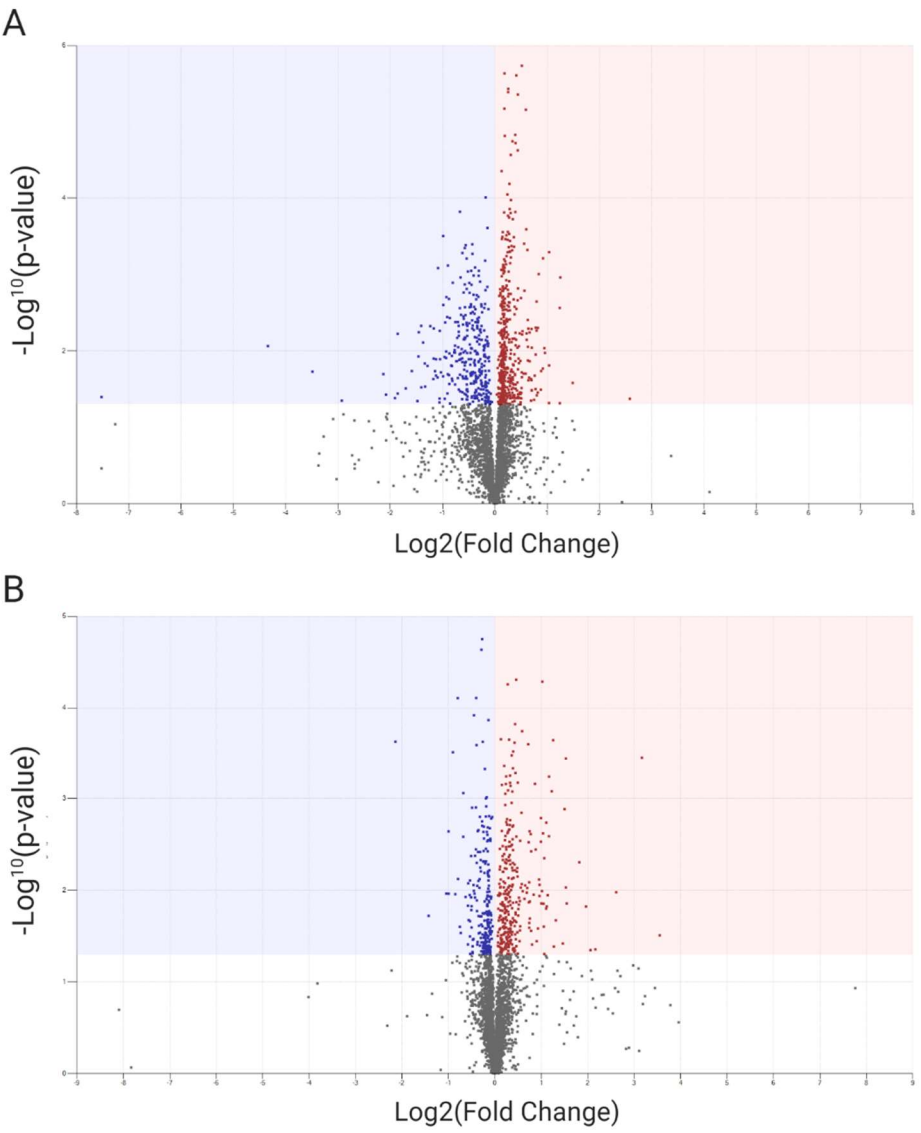

Figure 24. P75 deficient sciatic nerves from P6 mice have markedly altered lipid profiles relative to wild type. (A) Volcano plot showing the distribution of lipid compounds detected the positive mode. A pairwise comparison based on significance criteria for p-value. P-values were generated by ANOVA, with a threshold of significance set at P-value ≤0.5, threshold indicated by blue (negative fold change) red (positive fold change) rectangles with individual compounds represented by dots. A total of 3583 compounds were detected (329 increased in fold change, 462 decreased in fold change). (B) Volcano plot showing the distribution of lipid compounds detected in the negative mode. A pairwise comparison based on significance criteria for p-value. P-values were generated by ANOVA, with a threshold of significance set at P-value ≤0.5, threshold indicated by blue (negative fold change) red (positive fold change) rectangles with individual compounds represented by dots. A total of 3714 compounds were detected (237 increased in fold change), 312 (decreased in fold change).

P75 null nerves reveal a robust accumulation of monolysocardiolipin

Each significantly altered lipid compound was queried against published databases and assigned a putative structure annotation/identification. Levels of confidence in the identification of each compound was ranked from L2 (high)-L5 (low) and only those with L2 (experimental fragment data consistent with database match) and L3a (classification based on firm molecular formula and mass data) were considered for further analysis. Using these criteria, 186 (83 with positive fold change, 103 with negative fold change) total compounds were identified in the positive mode (Fig. 25 A, Table 7). In the negative mod 106 (66 with positive fold change, 40 with negative fold change) compounds were identified (Fig. 25 B, Table 6).

Curiously, while hundreds of lipid compounds in $p75^{KO}$ nerves displayed significant changes in abundance relative to WT controls, only nine had were changed by more than 2.0 fold (Table 4). By far the lipid species that was most increased was monolysocardiolipin (66:12) with a 11.73 positive fold change above WT samples. Monolysocardiolipins (MLCL) are intermediate species in the cardiolipin remodeling pathway localized predominately to the inner membrane of mitochondria. Cardiolipin is a phospholipid with four acyl side chains which maintains mitochondrial cristae curvature and stabilizes respiratory chain super complexes (Pfeiffer *et al.*, 2003). Mature cardiolipin is formed, in part, by the acylation of MLCL, in a process called cardiolipin remodeling (Boyd, Alder and May, 2018). MLCL levels are generally low in normal tissues, but aberrant MLCL accumulation has been noted in patients with Barth syndrome, a primarily cardiac disorder, and the neurodegenerative disorder, Tangier disease. While no definitive mechanisms of MLCL have been elucidated, increased MLCL is proposed to affect respiration and apoptotic signaling dynamics in mitochondria (Fobker *et al.*, 2001; Duncan, 2020). Primarily, its accumulation thought to disrupt/decrease mitochondrial respiration due to altered mitochondrial protein interactions and membrane structure destabilization, leading to respiratory chain collapse(Boyd, Alder and May, 2018; Duncan, 2020). However, it has also been proposed to reduce apoptotic signaling in oxidative stress conditions, as cardiolipin is more prone to oxidation, and potentially mimic the signaling of other toxic lysolipids (Fobker *et al.*, 2001; Li *et al.*, 2012).

Compound	Class	Annotation	P Value	q Value	Max Fold Change	Change
10.91_1341.8290m/z	Lysocardiolipin	MLCL(66:12)	0.031	0.239	11.73	Positive
1.45_390.2698m/z	Sulfonolipid	SL(20:0;O)	0.006	0.039	2.74	Positive
6.17_546.4059n	N-acyl ornithine	NAOrn(27:4)	0.029	0.084	2.52	Positive
9.97_1207.7692m/z	Ganglioside GM3	GM3(38:1;2O)	0.041	0.264	2.41	Positive
1.36_376.3598m/z	Diacylglycerol	DG(45:0)	0.023	0.074	2.26	Positive
6.02_450.3504m/z	Acylcarnitine	CAR(19:5)	0.021	0.071	2.18	Positive
7.84_307.2635m/z	Free fatty acid	FA(20:2)	0.001	0.036	2.03	Positive
12.55_1281.7861m/z	Ganglioside GM3	GM3(40:1;2O)	0.001	0.022	2.38	Negative
14.87_1362.1720m/z	Ox.Sphingomyelin	SM(78:4;3O)	0.011	0.162	2.07	Negative

Table 4. P75 null nerves have few large-scale changes in lipid abundance. Table of the identified lipid compounds with the largest max fold change measured in $p75^{KO}$ relative to WT controls. Abbreviations are as follows, Ox., Oxidized; GM3, monosialodihexosylganglioside; m/z, mass (m) to charge (z) ratio.

Interestingly , several cardiolipin species appear to be mildly decreased in $p75^{KO}$ nerves in both the negative (5%) and positive mode (15%) (Fig. 25 A,B). This suggests that cardiolipin remodeling, or degradation, may be widely disrupted in p75 deficient neurons, glia, or both. However, unlike the (66:12) MLCL species, which was robustly increased in abundance, the decrease in each cardiolipin species was less than 2 fold. Additionally, no other MLCL species had significantly altered abundance, making an interpretation of the dynamics of cardiolipin pathway dysregulation in $p75^{KO}$ mice difficult.

P75 null nerves display prominent dysregulation of fatty acid metabolism, membrane lipids, and ceramide pathways.

As $p75^{KO}$ nerves were shown to have many significantly altered lipids, but few which had large changes in abundance, we next asked whether any structural/functional classes seemed altered. Strikingly, out of 83 lipid compounds with a significant increase in abundance in the positive ionization mode that met the L2/L3a criteria, 37% were triacylglycerols (TAG) (Fig. 25 A). In contrast, no TAG species were significantly decreased in $p75^{KO}$ nerves (Fig. 25 A-D). Generally stored in lipid droplets, TAGs are neutral lipids formed from diacylglycerols (DAG) and fatty acyl-CoAs (derived from fatty

acids) (Welte, 2015). Interestingly, DAG species were found to be both increased (10%) and decreased (8%) in p75^{KO} nerves (25 A,B). Also, several species of Very Long-Chain Fatty Acids (over 20 carbon chains in length) were found to be increased in p75^{KO} nerves compared to control (Fig. 25C). Together, these changes indicate there are broad alterations in general fatty acid metabolism/energy storage in p75^{KO} nerves.

P75^{KO} mice retain a hypomyelination phenotype into adulthood (Cosgaya, Chan and Shooter, 2002). Therefore, we expected p75^{KO} nerves would display decreases in major membrane lipids species such as glycerophospholipids (GPLs), which together account for about 20% of myelin membrane phospholipids (Chrast Roman *et al.*, 2011). Interestingly, while many of the significantly altered compounds were membrane GPL species that were decreased (53% and 47% of total altered species in the positive and negative modes, respectfully), several species were increased (5% and 29% in the positive and negative mode, respectfully) (Fig. 25 A-D). Sphingomyelin species, which are membrane lipids that compose 10-35% of peripheral myelin, had similar alterations, with some species significantly increased and others decreased in P75^{KO} nerves (Chrast Roman *et al.*, 2011) (Fig. 25 A-D). These results suggest that p75^{KO} membrane lipids may not be uniformly decreased due reduced myelin surface area. Instead, membrane composition/lipid ratios may be altered in p75 deficient axons, glia, or both.

We also noted dysregulation of ceramide lipid compounds in the lipid profiles of p75^{KO} nerves. Ceramides are central components of sphingolipid metabolism with diverse biological function, including regulating inflammatory signaling, apoptosis, and metabolism. Additionally, their accumulation has been noted in several neurodegenerative disorders, including Farber disease, and Niemann-Pick Type A and B (Aerts *et al.*, 2008; Rombach *et al.*, 2010; Schuchman and Desnick, 2017). Intriguingly, p75 signaling can stimulate sphingomyelinase to generate ceramide in several cell types and in cultured Schwann cells has been shown to increase intracellular ceramide pools leading to apoptotic signaling(Dobrowsky *et al.*, 1994; Hitoshi Hirata *et al.*, 2001; Brann *et al.*, 2002). However, as with membrane GPLs, ceramides in p75^{KO} nerves appear to be fundamentally dysregulated, with many species showing increased abundance, and

others significantly decreased levels, suggesting p75^{KO} nerves have complex alterations in ceramide metabolism, and potentially, signaling (Figure 25 A, B).

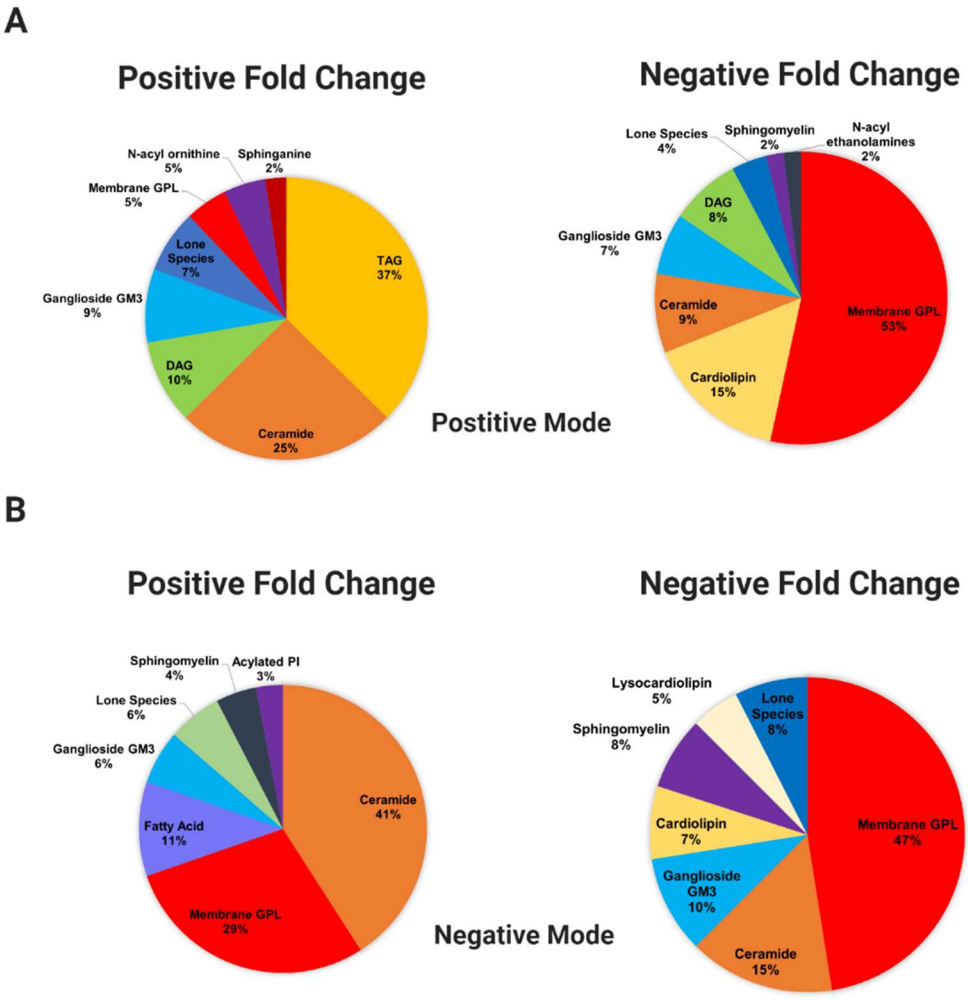

Figure 25. p75 null nerves have altered abundance of lipids in multiple lipid pathways. Lipid species with significantly altered abundance were assigned to metabolic groups/pathways based on their structure (class). Compounds that did not belong to pathways with more than one lipid altered were classified as lone species for brevity. (A) The percentage of lipids within each group/pathway that had significant positive fold change (p75^{KO} vs WT) in positive mode (N=83). (B) The percentage of lipids within each group/pathway that had significant negative fold change (p75^{KO} vs WT) in positive mode (N=106) (C) The percentage of lipids within each group/pathway that had significant positive fold change (p75^{KO} vs WT) in negative mode (N=66) (D) The percentage of lipids within each group/pathway that had significant negative fold change (p75^{KO} vs WT) in negative mode (N=40).

Discussion

Our findings suggest that deletion of p75 signaling does result in extensive alterations in peripheral nerve lipid dynamics. Over a hundred lipid species were found to have altered abundance in $p75^{KO}$ nerves compared to WT. Taken individually those alterations were subtle with robust accumulation of only one compound noted (MLCL), while most lipid compounds had a significant but less than 2-fold change in abundance. However, many significantly changed lipid species are involved in pathways that have been noted to be altered in response to oxidative stress and potentially neurotoxic pathway activation.

For instance, the prominent alterations in TAG species, coupled with altered levels of DAG compounds and increased abundance of some species of very long-chain fatty acids, is indicative of wide-spread alterations in fatty acid metabolism and energy storage. Studies have shown that increased oxidative stress, leading to altered ER and mitochondrial function and the accumulation of poly-unsaturated fatty acids, triggers the incorporation of cellular FAs into TAGs ((Liu *et al.*, 2015; Henne, Reese and Goodman, 2018; Jin *et al.*, 2018; Bocca *et al.*, 2019). This is thought to be primarily a protective measure to sequester potentially toxic FA lipids away in lipid droplets for later catabolism(Welte, 2015). However, increased lipid droplets (indicating increased TAG accumulation and storage) have been shown to accumulated in glia, both due to glial derived FA dysregulation, and in response to mitochondrial damage in neighboring neurons (Liu *et al.*, 2015). Consequently, droplet formation in glia may be an early marker for neurodegeneration. Additionally, while the dynamics of TAG accumulation have not been fully characterized in peripheral nerves, increases in TAG species have been associated with several neuropathies including CMT2, HSN1, CMT1E, and CMT1A(Marshall *et al.*, 2014; Zhou *et al.*, 2019; Giudetti *et al.*, 2020; Visigalli *et al.*, 2020).

That we observed both significantly increased as well as decreased abundance membrane GPLS and sphingomyelins was surprising. Although samples were taken from myelinating rather than adult nerves, we expected to see a uniform reduction in

membrane lipids consistent with later hypomyelination (which logically requires the synthesis of less membrane). However, this finding is consistent with a recent study which also found alterations in sphingolipid and GPL metabolism in lipid profiles analyzed from both a rat model of CMT1A, and samples taken from patients with CMT1. Similar to our results, they found that while many membrane species were significantly reduced, several others were aberrantly accumulated, indicating metabolic dysfunction and changes in membrane composition and signaling (Visigalli *et al.*, 2015). Therefore, GPL and sphingolipid metabolic dysregulation could be a shared mechanism in, or consequence of, peripheral neuropathy.

The alterations in ceramide and cardiolipin pathways we detected in $p75^{KO}$ nerves are also indicative of substantial shifts in the metabolic activity. Ceramides are potent secondary messengers, as well as central elements in sphingolipid metabolism. Consequently, dysregulation of ceramide signaling and metabolism have incredibly diverse results on cell function (Fisher-Wellman *et al.*, 2020). As previously mentioned, accumulation of ceramide species has been noted in multiple neurodegenerative diseases (Aerts *et al.*, 2008; Rombach *et al.*, 2010; Schuchman and Desnick, 2017). However, the impact of the altered ceramide abundance we see in $p75^{KO}$ is hard to evaluate without further parsing of the specific ceramide species that are dysregulated. Likewise, the consequences of the alterations we see in the cardiolipin pathway are difficult to fully assess. Decreased cardiolipin is associated with a reduction in mitochondrial respiration and organization (Aufschnaiter *et al.*, 2017). However, cardiolipin is also theorized to play a major role in mitochondria in the initiation of oxidative stress induced apoptosis. Cardiolipin is redistributed in stressed mitochondria to the outer membrane where associates with cytochrome C and is readily oxidized by hydrogen peroxide and other oxidants (allowing eventual cytochrome C release from the mitochondria) (Pope, Land and Heales, 2008). Therefore, its reduction along with a buildup of MLCL (which generally is ER membrane bound), may reflect a cytoprotective response (Pope, Land and Heales, 2008). On the other hand, MLCL accumulates in Tangier disease and Broth syndrome and has been suggested to contribute to cytotoxicity and pro-apoptotic pathway activation (Fobker *et al.*, 2001; Duncan, 2020).

Taken together, these results reveal that deletion of p75 results in significant alterations in nerve lipid profiles. Furthermore, many alterations were found in lipid pathways associated with oxidative damage and neurodegeneration, thus, their dysregulation may contribute to the neurodegeneration we observed in the peripheral sensory neurons of $p75^{KO}$ mice.

Project Discussion

Conclusions and Future Directions

In this study I sought to clarify the roles of the p75 neurotrophin receptor in developing nerves by using two conditional p75 deletion mouse models to isolate and parse the role of p75 in peripheral neurons vs. Schwann cells. Unexpectedly, I discovered that loss of p75 in Schwann cells leads to DRG neuron loss and hypoalgesia, while neuronal p75 disruption failed to provoke DRG neuron loss. Additionally, I found that cholesterol biosynthesis is disrupted in p75 deficient Schwann cells, resulting in the accumulation of a neurotoxic lipid, 7-DHC, in nerves. Accordingly, induction of *dhcr7* in p75 deficient Schwann cells ameliorated the observed neuronal loss. Therefore, I propose that p75 plays a key role in the regulation of cholesterol biosynthesis in developing Schwann cells and that alteration of that catabolism in p75 null Schwann cells promotes neurodegeneration through 7-DHC induced lipotoxicity. However, there are several aspects of the pathomechanism of neurodegeneration in the $p75^{KO}$ and Dhh-$p75^{\Delta}$ models that remain to be explored in future studies.

I determined, contrary to previous suppositions, that the majority of DRG neuron loss in p75 null mice occurs between E17.5 and P6 (Lee *et al.*, 1992; Lee, Davies and Jaenisch, 1994; Murray, Bartlett and Cheema, 1999; Cosgaya, Chan and Shooter, 2002), which is well after the period of naturally occurring apoptosis (Oppenheim, 1991; Marmigère and Carroll, 2014). However, in the future, a more nuanced evaluation of the

progression of neuronal death in $p75^{KO}$ and Dhh-$p75^{\Delta}$ would greatly enhance understanding of the dynamics of neurodegeneration in p75 deficient mice. To chart a full timeline of the neuron loss, DRGs from $p75^{KO}$ and Dhh-$p75^{\Delta}$ could be assessed periodically for levels of neuronal loss from E17.5 to P6. Additionally, as apoptosis is the most widespread form of neuron death during development, DRGs could examined for apoptotic markers such as condensed chromatin, increased cleaved Caspase-3, or DNA fragmentation (Lossi, Castagna and Merighi, 2015a). This would allow for later analysis of altered pathway activation in DRGs at timepoints just prior to notable neuron loss.

Better understanding the exact kinetics of neuron death would be especially advantageous, because the primary mechanisms of 7-DHC induced DRG neuron death in $p75^{KO}$ and Dhh-$p75^{\Delta}$ mice remain to be elucidated. 7-DHC, and its metabolic derivatives, have been frequently theorized to cause neurodegeneration in the CNS through elevated oxidative stress (Tulenko *et al.*, 2006; Korade *et al.*, 2010; Porter and Herman, 2011; Haldar *et al.*, 2012). Additionally, the significant upregulation of several TAG species in our lipidomic study, may be indicative of mitochondrial dysfunction, a common result of oxidative damage (Liu *et al.*, 2015). Therefore, it would be interesting to determine if a firm connection could be made between oxidative damage, in DRGs and/or Schwann cells, and neurodegeneration. For instance, a connection could be made through an assessment of ROS levels in $p75^{KO}$ and Dhh-$p75^{\Delta}$ DRGs and nerves, or activation/upregulation of antioxidant responsive element (ARE) pathway regulators such as Liver X Receptor and Nrf2 (Hichor *et al.*, 2018). Additionally, cultured DRG neurons could be treated with 7-DHC and evaluated for progressive ROS accumulation and decreased mitochondrial function(Redmann *et al.*, 2018).

Increased understanding of the signalling dyanamics, and timeline of neuronal death in the p75 null mice may also help understand why there was such a divergence from anticipated phenotypes in both conditional deletion models. As stated previously, we found that approximately 5.7% of DRG neurons still expressed p75 in Thy1-$p75^{\Delta}$ mice The incomplete deletion of p75 could account for the difference between the 50% loss of neurons in the total knock out compared to a 30% loss in the Schwann cell deletion of p75. However, if our prediction that neuronal death occurs after PCD/NOND is accurate,

any neuron loss found in an alternative conditional neuron deletion model would also likely be simularly delayed/due to alternative mechanisms. Also, conditional deletion in other cells, such as sattalitte or perinerial glia, may determine if the total knockouts hypomyelination phenotype, which we also did observe after Schwann cel deletion, is dependent on axonal and SC p75 distruption, or the result of other mechansims.

The underlying mechanisms facilitating the transfer of 7DHC from Schwann cells to neurons is another potential avenue for future exploration. One possibility is transfer during sterol receptor mediated exchange of sterols from glia to axons during development, as has been well characterized in the central nervous system and theorized to occur in the periphery (Saher and Simons, 2010). Alternatively, transfer could occur through axonal incorporation of Schwann cell derived exosomes, vesicles which are largely enriched in cholesterol and have been shown to readily integrate 7-DHC (St. Clair and London, 2019). This seems especially likely given that exosome transfer between Schwann cells and axons has been suggested to occur regularly during development and has been shown to profoundly impact sensory neuron health in disease models (Lopez-Verrilli and Court, 2012; Zhou *et al.*, 2018; L. Wang, Chopp, Szalad, X. Lu, *et al.*, 2020). The primary mode of 7-DHC efflux from Schwann cells could be determined through collection of Schwann cell conditioned media after C-13 labelled glucose treatment as described in Chapter 3. Exosomes could be isolated from media through ultracentrifugation, and both could be assessed for the levels of C-13 7-DHC using LC-MS/MS (L. Wang, Chopp, Szalad, X. R. Lu, *et al.*, 2020).

One of the key remaining questions in our study is why DRG neurons are the primary cell type affected by 7-DHC accumulation in nerves. Protective signaling in Schwan cells, such as the efflux of extraneous 7-DHC or robust antioxidant expression, may explain why myelin profiles are seemingly unaffected in Dhh-P75$^{\Delta}$ mice and Schwann cells do not die. Our data does not suggest, however, that Schwann cells are not adversely affected by 7-DHC accumulation, only that they are better able to compensate and retain function during development. Therefore, it would be interesting to evaluate whether Dhh-p75$^{\Delta}$ mice have decreased ability to remyelinate after sciatic nerve injury or feature increased neurological impairments at advanced ages.

Although the number of motor neurons in Dhh-p75$^{\Delta}$ mice was not determined here, there was no overt indication of motor impairment and in global p75^{KO} mice there is no reduction in lower motor neurons (Murray, Bartlett and Cheema, 1999). The preservation of spinal motor neurons in p75 deficient models, especially as they, like DRGs, are so closely associated with Schwann cells, is quite perplexing. There are two distinct possibilities, either they are not exposed to the same levels of 7-DHC as DRG neurons, perhaps through reduced cellular uptake, or they are inherently more resistant to the neurotoxic effects of 7-DHC than sensory neurons. A full assessment of Dhh-p75$^{\Delta}$ spinal motor neuron morphology, conduction, and response to 7-DHC exposure would be necessary to address these questions in the future.

Significance

The significance of this work is two-fold. First, it adds additional weight to recent studies that contradict the previously assumed roles of p75 in the developing PNS. P75 signaling in DRG neurons has long been assumed to be a main contributor to the survival signaling preventing excess embryonic DRG death during naturally occurring cell death, in accordance with the neurotrophic hypothesis (Lee *et al.*, 1992; Lee, Davies and Jaenisch, 1994; Murray, Bartlett and Cheema, 1999). Additionally, due to the hypomyelination phenotype in p75^{KO} mice, it was assumed that proper myelin formation and thickness was dependent on Schwann cell p75 signaling (Cosgaya, Chan and Shooter, 2002). That we see no neuronal loss in our Thy1-p75$^{\Delta}$ model joins studies such as Qin et al. (2020) and Chen et al. (2017) in suggesting that deficiency in p75 signaling is not responsible for the majority of DRG loss noted in p75^{KO} mice . Likewise, our failure to observe evidence of persistent hypomyelination in Dhh-p75$^{\Delta}$ mice, a result echoed recently in a myelin protein zero-Cre (MPZ-Cre) driven Schwann cell conditional p75 deletion model, suggests that myelin thickness is not regulated solely by Schwann cell p75 during development(Gonçalves, Jager, *et al.*, 2020). Taken together these results substantially shift our understanding of p75 signaling in PNS development.

Secondly, the unique lipid signaling between Schwann cells and neurons described here corroborates a growing body of literature indicating that Schwann cell lipid metabolism has a profound effect on neuron function and survival (Jha and Morrison, 2018). It has long been clear that Schwann cells are essential for the survival of sensory neurons (Davies, 1998; Woldeyesus *et al.*, 1999; Chen *et al.*, 2003). Additionally, as reviewed fully in in Chapter 1, there has recently been a growing acknowledgment that neurotoxic lipid accumulation can contribute to pathology of neuropathy. However, so far studies exploring this phenomenon have largely involved inherited diseases with known lipid biogenic dysfunction, or mouse models featuring directed disruption of Schwann cell mitochondrial metabolism (Viader *et al.*, 2013; Dali *et al.*, 2015; Kramer, Bielawski, Kistner-Griffin, *et al.*, 2015; Dodge, 2017; M C Perez-Matos, Morales-Alvarez and Mendivil, 2017). Our findings that disruption of Schwann cell p75 signaling during development results in pronounced sensory neuron loss due to 7-DHC accumulation, as well as significant alterations in nerve lipid profiles, suggests that alteration of pathways regulating Schwann cell metabolism may substantially impact the development of neuropathy. Thus, this novel mechanism of Schwann cell metabolic dysfunction provoked neurodegeneration contributes to our understanding of the complex pathophysiology of acquired neuropathies.

Appendix I

The Role of NFκB in Inherited Neuropathy

Introduction

As previously detailed in Chapter 1, myelin plays a key role in axonal support, to the extent that many neuropathies involve dysfunctional myelin formation and/or maintenance. Several key examples of this are found in the pathologies of Charcot-Marie-Tooth (CMT) disease, also known as hereditary motor and sensory neuropathy (HMSN)(Pareyson and Marchesi, 2009). This appendix will briefly detail our investigations into the potential pathological contributions of the NFκB signaling pathway to de-/dysmyelinating neuropathology.

Charcot-Marie-Tooth Disease

CMT was first documented in 1886 by French neurologists Jean-Marin Charcot and Pierre Marie, and, independently, England's Howard Tooth. These physicians described patients exhibiting sensory loss, muscle weakness, absent reflexes, and frequent atrophy of distal limbs (Tooth, 1886; Pareyson, Scaioli and Laurà, 2006; Dyck and Lambert, 2014). Today, CMT is recognized as the most common inherited neuropathy with an estimated prevalence of around 1 in 2500 individuals (Paassen *et al.*, 2014). Over time, advances in diagnostics and genetic testing have revealed CMT to be a heterogeneous group of inherited neuropathies, necessitating a complex sub-classification system based on type of genetic mutation, symptomatology, and inheritance patterns (Timmerman, Strickland and Züchner, 2014).

Interestingly, while over 100 genes have been implicated in CMT pathology the majority of CMT cases fall under the broad category of de-/dysmyelinating CMT, featuring primary or predominant dysfunction in myelinating Schwann cells (Stavrou *et*

al., 2020). De-/dysmyelinating CMT is typically characterized by severe reductions in motor conduction velocity and the notable presence of myelin structural abnormalities, including segmental and recurrent demyelination, hypomyelination (reduced myelin thickness), and myelin decompaction, preceding secondary axonal loss (Dyck and Lambert, 2014). Several of the causative mutations in the de-/dysmyelinating form of CMT have been pinpointed to mutations involving proteins enriched in compact myelin (Timmerman, Strickland and Züchner, 2014). For example, the most common cause of CMT has been linked to mutations in the gene encoding Peripheral Myelin Protein 22 (PMP22). PMP22 is a tetraspan membrane glycoprotein of debated function which makes up only 2-5% of compact myelin (Li *et al.*, 2013). Nonetheless, ~50 percent of patients with de/dysmyelinating CMT are classified as having CMT1A, caused by 1.5Mb duplication at the p11.2 locus of Chromosome which includes both the promoter and exons for the gene encoding PMP22, *PMP22* (Vance *et al.*, 1991; Nelis *et al.*, 1996; Li *et al.*, 2013). Additionally, the second most common form of CMT, known as hereditary neuropathy with liability to pressure palsy (HNPP) is associated loss of one PMP22 allele. Finally, while much rarer than CMT1A, several PMP22 point mutations also result in CMT, classified as CMT1E. Another common form of CMT, accounting for roughly 5% of patients is classified as CMT1B (DiVincenzo *et al.*, 2014). CMT1B is due to point mutations in Myelin Protein Zero (MPZ/P0), a membrane glycoprotein of the immunoglobulin superfamily that makes up 50 percent of compact myelin and plays a critical structural role (Bai, Patzko and Shy, 2013).

CMT1 Pathology

While many of the causative mutations in de-/dysmyelinating CMT are known, our understanding CMT pathological mechanisms remains incomplete. One prominent theory is that altered levels of affected myelin proteins in myelin membranes, and/or loss-of-function, is the main cause of the myelin dysfunction observed in CMT1. However *PMP22* deletion results in HNPP, a very mild form of CMT that has a very different pathology from PMP22 duplication (CMT1A) or PMP22 point mutations (CMT1E), suggesting that mutations in PMP22 are more likely toxic gain-of-function than loss of function (Paassen

et al., 2014). Likewise, haploinsufficiency of MPZ causes a much less severe, and phenotypically distinct form of neuropathy in mice compared to MPZ point mutations (Shy *et al.*, 2004; Saporta *et al.*, 2012).

There is also evidence that myelin abnormalities in CMT1A are not solely due to high expression of PMP22. PMP22 levels are throttled even under normal conditions in Schwann cells, with around 80% of PMP22 being undergoing proteasomal endoplasmic reticulum-associated degradation before incorporation into the myelin membrane (Pareek *et al.*, 1997; Stavrou *et al.*, 2020). Therefore, it has been suggested that high levels of PMP22 accumulate due to interrupted degradation may contribute towards CMT1A pathology. Accordingly, dysfunctional/disrupted trafficking of PMP22, to the point of aggregation, has been reported in both CMT1A mouse models and in patient derived cells (Fortun *et al.*, 2006; Lee *et al.*, 2018). However, evidence for such aggregation in CMT1 patient nerve biopsies is limited (Hanemann *et al.*, 2000). Moreover, phenotypic presentation is highly variable in CMT1A patients, even amongst family members where less genetic variability can be assumed, and PMP22 protein and mRNA levels do not correlate with the degree of neurological impairment (Katona *et al.*, 2009; Visigalli *et al.*, 2020). This divide between myelin protein levels/functional status and phenotypic outcomes in CMT1 suggests that CMT pathology may be amplified by the initiation of additional maladaptive cellular mechanisms in a gain-of-function manner.

One commonly proposed maladaptive pathway involved in several forms of CMT is sustained unfolded protein response (UPR) pathway activation, resulting from the aggregation of mutant/excess proteins within Schwann cell Endoplasmic Reticulum (ER). The Unfolded Protein Response pathway (UPR) is a group of interconnected signal transduction pathways activated by specialized ER localized transmembrane proteins capable of detecting the presence of accumulated misfolded, or unfolded, proteins (Fig. 25). While transient UPR activation often ameliorates ER stress, prolonged UPR activation has been implicated in several disease pathologies in myelinating cells(Clayton and Popko, 2016; Lin and Stone, 2020). For example, excess UPR activation has been linked to a form of CMT1B resulting from a myelin protein zero (MPZ) serine 63 deletion

point mutation, which features maladaptive activation of the C/EBP homologous protein (CHOP) transcription factor, leading to myelin abnormalities(D'Antonio *et al.*, 2013). Additionally, activation of the Ire1α arm of the Unfolded Protein Response (UPR) has been noted in the Trembler-J (TrJ) mouse model. TrJ mice, a model of CMT1E, have a spontaneously occurring leucine 16 to proline point mutation of PMP22 which results in severe neuropathy (Okamoto *et al.*, 2013).

Interestingly, it has been noted many UPR regulated pathways have additional roles in Schwann cell development as key modulations of maturation, myelination, and repair (Nickols *et al.*, 2003; Mirsky *et al.*, 2008; Arthur-Farraj *et al.*, 2012; Yang *et al.*, 2012). This has led to speculation that their aberrant activation may contribute to dysregulation of Schwann cell myelination, and demyelinating pathology. For example, the presence of MAPK/ERK1/2 is required during nerve development for both Schwann cell precursor maturation, and later for the regulation of myelin formation(Mirsky *et al.*, 2008). Additionally, ERK1/2 can also be activated by UPR pathway activation through IRE1α kinase activity(Darling and Cook, 2014). However, acute activation of ERK in adulthood provokes SC dedifferentiation and demyelination and prolonged MAPK/ERK activation in adulthood delayed repair after injury (Cervellini 2017). Other UPR activated pathways with dual roles in Schwann cell development and myelination include the mitogen activated protein (MAP) family Kinase- p38, c-jun N-terminal kinase (JNK), and the nuclear factor kappa-light-chain-enhancer of activated B cells (NFκB) pathway (Nickols *et al.*, 2003; Mirsky *et al.*, 2008; Arthur-Farraj *et al.*, 2012; Yang *et al.*, 2012).

NFκB Signaling in Neuropathy

The NFκB pathway is an especially striking candidate for maladaptive UPR signaling due to its pervasive function in several biological processes, and additional role in Schwann cell maturation. NFκB subunits, including RelA (p65), RelB, c-rel, p50, and p52 are expressed in almost all cell types and regulate numerous adaptive and potentially maladaptive processes such as inflammation, immunity, differentiation, cell growth, and apoptosis (Ghosh and Dass, 2016). While canonical activation of NFκB occurs through

multiple surface membrane receptors, it is also activated by the Ire1α and Perk pathways of the UPR (Tam *et al.*, 2012; Ghosh and Dass, 2016) (Fig. 26). In developing Schwann cells, NFκB is activated by NRG1 type III during early stages of myelin formation (Nickols et al., 2003; (Limpert and Carter, 2010). Subsequently, the p65 and p50 NFκB subunits heterodimerize and regulate the expression of Oct6, a transcription factor which regulates the timing of myelin programing(Bermingham *et al.*, 1996; Jaegle *et al.*, 2003; Yoon, Korade and Carter, 2008).

Increased activation of NFκB has been noted in several neuropathies including diabetic neuropathy, HNPP, and CIPN. Although, the pathological mechanisms proposed in these conditions have primarily focused on potential neuroinflammatory effects(Cameron and Cotter, 2008; Bekircan-Kurt, Tan and Erdem Özdamar, 2015; Alé *et al.*, 2016). However, our lab previously found that treatment of DRG myelinated co-cultures with an adenovirus overexpressing the p65 subunit, inhibited Schwann cell myelination (data not shown). Additionally, our lab has previously noted NFκB activation in adult TrJ nerves (data not shown). Therefore, we hypothesized that aberrant activation of the NFκB could, as in the case of MAPK/ERK, prompt dysregulation of Schwann cell myelin formation and contribute to the development of de-/dysmyelinating pathology.

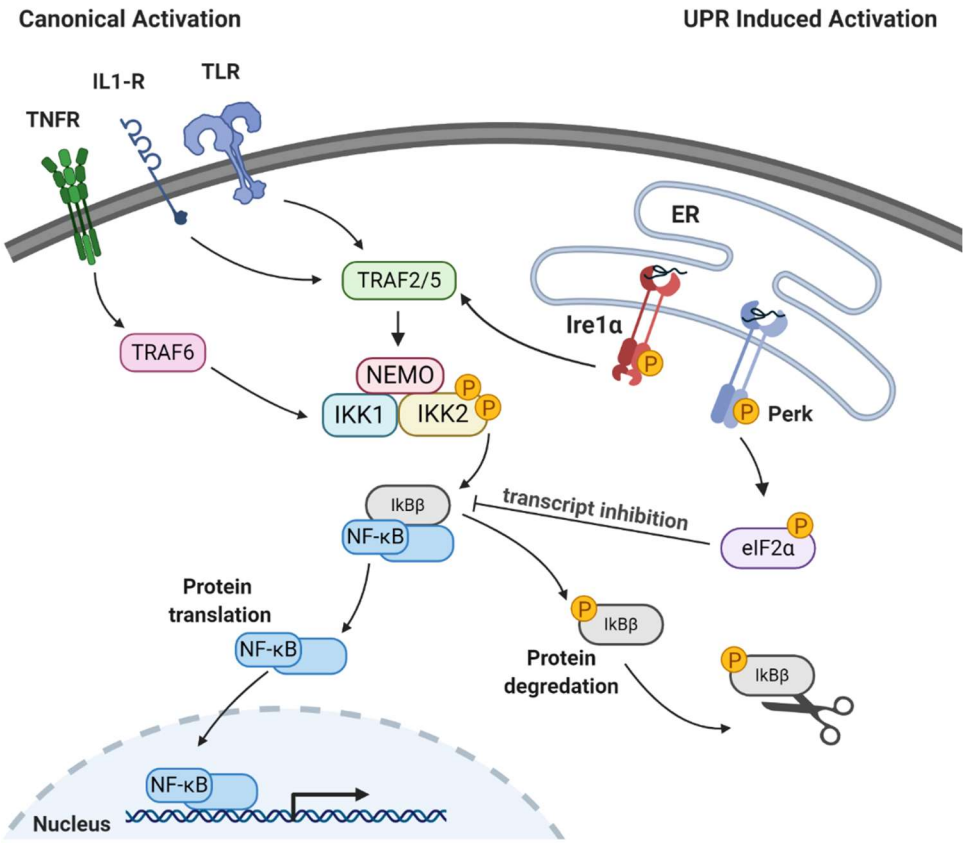

Figure 26. Activation of NF-κB signaling through canonical and UPR Pathways. Upstream activation from surface receptors (TNFR, IL1-R, TLR) or the UPR pathway receptor Ire1α leads to the phosphorylation of the NFκB inhibitor, IκBβ, by the IKK2 subunit of the IKK complex (IKK1, IKK2, NEMO). This triggers the release of NFκB subunits which translocate to the nucleus following degradation of IκBβ through the ubiquitin-proteasome system. The UPR receptor Perk also leads to NFκB activation through transcriptional inhibition of IκBβ after eIF2α activation. Abbreviations are as follows, UPR; Unfolded Protein Response; TNFR, Tumor necrosis factor receptor; IL1-R, interleukin-1 receptor; TLR, Toll like receptor; ER, Endoplasmic Reticulum; Ire1α, inositol-requiring enzyme 1 α; Perk, protein kinase RNA-like endoplasmic reticulum kinase; EIF2α, Eukaryotic Initiation Factor 2 alpha; NEMO, NF-kappa-B essential modulator; IκBβ, inhibitor of nuclear factor kappa B β; IKK, IκB kinase; NFκB, nuclear factor kappa-light-chain-enhancer of activated B cells

Methods

Nerve Conduction Studies

Mice were anesthetized using a precision vaporizer dispensing isoflurane (4% for induction; 1.5% for maintenance during the procedure). Uninsulated pins (27 gauge, sterilized by glass bead sterilizer) were inserted in the sciatic notch and above the ankle and knee (popliteal fossa) for stimulation. A grounding electrode was inserted through belly skin. One recording electrode was inserted in the medial side of the foot pad, and a reference electrode was inserted proximally. The tibial nerve was stimulated at the distal and proximal sites starting with 2-3mA and increasing until a consistent CMAP amplitude was obtained.

Electron Microscopy and Myelin Analysis

Mice were perfused with a 2% glutaraldehyde and 2% paraformaldehyde solution in 0.1M cacodylate buffer. Approximately 4 mm sciatic nerve sections were extracted 0.5 cm distal from the sciatic notch while irrigating the area with additional fixative. The nerves were post fixed in the same solution and stored a 4C until incubation in 1% osmium for 1hr at RT then 0.5% osmium overnight. Nerves were embedded in resin and 1µm thin sections were obtained before being and dyed with toluidine blue mounted in DPX solution. Sciatic nerve cross sections were imaged in brightfield on a Nikon Eclipse Ti scope with DS-Qi2 camera (Nikon) and NIS-Elements (https://www.microscope.healthcare.nikon.com/products/software/nis-elements) at 20x magnification and images were stitched together to form an entire cross section. Blinded individuals analyzed whole cross sections for number of myelinated axons per cross section, as well as numbers of abnormally myelinated axons.

Immunofluorescence

Sciatic nerves were extracted from adult control and IKKON mice were fixed in 10% neutral buffered formalin and embedded in paraffin. After embedding, sciatic nerves were sectioned at 5 μm thickness using a Leitz 1512 microtome, before deparaffinization and rehydration. Then samples were placed in a pressure cooker for 15 min (GoWise, USA) within a copulin jar filled with citrate buffer antigen retrieval solution (10mM Citric Acid, 0.05% Tween 20, pH 6.0). After cooling to RT, samples were rinsed in PBS and permeabilized for 10 min with 0.1% Triton-X (Sigma-Aldrich Cat#T8787). They were then blocked with 5% Normal Goat Serum (Gibco Cat# 16210064) for 1hr at RT before being incubated overnight in a primary anti-rabbit polyclonal p65 antibody (Rockland Cat#100-4165). Samples were rinsed three times with PBS and incubated with a secondary 596-Alexa Flour Goat anti-Rabbit antibody (Invitrogen Cat# A-11012) for 1 hr at RT before being rinsed with PBS and mounted with Prolong anti-fade reagent with DAPI (Life Technologies Cat#P36931).

Immunoblot

Sciatic nerves were extracted from adult IKKON and control mice and immediately frozen on dry ice. Freeze dried nerves were ground to a powder using a pestle and resuspended in NP-40 lysis buffer with a PhosSTOP phosphatase inhibitor cocktail (Sigma-Aldrich Cat# 4906845001) and sodium vanadate. A Bradford assay was preformed to determine protein concentration. 25 micrograms of protein lysate was boiled for 10 minutes at 100^{o}C in 6X SDS buffer before being loaded and run on a 7% acrylamide SDS gel. Proteins were transferred at 300 millivolts for 1.5 hours onto a nitrocellulose membrane and blocked with 5% BSA/PBS for 1hr at RT. Blots were probed with Anti-Flag (1:1000) (Sigma-Aldrich Cat#F1-50UG) and anti-tubulin (1:1000) primary antibodies (Calbiochem Cat#. CP06) and an anti-mouse HRP secondary (Promega Cat#W402).Blots were exposed using an Amersham Imager 600 version 1.2.0804.

Tail suspension

Adult mice were grasped at the base of the tail and suspended for 15 seconds while evaluated (pass/fail) on their ability to maintain a stable splay reflex formation without the presence of trembling, paw curling, lateral (non-fully extended) limb positioning. The task was repeated 5 times per session with brief breaks in between trials. Mice were assigned either 0= no failed trails, 1=1-2 failed trails, or 2=3 or more failed trails.

Results

IKK2SSEE is expressed in IKKON sciatic nerves.

To test the hypothesis that aberrant NFκB activation contributes to de-/dysmyelination, we utilized R26StopIKK2SSEE mice crossed with the Dhh-Cre transgenic line, hereafter referred to as IKKON mice (Fig. 27A). The Rosa26IKK2SSEE line carries a floxed allele expressing a constitutively active form of IKK2, a member of the IKK complex. IKK is a linchpin of both the canonical and alternative pathway activation of NFκB and consists of two kinases IKK1 (or IKKα) and IKK2 (IKKβ) and a regulatory subunit, NFκB essential modulator (NEMO or IKKγ). Phosphorylation of either IKK1 or IKK2 activates the IKK complex and results in phosphorylation and subsequent degradation of IκB, an inhibitor responsible for the sequestration of NFκB subunit dimers in the cytoplasm (Fig. 26). Therefore, the presence of IKK2SSEE, which mimics IKK2 phosphorylation through substitution of two glutamates in place of serines in the activation loop of the kinase domain, indirectly results in constitutively active NFκB signaling through the continuous degradation of IkB. We crossed this line with a Schwann cell specific transgenic line, Dhh-Cre, to target the activation of NFκB to Schwann cells, and Schwann cell precursors, beginning at E13.5 (Sasaki *et al.*, 2006; Otero *et al.*, 2012).

Firstly, IKK2SSEE expression in the IKKON model was confirmed. Sciatic nerves were extracted from 6-8 week old IKKON mice and littermate (Dhh-Cre negative) controls. To avoid detection of endogenous IKK2, we performed an anti-Flag western blot, specifically detecting the Flag tagged IKK2SSEE protein. Flg-IKK2SSEE, consistent with the

expected size of IKK2 (~87kda) was detected in IKKON sciatic nerve lysates only, indicating that recombination was successful and exclusive to IKKON nerves (Woronicz *et al.*, 1997) (Fig. 27 B).

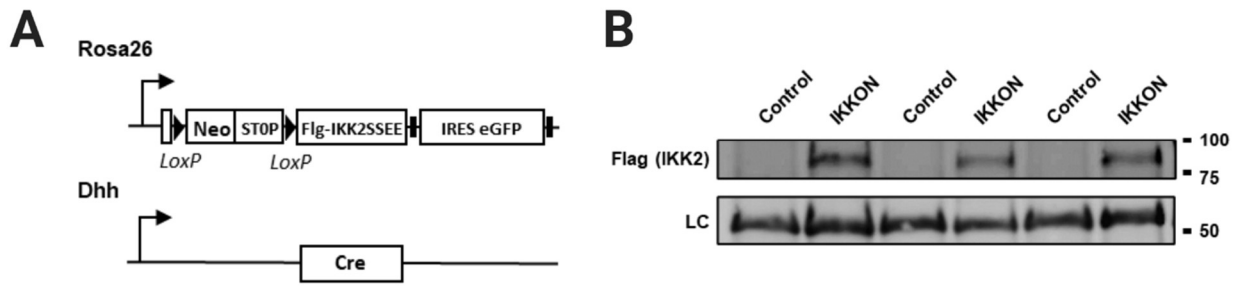

Figure 27. IKK2SSEE is expressed in the IKKON mouse model. (A) Schematic of IKKON cross. The IKK2SSEE cassette is localized to the Rosa26 locus (top) while the Dhh-Cre allele features Cre expression under the control of the Desert Hedgehog (Dhh) promoter (bottom) (B) Anti-Flag immunoblot of sciatic nerve lysates (top). IKK2SSEE-Flg was detected solely in IKKON mice, and not control, Dhh-Cre negative littermates (N=3 for each genotype). Anti-Tubulin serves as a loading control, LC, on the same membrane (bottom).

NFκB expression is altered in IKKON Schwann cells

As activation of the NFκB pathway in the IKKON model is indirect, we next examined whether the presence of IKK2SSEE in IKKON Schwann cells was sufficient to provoke alterations in NFκB signaling. Therefore, sciatic nerves were extracted from 6-8 week IKKON mice and immunostained for p65, a primary subunit of NFκB (Ghosh and Dass, 2016). Longitudinal nerve sections suggested increased levels of p65, with greater signal overlap in DAPI stained Schwann cell nuclei (Fig. 28 A). However, p65 localization in Schwann cells was difficult to determine, due to the presence of apparent axonal p65 expression. Therefore, we next examined p65 staining in nerve cross sections which showed that while there was consistent low level p65 signal in IKKON and control axons, p65 localization was more highly expressed in Schwann cells surrounding axons (Fig. 28 B). IKKON Schwann cells exhibited both greater intensity of p65 signaling, as well as

p65 nuclear localization, indicating the presence of IKK2SSEE in Schwann cells was sufficient to activate NFκB.

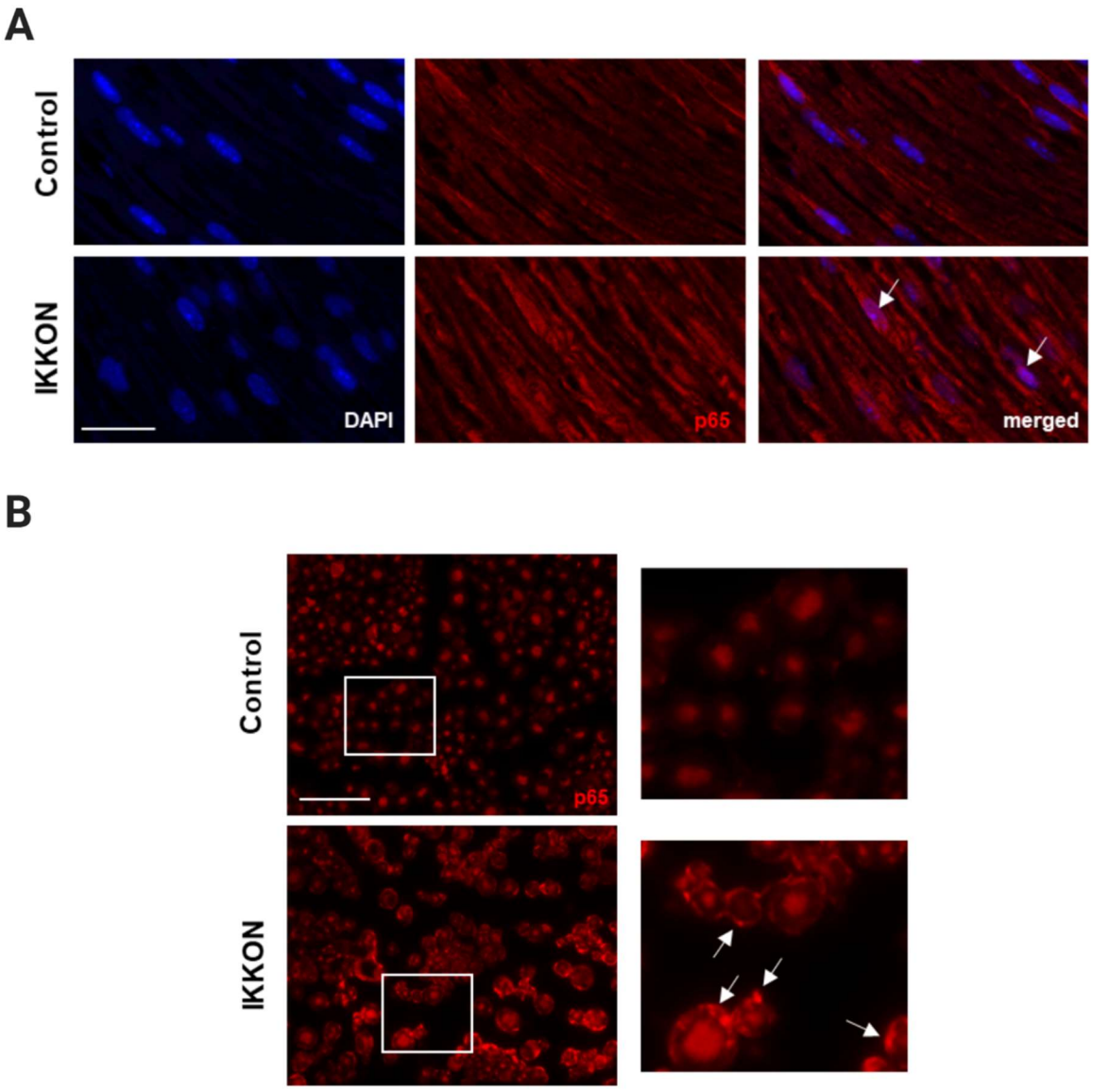

Figure 28. The NFκB pathway is activated in IKKON Schwann cells.(A) Immunofluorescence staining for p65 in longitudinal sciatic nerve sections (5 μm) extracted from IKKON and control 6-8 week old mice. Scale Bar, 25 μm. P65 staining intensity was increased in IKKON samples and appears to converge with Schwann cell nuclei (white arrows) as identified by DAPI. (B) Immunofluorescence staining for p65 in sciatic nerve cross sections (5 μm). Consistent axonal p65 staining was evident in both control and IKKON sciatic nerve cross sections. IKKON cross sections featured both more signal intensity, and areas of highly clustered p65 (white arrows).

IKK2SSEE expression in mice does not prompt aberrant formation of myelination or axonal loss

To determine if IKK2SSEE expression in Schwann cells provokes abnormal myelin formation, or demyelination, we analyzed myelin profiles of IKKON and control mice at 3 months. Sciatic nerves were extracted from adult mice and cross sections were analyzed by brightfield microscopy (Fig. 29 A). As de-/dysmyelination often results in secondary axonal degeneration we quantified the number of myelinated axons and noted no difference between IKKONs and litter controls (Pareyson and Marchesi, 2009)(Fig. 29 B). Additionally, we noted no obvious alterations in myelin thickness, nor any increase in the amount of abnormally myelinated axons in IKKON nerves (Fig. 29 C) From this we concluded that constitutive activation of NFκB in IKKON mice does not result in major myelin abnormalities, at least in early adulthood.

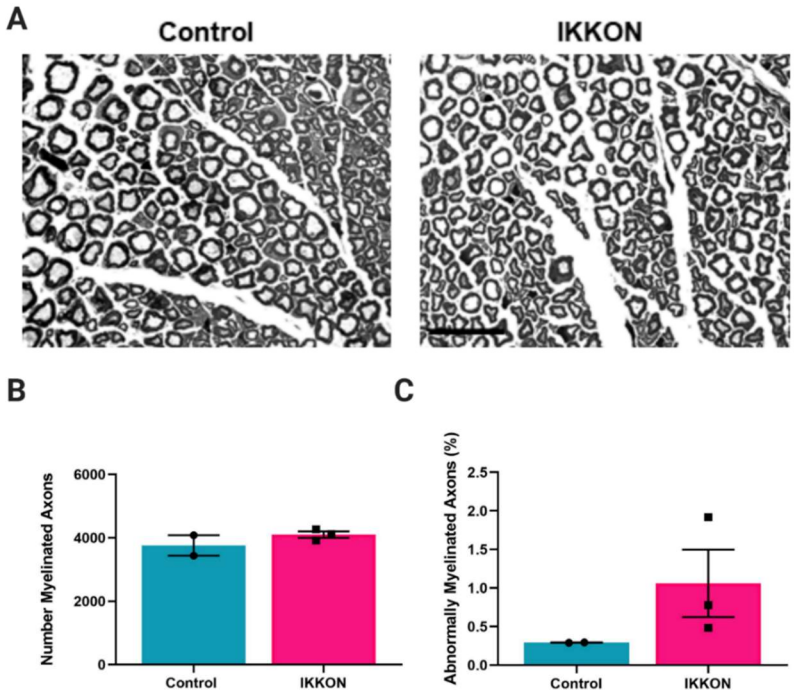

Figure 29. IKKON mice display normal myelin profiles at 3 months. (A) Myelin profiles from IKKON and control mice. Scale bar=50µm (B) Quantification of total number of myelinated axons within whole sciatic nerve cross sections from control (N=2) and IKKON (N=3) mice revealed no loss of myelinated axons in IKKON sciatic nerves. (C) Quantification of the percentage of ≥ 1 µm diameter axons in whole sciatic nerve cross sections which feature either absent, or clearly abnormal myelin. Control (N=2), IKKON (N=3).

IKKON mice have no deficits in nerve conduction

De-/dysmyelination is often associated with altered axonal conduction(Azhary *et al.*, 2010). Therefore, we next examined IKKON mice for evidence of abnormal sciatic nerve conduction. Nerve conduction velocities were derived from compound muscle action potential (CAMP) recordings taken from the foot muscles of IKKON and control mice, after electrical stimulation of the sciatic nerve. We found that average nerve conduction velocity (m/s) was not significantly altered in IKKON mice at 1 month, and repeated testing at 2 and 3 months revealed no changes in NCV (Fig. 30 A). Additionally, we saw no significant changes in the average amplitudes of recorded CAMPs after stimulation of the sciatic nerve at proximal or distal sites at 1 month, nor changes in CAMP amplitudes over time (Fig 30 B, C). Taken together these data indicate that IKKON mice have no detectible deficits in sciatic nerve conduction, even up to 3 months of age.

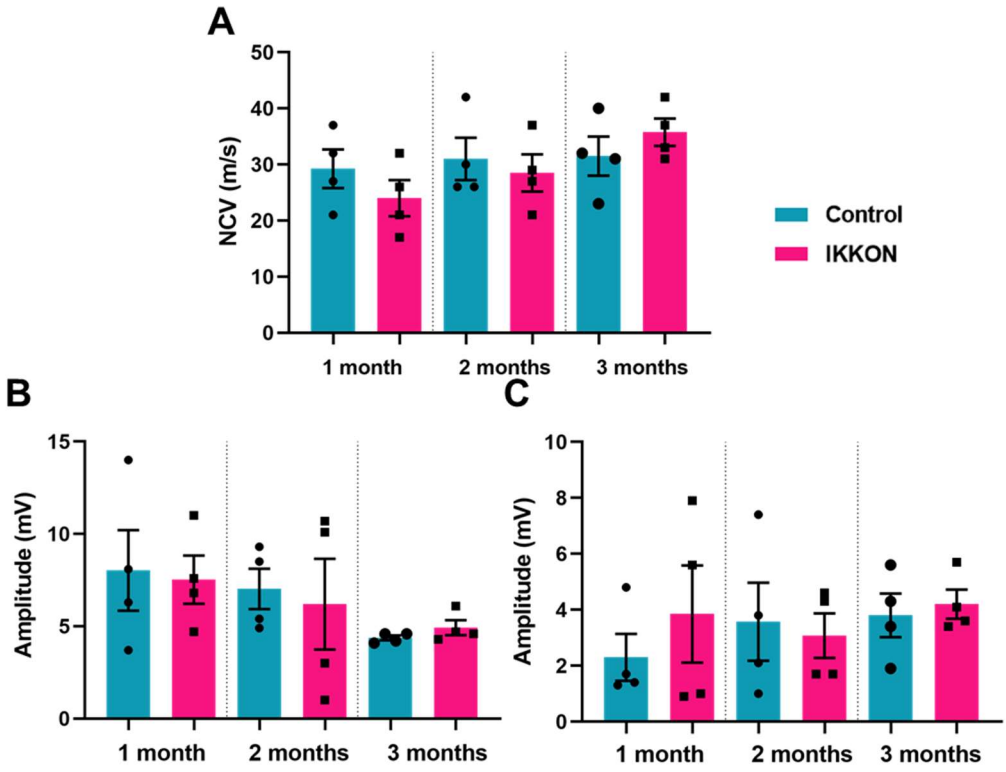

Figure 30. IKKON mice do not exhibit deficiencies in nerve conduction velocities or compound muscle action potential amplitude. (A) Average nerve conduction velocities derived by recording from foot muscles after proximal stimulation of sciatic nerves in 1, 2, 3 month old IKKON and control mice. IKKON mice display no initial deficits in NCV at 1 month, nor deterioration over time. (B) Average amplitude of compound muscle action potential (CAMP) recordings from IKKON and control foot muscles after stimulation at the ankle. (C) Average amplitude of CAMP recordings from foot muscles after stimulation at the popliteal fossa (knee). IKKON mice display no early deficiency, or deterioration, in CAMP amplitude over time. N=4 mice of each genotype, with repeated recordings from the same mice each month. mV, millivolt; m/s, meter per second. Data are shown as mean ± SEM.

IKKON mice have no significant changes motor function

As both sensory and motor neurons can be impaired by de/-dysmyelination, we investigated whether IKKON mice have motor/reflex deficits(Reilly, 2009). Motor function in IKKON mice was assessed using tail suspension. Mice were gently suspended by base of the tail and their ability to achieve and hold a reflexive paw splay formation for 15 seconds was evaluated. Five trials were recorded per mouse, with an inability to extend either limb fully, evidence of shaking/trembling, or clasped toes classified as a failed trial. IKKON mice performed similarly to control mice and displayed no overt evidence of muscle atrophy, suggesting that motor function is not disrupted in adult IKKON mice (Fig. 30).

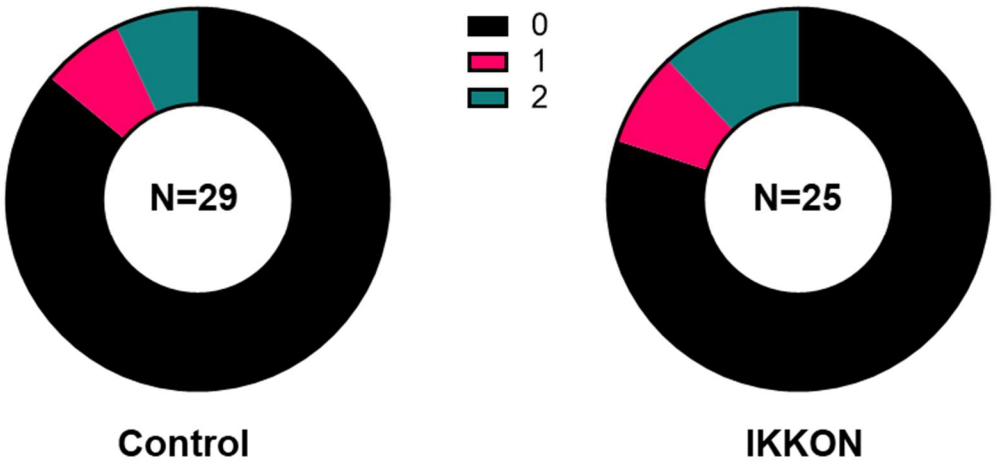

Figure 31. IKKON mice displayed no motor function abnormalities as measured by a tail suspension splay reflex. (A)Percentage of mice which achieved a reflexive paw splay formation in all trials (0), had a single failed trial out of five suspension trials (1) or displayed repeated abnormal splay formations over five trials (2). N=29 control mice. N=25 IKKON mice.

Elimination of NFκB signaling is detrimental to Trembler mice

The aberrant activation of NFκB in IKKON mice was not sufficient to provoke a de-/dysmyelinating phenotype, indicating that aberrant activation of NFκB in Schwann cells does not result in nerve pathology. Therefore, we next asked the converse; does deletion of NFκB in an existing model of de-/dysmyelinating CMT ameliorate neurological deficits. To test this, we first generated mice with conditional Schwann cell deletion of NFκB by crossing mice carrying a homozygous floxed null allele of IKK2 with the Dhh-Cre mice. We then crossed the resulting conditional IKK2 knock out (NFcKO) mice with Trembler-J (TrJ) heterozygous mice, which have a pathological mutation in PMP22 (L16P). The resulting TrJ/NFcKO mice, should have elimination of Schwann cell NFκB pathway signaling after E13.5 as well as a single copy of the L16P PMP22 mutation. Startlingly, TrJ/NFcKO mice displayed much more extreme neuropathic deficits than TrJ littermates. In addition to displaying smaller stature, and increased limb atrophy, ¾ TrJ/NFcKO (6 out of 8) mice developed complete hindlimb paralysis by the third week of life. In contrast, TrJ/DhhCre negative littermates showed no evidence of phenotype alterations/worsening neuropathy. Consequently, the experiment was terminated for humane reasons.

Discussion and Future Directions

Our results do not support the hypothesis that aberrant activation of the NFκB during development contributes to de-/dysmyelinating pathology in Schwann cells. Expression of IKK2SSEE was detected in sciatic nerve lysates of IKKON mice, and activation of NFκB pathway. However, IKKON mice developed no significant anatomical or behavioral neuropathic deficits. While it is possible IKKON may acquire neurological impairments as they age further or may have reduced ability to recover from nerve injury, these data suggest that IKKON mice do not have problems forming or maintaining myelin. There are two highly plausible explanations for this, either the IKKON do not have altered NFκB activity to the extent required to be detrimental to nerve development/maintenance,

or aberrant activation of NFκB pathway in isolation is tolerated by, even perhaps beneficial to, Schwann cells in some situations.

The first theory, that IKKON mice do not amplify NFκB activity to the extent required to provoke adverse outcomes in myelination is feasible and requires further investigation. NFκB activity in IKKON mice may be limited either by incomplete recombination or IKK2SSEE function in Schwann cells, or compensatory mechanisms. Schwann cell Cre expression is noted to be high in Dhh-Cre model, and IKK2SSEE expression was clearly visible by immunoblot in nerve lysates(Jaegle *et al.*, 2003). However, especially since IKK2SSEE is an enzyme, the degree of expression or penetrance may not have been sufficient to provoke widespread NFκB activation in Schwann cells. Additionally compensatory mechanisms may inhibit the effect of long term IKK2SSEE expression, as NFκB is prone to autoregulatory negative feedback inhibition, including by the IkBα subunit of the IkB complex, which is not degraded after IKK2 phosphorylation of IkBβ(Renner and Schmitz, 2009; Shih *et al.*, 2009). However, that we observed both an increase in p65 immunofluorescence signal in IKKON nerves, as well as changes in the localization within Schwann cells, suggests NFκB signaling is at least partially altered in IKKON mice.

To better evaluate the dynamics of NFκB activation in IKKON Schwann cells, NFκB activity should be directly quantified. This could be accomplished through electrophoretic mobility shift assay (EMSA), dual-luciferase assay, or both. If NFκB activation is compromised by compensatory mechanisms, or deficient expression, then an alternative model could be selected.

While our IKKON data does not support our initial hypothesis, the results of the TrJ/NFcKO seem to actively contradict it. If sustained NFκB activation promotes de-/dysmyelination we would expect that elimination of NFκB signaling in TrJ Schwann cells would lessen the degree of neurological impairment. Instead, we saw a robust worsening of the TrJ phenotype, to the point of hind limb paralysis, indicating that reducing NFκB signaling is detrimental to TrJ nerve pathology. However, these results could be either due to beneficial effects of NFκB signaling in the TrJ pathology, or to negative effects from eliminating NFκB signaling during development, or both. NFκB signaling is thought

to regulate both myelin formation, and repair mechanisms(Bermingham *et al.*, 1996; Jaegle *et al.*, 2003; Yoon, Korade and Carter, 2008; Morton *et al.*, 2012). NFκB is activated in Schwann cells during myelin formation and *in vitro* results demonstrated that blocking or deleting NFκB reduced myelin formation (Nickols et al., 2003). However, conditional deletion of IKK2 in Schwann cells, which blocked NFκB activation, did not impair myelination *in vivo* (Morton *et al.*, 2013). Therefore, it is possible that compensatory mechanisms allow myelin to form *in vivo*, but if there is an underlying pathology (e.g., TrJ), then loss of NFκB signaling exacerbates the dysmyelination. On the other hand, NFκB signaling during pathology is thought to help in the recruitment of macrophages, but it remains controversial as to whether the presence of these immune cells is beneficial or detrimental (Martini *et al.*, 2008; Smith *et al.*, 2009). Therefore, the more severe phenotype observed in the TrJ/NFcKO mice could also reflect the loss of beneficial macrophage recruitment.

To determine whether NFκB is important for Schwann cells to form myelin, which is impaired in TrJ mice, or critical for recruiting macrophages, which may be beneficial in TrJ pathology, an inducible Cre line could be utilized to delete IKK only after a baseline assessment of neuropathy was established. Then mice could be monitored for evidence of deterioration. Macrophage recruitment could also be evaluated, comparing WT and the conditional knock out. Since TrJ is a model of a rare, pathologically distinct form of CMT1, deletion of NFκB in other models of CMT, such as the CMT1A mimic C3 model may assist in evaluating whether suppression of NFκB is widely detrimental in de-/dysmyelinating CMT pathology (Verhamme *et al.*, 2011).

Our data in this project was entirely counter to what we expected. However, our TrJ/NFcKO results do suggest there is a clear link between NFκB pathway deletion and the magnification of neuropathic symptoms. Further exploration of this connection may offer greater insight into the true role of NFκB in neuropathy and in normal development. If NFκB signaling is indeed a beneficial pathway in some instances of neuropathy, or if its elimination during development has adverse effects on the ability to tolerate later neurotoxic insults, such as frequently occur in chemotherapy or diabetes, it would be an important consideration when evaluating future therapeutics. Especially, considering

many recent studies have focused on developing treatments reducing NFκB signaling, and other potentially inflammatory signaling pathways in neuropathy and other diseases (Cameron and Cotter, 2008; Epstein, Sanderson and Macdonald, 2010; Jani *et al.*, 2010; Suryavanshi and Kulkarni, 2017) .

Appendix II

Supplementary Tables and Bibliography

Table of Reagents

REAGENT or RESOURCE	SOURCE	IDENTIFIER
Antibodies		
V5	Invitrogen	Cat# R960-25
actin	Santa Cruz Biotechnology	Cat# SC-32251
Tubulin	Santa Cruz Biotechnology	Cat# SC-8035 RRID:AB_628408
SREBP2	BD Biosciences	Cat#557037 RRID:AB_396560
ErbB2	Santa Cruz Biotechnology	Cat# SC-284
ErbB3	Santa Cruz Biotechnology	Cat# SC-285, SC-7390
Phospho Tyrosine (4G10)	Millipore	Cat# 05-321
Phospho Tyrosine (PY99)	Santa Cruz Biotechnology	Cat# SC-7020
596-Alexa Flour Goat anti-Rabbit	Invitrogen	Cat# A-11012
596-Alexa Flour Goat anti-Mouse	Invitrogen	Cat#A-11031 RRID:AB_141369
Chemicals, Peptides, and Recombinant Proteins		
PFA	Sigma-Aldrich	Cat# P6148
7-DHC	Sigma-Aldrich	Cat#30800-5G-F
C13-Glucose	Cambridge Isotope Lab	CLM-1396-0
Chloroform	Sigma-Aldrich	Cat#270636
Methanol	Fisher Scientific	Cat#A412P-4
Fish Gelatin	Sigma-Aldrich	Cat#G7765
Triton-X	Sigma Aldrich	Cat#T8787
Ethyl alcohol, Pure	Sigma-Aldrich	Cat# SHBJ7192
Trypsin	Worthington	Cat#LS003708

Nerve growth factor	Alomone	N-100
GGF-Recombinant Human NRG1-beta 1/HRG1-beta 1 EGF Domain Protein	*R&D* Systems	Cat# 396-HB
Collagenase	Sigma-Aldrich	Cat# C5894-50MG
Poly-D-lysine	Fisher Scientific	Cat# 215017525
Laminin	Fisher Scientific	Cat # 354232
Xylenes	Fisher Scientific	Cat# X3F-1Gal
DPX mounting media	Electron Microscopy Solutions	Cat#13512
Toluidine Blue	Sigma-Aldrich	Cat# 89640-5G
RNAse Inhibitor	Invitrogen	Cat#N8080119
TRIzol™	Invitrogen	Cat#15596026
Hoechst 33258	Molecular Probes	Cat#H-3569
100x N2	Gibco	Cat# 17502-048
Collagen Type 1A	Sigma Aldrich	Cat#C3867
50x B27	Gibco	Cat#17504-044
Dnase I	Sigma-Aldrich	Cat #D5025
Forskolin	Sigma-Aldrich	F6886-10MG
Experimental Models: Organisms/Strains		
P75-floxed ($p75^{fl/fl}$) mice		Bogenmann et al., 2011
Thy1-cre	The Jackson Laboratory	Stock # 006143 RRID:IMSR_JAX:006143
Dhh-cre	The Jackson Laboratory	Stock # 012929 RRID:IMSR_JAX:012929
P75 knockout	The Jackson Laboratory	Stock # 002213 RRID:IMSR_JAX:002213
C57BL/6J (WT)	The Jackson Laboratory	Stock #000664 RRID:IMSR_JAX:000664
Sequence Based Reagents		
RNAscope® Positive Control Probe- Mm-Ppib-C2	ACDbio	Cat#313911-C2
RNAscope® Negative Control Probe- DapB	ACDbio	Cat#310043
RNAscope® Probe- Mm-Ntrk1-C3	ACDbio	Cat#435791-C3

RNAscope® Probe- Mm-Ntrk2	ACDbio	Cat#423611
RNAscope® Probe- Mm-Ntrk3-C2	ACDbio	Cat#423621-C2
RNAscope® Probe- Mm-Ret-C2	ACDbio	Cat#431791-C2
TaqMan qPCR assay mouse 7-dhcr	IDT	Assay number Mm00514571_m1
TaqMan qPCR assay mouse Gapdh	IDT	Assay number Mm99999915_g1
Recombinant DNA		
pLX304 vector	Addgene	#25890
DHCR7-pLX304	CCSB-Broad Lentiviral Expression Collection	ccsbBroad304_06097
psPax2	Addgene	#12260
pMD2.G	Addgene	#12259
NRG 1-Type III	Dr. Doug Falls	
pSIREN-RetroQ-ZsGreen1-ErbB2i-a AAGTCTCACAGAGATCCTG	This paper	
pSIREN-RetroQ-ZsGreen1-ErbB2i-b ACCACGTCAAGATTACAGA	This paper	
pSIREN-RetroQ-ZsGreen1-ErbB2i-c ATCATAGTGGTATCTGTGA	This paper	
pSIREN-RetroQ-ZsGreen1-ErbB3i-a TCTGGACTTCCTCATCACC	This paper	
pSIREN-RetroQ-ZsGreen1-ErbB3i-b GAACTTGAATGTCACATCC	This paper	
pSIREN-RetroQ-ZsGreen1-ErbB3i-c CCTGACAAGATGGAAGTAGAT	This paper	
pSIREN-RetroQ-ZsGreen1-p75i-a		Vilar et al., 2009
Software and Algorithms		

FIJI	FIJI/NIH	https://fiji.sc/
Prism 6/7	GraphPad Software	http://www.graphpad.com/scientific-software/prism/
NIS-Elements	Nikon	https://www.microscope.healthcare.nikon.com/products/software/nis-elements
AMT	Advanced Microscopy Techniques	http://www.amtimaging.com/www11/english/product_e.html#soft
MetaXpress® 4	Molecular Devices	https://www.moleculardevices.com/products/cellular-imaging-systems/acquisition-and-analysis-software/metaxpress#gref
Other		
RNAscope® Multiplex Fluorescent Reagent Kit v2	ACDbio	Cat# 323100
TSA® Plus Cyanine 3 (Cy3) detection kit	Perkin Elmer	Cat# NEL744001KT
RNeasy Mini Kit (50)	Qiagen	Cat# 74104
High-Capacity cDNA Reverse Transcription Kit	Thermo Fischer	Cat# 4368814
BCA Protein Assay Kit	Pierce	Cat#23225
Costar 96 well culture cluster	Costar	Cat# 3595
Taqman Fast Advanced Master Mix	Invitrogen	Cat#4444556
Hyclone Fetal Bovine Serum	Hyclone	Cat#SH30088.03
Fetal Bovine Serum	Omega Scientific	Cat#FB-01
DMEM, high glucose, pyruvate	Gibco	Cat#11995-065
Prolong Antifade Reagent w/DAPI	Life Technologies	Cat#P36931

Table 5. Comprehensive List of Reagents

UPLC-MS/MS Tables

Compound	Class	Annotation	P Value	q Value	Max Fold Change	Direction
7.84_307.2635m/z	Free fatty acid	FA(20:2)	5.20E-05	0.036	2.03	Positive
9.97_1207.7692m/z	Ganglioside GM3	GM3(38:1;2O)	0.041	0.264	2.41	Positive
10.91_1341.8290m/z	Lysocardiolipin	MLCL(66:12)	0.031	0.239	11.73	Positive
14.93_637.6037n	Ceramide alpha-hydroxy fatty acid-sphingosine	Cer_AS(18:1/22:0;2O)	0.015	0.177	1.21	Positive
15.43_668.6227m/z	Ceramide non-hydroxyfatty acid-dihydrosphingosine	Cer_NDS(40:0;2O)	0.022	0.208	1.26	Positive
16.01_696.6543m/z	Ceramide non-hydroxyfatty acid-dihydrosphingosine	Cer_NDS(18:0/24:0;2O)	0.032	0.245	1.25	Positive
7.10_374.2461m/z	Ceramide non-hydroxyfatty acid-sphingosine	Cer_NS(20:2;2O)	0.008	0.144	1.93	Positive
9.31_374.2464m/z	Ceramide non-hydroxyfatty acid-sphingosine	Cer_NS(20:2;2O)	0.011	0.162	1.78	Positive
8.60_374.2465m/z	Ceramide non-hydroxyfatty acid-sphingosine	Cer_NS(20:2;2O)	0.039	0.263	1.74	Positive
7.84_374.2461m/z	Ceramide non-hydroxyfatty acid-sphingosine	Cer_NS(20:2;2O)	0.014	0.171	1.66	Positive
11.67_1005.5358m/z	Diacylated phosphatidylinositol monomannoside	Ac2PIM1(32:1)	0.030	0.238	1.13	Positive
5.19_1169.7733m/z	Digalactosyldiacylglycerol	DGDG(50:5)	0.011	0.162	1.22	Positive
5.13_552.3213m/z	Ether-linked lysophosphatidylethanolamine	LPE(O-22:3)	0.029	0.233	1.16	Positive
7.80_523.3443m/z	Ether-linked lysophosphatidylglycerol	LPG(O-20:1)	0.027	0.225	1.23	Positive
19.29_764.5840m/z	Ether-linked phosphatidylcholine	PC(O-32:0)	0.050	0.279	1.10	Positive
15.66_756.5948m/z	Ether-linked phosphatidylethanolamine	PE(P-18:0/20:1)	0.002	0.091	1.24	Positive
15.03_704.5612m/z	Ether-linked phosphatidylethanolamine	PE(O-18:0/16:0)	0.002	0.091	1.19	Positive
14.75_667.6126n	Ether-linked phosphatidylethanolamine	PE(P-18:0/16:0)	0.011	0.162	1.14	Positive

15.61_782.6135m/z	Ether-linked phosphatidylethanolamine	PE(O-18:2_22:1)	0.001	0.062	1.11	Positive
14.77_754.5780m/z	Ether-linked phosphatidylethanolamine	PE(P-18:1/20:1)	0.000	0.043	1.10	Positive
7.07_399.2525m/z	Fatty acid ester of hydroxyl fatty acid	FAHFA(25:6)	0.028	0.230	1.46	Positive
7.04_305.2493m/z	Free fatty acid	FA(20:3)	0.002	0.090	1.99	Positive
11.39_365.3435m/z	Free fatty acid	FA(24:1)	0.000	0.043	1.65	Positive
6.63_305.2495m/z	Free fatty acid	FA(20:3)	0.013	0.171	1.45	Positive
7.53_357.2808m/z	Free fatty acid	FA(24:5)	0.036	0.257	1.45	Positive
9.25_409.3121m/z	Free fatty acid	FA(28:7)	0.045	0.271	1.14	Positive
14.52_1265.8498m/z	Ganglioside GM3	GM3(42:0;2O)	0.010	0.159	1.28	Positive
15.66_1584.1709m/z	Ganglioside GM3	GM3(65:2;2O)	0.039	0.263	1.18	Positive
14.55_1672.2248m/z	Ganglioside GM3	GM3(68:2;2O)	0.022	0.206	1.06	Positive
14.95_785.6759n	Hexosylceramide non-hydroxyfatty acid-dihydrosphingosine	HexCer_NDS(40:0;2O)	0.001	0.078	1.28	Positive
11.04_518.3720m/z	Hexosylceramide non-hydroxyfatty acid-dihydrosphingosine	HexCer_NDS(21:0;2O)	0.019	0.193	1.23	Positive
15.35_811.6941n	Hexosylceramide non-hydroxyfatty acid-sphingosine	HexCer_NS(18:1_24:0;2O)	0.001	0.058	1.36	Positive
14.72_828.6620m/z	Hexosylceramide non-hydroxyfatty acid-sphingosine	HexCer_NS(18:1_22:0;2O)	0.000	0.043	1.34	Positive
15.91_884.7181m/z	Hexosylceramide non-hydroxyfatty acid-sphingosine	HexCer_NS(44:1;2O)	0.005	0.118	1.25	Positive
15.05_842.6766m/z	Hexosylceramide non-hydroxyfatty acid-sphingosine	HexCer_NS(18:1_23:0;2O)	0.010	0.159	1.19	Positive
14.67_854.6772m/z	Hexosylceramide non-hydroxyfatty acid-sphingosine	HexCer_NS(20:2_22:0;2O)	0.005	0.118	1.17	Positive
14.92_811.6935n	Hexosylceramide non-hydroxyfatty acid-sphingosine	HexCer_NS(42:1;2O)	0.008	0.152	1.16	Positive
13.98_826.6448m/z	Hexosylceramide non-hydroxyfatty acid-sphingosine	HexCer_NS(40:2;2O)	0.003	0.101	1.12	Positive
15.28_837.7044n	Hexosylceramide non-hydroxyfatty acid-sphingosine	HexCer_NS(18:1_26:1;2O)	0.021	0.206	1.10	Positive
4.15_612.3326m/z	Lysophophatidylcholine	LPC 22:6	0.031	0.238	1.28	Positive
4.75_590.3489m/z	Lysophophatidylcholine	LPC 20:3	0.029	0.233	1.19	Positive
5.03_480.3101m/z	Lysophosphatidylethanolamine	LPE 18:0	0.045	0.271	1.10	Positive
7.33_642.4133m/z	Monomethyl-Phosphatidylethanolamine	MMPE(28:3))	0.012	0.166	1.55	Positive

9.33_542.3519m/z	Oxidized sulfonolipid	SL(29:3;2O)	0.002	0.091	1.30	Positive
15.84_856.6116m/z	Phosphatidylcholine	PC 18:0_20:3	0.009	0.154	1.29	Positive
16.71_828.6441m/z	Phosphatidylethanolamine	PE 42:1	0.021	0.206	1.20	Positive
15.08_772.5877m/z	Phosphatidylethanolamine	PE 38:1	0.003	0.095	1.16	Positive
15.82_826.6275m/z	Phosphatidylethanolamine	PE 18:1_24:1	0.004	0.112	1.12	Positive
11.11_684.4636m/z	Phosphatidylethanolamine	PE 16:0_16:3	0.046	0.273	1.11	Positive
12.00_809.5197m/z	Phosphatidylinositol	PI 16:0_16:0	0.002	0.091	1.11	Positive
22.78_872.6386m/z	Phosphatidylserine	PS 42:1	0.015	0.176	1.14	Positive
22.80_799.5655n	Phosphatidylserine	PS 22:0_18:1	0.011	0.162	1.07	Positive
22.80_842.5949m/z	Phosphatidylserine	PS 18:1_22:1	0.011	0.162	1.07	Positive
21.51_831.6633m/z	Sphingomyelin	SM(40:1;2O)	0.001	0.062	1.26	Positive
20.18_857.6799m/z	Sphingomyelin	SM(42:2;2O)	0.025	0.223	1.17	Positive
20.11_993.6538m/z	Sphingomyelin	SM(54:13;2O)	0.016	0.183	1.16	Positive
13.90_876.6275m/z	Sulfatide	SHexCer(41:1);2O)	0.002	0.091	1.24	Positive
9.25_1337.7588m/z	Triacylated phosphatidylinositol dimannoside	Ac3PIM2(43:0)	0.003	0.100	1.29	Positive
13.57_998.5892m/z	Trihexosylceramide	Hex3Cer(29:1;2O)	0.007	0.140	1.40	Positive
21.69_1673.3717m/z	Trihexosylceramide	Hex3Cer(77:0;2O)	0.029	0.233	1.30	Positive
15.56_1687.2822m/z	Trihexosylceramide	Hex3Cer(79:7;2O)	0.006	0.126	1.29	Positive
22.78_1002.5682m/z	Trihexosylceramide	Hex3Cer(30:1;2O)	0.026	0.223	1.26	Positive
13.53_1024.6057m/z	Trihexosylceramide	Hex3Cer(31:2;2O)	0.012	0.164	1.17	Positive
5.14_1597.1454m/z	Trihexosylceramide	Hex3Cer(73:10;2O)	0.042	0.266	1.16	Positive
18.35_1010.5744m/z	Trihexosylceramide	Hex3Cer(34:7;2O)	0.019	0.197	1.09	Positive
7.32_605.4460m/z	Esterified deoxycholic acid	ST 24:1;O4/11:0	0.040	0.264	1.18	Positive
14.87_1362.1720m/z	Oxidized sphingomyelin	SM(78:4;3O)	0.011	0.162	2.07	Negative
12.69_902.6070m/z	Oxidized ceramide phosphoethanolamine	PI-Cer(42:3;3O)	0.000	0.043	1.31	Negative
12.02_900.5848m/z	Phosphatidylcholine	PC 42:9	0.000	0.036	1.22	Negative
13.78_1626.2016m/z	Ganglioside GM3	GM3(68:2;2O)	0.000	0.036	1.21	Negative
11.50_712.4950m/z	Phosphatidylethanolamine	PE 16:1_18:2	0.002	0.091	1.21	Negative
12.43_1425.0376m/z	Dihexosylceramide	Hex2Cer(73:10;2O)	0.030	0.238	1.20	Negative
12.51_1456.0439m/z	Cardiolipin	CL(72:4)	0.018	0.191	1.20	Negative

12.28_1428.0157m/z	Cardiolipin	CL(70:4)	0.037	0.259	1.19	Negative
11.50_551.4932n	Ceramide non-hydroxyfatty acid-phytospingosine	Cer_NP(34:2;3O)	0.040	0.264	1.19	Negative
11.06_736.4952m/z	Phosphatidylethanolamine	PE 18:2_18:3	0.002	0.091	1.19	Negative
14.49_1390.1651m/z	Sphingomyelin	SM(81:9;2O)	0.048	0.277	1.18	Negative
9.72_803.4674m/z	Phosphatidylinositol	PI(32:3)	0.002	0.091	1.18	Negative
11.42_686.4803m/z	Phosphatidylethanolamine	PE 14:0_18:2	0.003	0.095	1.18	Negative
14.49_758.5935m/z	N-acyl glycine	NAGly(43:4)	0.033	0.247	1.16	Negative
9.33_481.3379m/z	Free fatty acid	FA(30:8)	0.035	0.253	1.15	Negative
12.49_1430.0283m/z	Cardiolipin	CL(70:3)	0.030	0.236	1.14	Negative
14.90_1569.2515m/z	Trihexosylceramide	Hex3Cer(73:1;2O)	0.043	0.267	1.14	Negative
15.46_706.6387m/z	Ceramide non-hydroxyfatty acid-sphingosine	Cer_NS(43:2;2O)	0.017	0.188	1.13	Negative
12.53_740.5265m/z	Phosphatidylethanolamine	PE 18:1_18:2	0.002	0.091	1.13	Negative
1.43_1071.1125m/z	Ceramide non-hydroxyfatty acid-dihydrosphingosine	Cer_NDS(72:0;2O)	0.021	0.206	1.12	Negative
11.60_839.5206m/z	Diacylglyceryl glucuronide	DGGA(40:8)	0.014	0.176	1.12	Negative
12.31_688.4955m/z	Phosphatidylethanolamine	PE 14:0_18:1	0.004	0.105	1.11	Negative
13.78_1600.1741m/z	Lysocardiolipin	MLCL(84:9)	0.006	0.129	1.11	Negative
12.26_784.5165m/z	Phosphatidylserine	PS 36:3	0.019	0.196	1.11	Negative
11.93_738.5113m/z	Phosphatidylethanolamine	PE(36:4)	0.003	0.095	1.10	Negative
13.76_1572.1317m/z	Lysocardiolipin	MLCL(82:9)	0.000	0.043	1.10	Negative
12.26_790.5418m/z	Phosphatidylethanolamine	PE 18:1_22:5	0.008	0.146	1.10	Negative
12.48_714.5119m/z	Phosphatidylethanolamine	PE 16:0_18:2	0.007	0.140	1.09	Negative
11.44_762.5112m/z	Phosphatidylethanolamine	PE 18:2_20:4	0.009	0.153	1.09	Negative
11.26_736.4950m/z	Phosphatidylethanolamine	PE 16:1_20:4	0.017	0.188	1.09	Negative
12.86_1578.0888m/z	Ganglioside GM3	GM3(62:2;2O)	0.002	0.090	1.09	Negative
10.81_734.4838m/z	Phosphatidylethanolamine	PE 14:0_22:6	0.042	0.265	1.09	Negative
13.14_812.5474m/z	Phosphatidylserine	PS(38:3)	0.006	0.129	1.08	Negative
14.52_1656.2612m/z	Ganglioside GM3	GM3(70:1;2O)	0.012	0.163	1.08	Negative
12.86_1552.0818m/z	Ganglioside GM3	GM3(60:1;2O)	0.003	0.095	1.07	Negative
11.92_814.5335m/z	Phosphatidylethanolamine	PE 20:4_22:4	0.048	0.277	1.07	Negative

12.26_663.4867n	Phosphatidylethanolamine	PE 14:0_16:0	0.030	0.238	1.07	Negative
13.35_742.5437m/z	Phosphatidylethanolamine	PE 18:1_18:1	0.012	0.166	1.06	Negative
13.61_768.5580m/z	Phosphatidylethanolamine	PE 18:0_20:3	0.002	0.090	1.05	Negative
3.46_1318.1983m/z	Oxidized sphingomyelin	SM(77:1;3O)	0.029	0.233	1.05	Negative

Table 6. Lipid Compounds with Altered Abundance Recorded in Negative Mode. Levels in P6 Sciatic nerves $p75^{KO}$ compared to WT control. All lipids significantly altered (P≤ 0.05 by Anova) and with structure confidence level L3a or above. m/z; mass (m) to charge (z) ratio

Compound	Class	Annotation	P Value	q Value	Max Fold Change	Direction
12.55_1281.7861m/z	Ganglioside GM3	GM3(40:1;2O)	0.001	0.022	2.38	Negative
5.54_356.2594m/z	Phytosphingosine	SPB(18:0;3O)	0.002	0.030	1.74	Negative
12.00_1426.0087m/z	Ganglioside GM3	GM3(55:3;2O)	0.021	0.071	1.70	Negative
11.57_1253.7559m/z	Ganglioside GM3	GM3(38:1;2O)	0.000	0.017	1.54	Negative
18.88_1424.9520n	Cardiolipin	CL(70:6)	0.007	0.043	1.52	Negative
4.44_570.3487m/z	Oxidized lysophosphatidylcholine	OxLPC(18:1(OOO))	0.031	0.086	1.42	Negative
10.30_605.4614n	Phosphatidylcholine	PC 26:0	0.015	0.061	1.27	Negative
11.51_714.4971m/z	Phosphatidylethanolamine	PE 34:3	0.000	0.012	1.27	Negative
11.05_755.5014n	Phosphatidylethanolamine	PE 36:5	0.000	0.017	1.26	Negative
10.88_1221.8123m/z	Ganglioside GM3	GM3(40:0;2O)	0.032	0.087	1.25	Negative
10.81_736.4829m/z	Phosphatidylethanolamine	PE 14:0_22:6	0.000	0.017	1.25	Negative
11.85_717.4840n	Phosphatidylethanolamine	PE 18:1_18:3	0.000	0.010	1.24	Negative
11.16_711.4750n	Phosphatidylethanolamine	PE 34:4	0.001	0.018	1.24	Negative
11.43_688.4829m/z	Phosphatidylethanolamine	PE 14:0_18:2	0.000	0.003	1.24	Negative
11.18_698.5422m/z	Hexosylceramide non-hydroxyfatty acid-sphingosine	HexCer_NS(18:2_16:0;2O)	0.011	0.053	1.24	Negative

11.16_661.4605n	Phosphatidylethanolamine	PE 14:0_16:1	0.001	0.020	1.22	Negative
11.00_724.5069n	Monogalactosyldiacylglycerol	MGDG(14:0_18:3)	0.001	0.017	1.22	Negative
11.75_726.5777m/z	Hexosylceramide non-hydroxyfatty acid-sphingosine	HexCer_NS(18:1_18:1;2O)	0.000	0.011	1.22	Negative
12.55_777.5433n	Phosphatidylethanolamine	PE 18:1_18:2	0.000	0.016	1.21	Negative
11.11_758.4889m/z	Phosphatidylserine	PS 34:3	0.000	0.012	1.21	Negative
12.31_1456.0246m/z	Cardiolipin	CL(72:5)	0.000	0.017	1.20	Negative
14.16_638.5656m/z	Diacylglycerol	DG(18:1_18:1)	0.032	0.088	1.20	Negative
13.16_1412.0547m/z	Phosphatidylcholine	PC 82:20	0.023	0.073	1.20	Negative
12.02_721.5190n	Phosphatidylcholine	PC 30:1	0.002	0.028	1.19	Negative
12.31_689.4915n	Phosphatidylethanolamine	PE 14:0_18:1	0.000	0.001	1.19	Negative
11.13_671.5252n	Hexosylceramide non-hydroxyfatty acid-sphingosine	HexCer_NS(18:1_14:0;2O)	0.006	0.040	1.19	Negative
12.66_692.5133m/z	Phosphatidylcholine	PC 29:0	0.000	0.012	1.19	Negative
12.17_730.5294m/z	Phosphatidylcholine	PC 14:0_18:2	0.002	0.026	1.19	Negative
12.00_698.5339m/z	Hexosylceramide non-hydroxyfatty acid-sphingosine	HexCer_NS(18:1_16:1;2O)	0.001	0.017	1.18	Negative
12.48_716.5141m/z	Phosphatidylethanolamine	PE 16:1_18:1	0.000	0.016	1.18	Negative
12.55_837.5405n	Phosphatidylserine	PS 18:0_22:5	0.003	0.030	1.18	Negative
13.39_1603.2079m/z	Ganglioside GM3	GM3(65:2;2O)	0.039	0.097	1.18	Negative
12.64_756.5447m/z	Phosphatidylcholine	PC 16:0_18:3	0.004	0.036	1.18	Negative
12.28_615.5219m/z	Ether-linked diacylglycerol	DG(O-40:8)	0.006	0.039	1.17	Negative
12.28_792.5441m/z	Phosphatidylethanolamine	PE 18:1_22:5	0.009	0.049	1.17	Negative
13.11_814.5465m/z	Phosphatidylserine	PS 38:3	0.002	0.026	1.16	Negative
11.26_737.4903n	Phosphatidylethanolamine	PE 16:1_20:4	0.002	0.029	1.14	Negative
13.49_840.5638m/z	Phosphatidylserine	PS 40:4	0.034	0.090	1.14	Negative
11.92_816.5436m/z	Phosphatidylcholine	PC 17:2_22:6	0.013	0.056	1.14	Negative
11.43_723.5010m/z	Monogalactosyldiacylglycerol	MGDG(14:0_16:1)	0.001	0.020	1.14	Negative
14.13_862.6220m/z	Phosphatidylcholine	PC 42:6	0.029	0.083	1.14	Negative
13.16_723.5341n	Phosphatidylcholine	PC 30:0	0.000	0.001	1.14	Negative
12.46_1490.0385m/z	Cardiolipin	CL(76:7)	0.003	0.030	1.13	Negative
11.89_1527.0211n	Cardiolipin	CL(78:11)	0.003	0.033	1.13	Negative

10.17_257.2007m/z	Acylcarnitine	CAR(7:0)	0.001	0.019	1.13	Negative
14.21_745.5540n	Phosphatidylethanolamine	PE 36:1	0.046	0.103	1.13	Negative
12.43_888.5612n	Phosphatidylinositol	PI 38:3	0.010	0.051	1.13	Negative
14.23_1492.1297m/z	Phosphatidylcholine	PC 88:22	0.017	0.065	1.13	Negative
12.28_1601.0459n	Cardiolipin	CL(84:16)	0.003	0.030	1.13	Negative
13.35_744.5455m/z	Phosphatidylethanolamine	PE 18:1_18:1	0.004	0.036	1.13	Negative
12.36_1438.0078m/z	Cardiolipin	CL(72:5)	0.021	0.072	1.13	Negative
13.49_636.5455m/z	Diacylglycerol	DG 18:1_18:2	0.006	0.041	1.13	Negative
12.89_1466.0397m/z	Cardiolipin	CL(74:5)	0.019	0.069	1.12	Negative
13.55_758.5610m/z	Phosphatidylcholine	PC 34:2	0.005	0.039	1.12	Negative
11.87_714.4976m/z	Phosphatidylethanolamine	PE 16:0_18:3	0.027	0.080	1.12	Negative
11.34_674.4881n	Monogalactosyldiacylglycerol	MGDG(14:0_14:0)	0.027	0.080	1.12	Negative
11.44_763.5068n	Phosphatidylethanolamine	PE 18:2_20:4	0.012	0.055	1.12	Negative
11.94_1519.0723m/z	Phosphatidylcholine	PC 88:22	0.044	0.100	1.12	Negative
13.81_796.5759m/z	Phosphatidylethanolamine	PE 40:4	0.027	0.079	1.12	Negative
17.97_787.6008n	Phosphatidylcholine	PC 36:1	0.034	0.091	1.12	Negative
11.72_731.5397n	Phosphatidylcholine	PC 34:4	0.001	0.021	1.12	Negative
13.75_1580.1094m/z	Cardiolipin	CL(84:9)	0.038	0.095	1.12	Negative
13.21_820.5684m/z	Phosphatidylethanolamine	PE 42:6	0.005	0.039	1.12	Negative
12.73_1486.0351m/z	Cardiolipin	CL(76:9)	0.001	0.020	1.12	Negative
12.27_725.5581n	Hexosylceramide non-hydroxyfatty acid-sphingosine	HexCer_NS(18:2_18:0;2O)	0.003	0.033	1.12	Negative
13.63_747.6115n	Phosphatidylethanolamine	PE 18:0_20:3	0.002	0.028	1.12	Negative
11.59_840.5454m/z	Phosphatidylethanolamine	PE 22:4_22:6	0.011	0.054	1.11	Negative
12.74_1452.9975n	Cardiolipin	CL(72:6)	0.002	0.026	1.11	Negative
10.90_386.3731m/z	Ceramide non-hydroxyfatty acid-sphingosine	Cer_NDS(23:0;2O)	0.027	0.080	1.11	Negative
10.93_762.5000m/z	Phosphatidylethanolamine	PE 18:3_20:4	0.036	0.093	1.11	Negative
12.17_835.5256n	Phosphatidylserine	PS 40:6	0.010	0.051	1.11	Negative
12.81_1454.0436m/z	Ganglioside GM3	GM3(57:3;2O)	0.046	0.103	1.11	Negative
14.05_568.5591m/z	Ceramide non-hydroxyfatty acid-sphingosine	Cer_NDS(36:0;2O)	0.013	0.056	1.11	Negative

12.66_788.5345m/z	Phosphatidylserine	PS 36:2	0.007	0.042	1.10	Negative
12.78_775.5457n	Ether-linked lysophosphatidylethanolamine	PE(P-18:1/22:5)	0.015	0.061	1.10	Negative
11.11_884.5295n	Phosphatidylinositol	PI 38:5	0.022	0.073	1.10	Negative
9.51_749.4506m/z	Sphingomyelin	SM(35:7;2O)	0.038	0.095	1.10	Negative
12.35_1514.0399m/z	Cardiolipin	CL(78:9)	0.026	0.079	1.10	Negative
12.30_766.5292m/z	Phosphatidylethanolamine	PE 18:1_20:4	0.010	0.051	1.10	Negative
12.61_1574.0520m/z	Cardiolipin	CL(78:7)	0.032	0.088	1.10	Negative
14.52_663.6081n	Ceramide non-hydroxyfatty acid-sphingosine	Cer_NS(42:3;2O)	0.015	0.061	1.10	Negative
12.91_673.4971n	Ether-linked lysophosphatidylethanolamine	PE(P-32:1)	0.000	0.016	1.10	Negative
11.80_780.5431m/z	Phosphatidylcholine	PC 36:5	0.021	0.072	1.10	Negative
12.74_364.2568m/z	N-acyl ethanolamines	NAE(18:1)	0.006	0.041	1.09	Negative
11.69_860.5301n	Phosphatidylinositol	PI 36:3	0.006	0.040	1.09	Negative
12.84_1542.0708m/z	Cardiolipin	CL(80:9)	0.044	0.100	1.09	Negative
13.85_1492.0802m/z	Cardiolipin	CL(76:6)	0.019	0.069	1.09	Negative
11.89_746.5082n	Phosphatidylethanolamine	PE 38:6	0.047	0.104	1.09	Negative
13.19_1535.0684n	Cardiolipin	CL(78:7)	0.001	0.020	1.09	Negative
12.20_862.5461n	Phosphatidylinositol	PI 36:2	0.004	0.036	1.09	Negative
12.08_796.5785m/z	Monogalactosyldiacylglycerol	MGDG(18:1_18:3)	0.002	0.030	1.09	Negative
14.41_760.5771m/z	Phosphatidylcholine	PC 34:1	0.011	0.054	1.09	Negative
12.08_783.5341n	Phosphatidylcholine	PC 18:2_20:4	0.026	0.079	1.09	Negative
11.79_759.5523n	Phosphatidylethanolamine	PE 36:3	0.009	0.048	1.08	Negative
14.21_720.5457m/z	Phosphatidylcholine	PC 31:0	0.047	0.104	1.07	Negative
13.30_1485.0811n	Cardiolipin	CL(74:4)	0.036	0.093	1.07	Negative
12.38_364.2568m/z	N-acyl ethanolamines	NAE(18:1)	0.015	0.061	1.07	Negative
12.94_1482.0694m/z	Ganglioside GM3	GM3(59:3;2O)	0.044	0.101	1.07	Negative
11.61_809.5098n	Phosphatidylserine	PS 38:5	0.031	0.086	1.06	Negative
10.96_699.5494n	Hexosylceramide non-hydroxyfatty acid-sphingosine	HexCer_NS(18:1_16:0;2O)	0.025	0.076	1.06	Negative
12.64_753.6012n	Monogalactosyldiacylglycerol	MGDG(18:1_18:2)	0.046	0.103	1.05	Negative

12.03_626.5031n	Vitamin E	VAE 24:5	0.046	0.103	1.05	Negative
9.86_813.6744m/z	Sphingomyelin	SM(42:2;2O)	0.036	0.093	1.05	Negative
1.45_390.2698m/z	Sulfonolipid	SL(20:0;O)	0.006	0.039	2.74	Positive
6.17_546.4059n	N-acyl ornithine	NAOrn(27:4)	0.029	0.084	2.52	Positive
1.36_376.3598m/z	Diacylglycerol	DG(45:0)	0.023	0.074	2.26	Positive
6.02_450.3504m/z	Acylcarnitine	CAR(19:5)	0.021	0.071	2.18	Positive
8.85_432.3190n	Ether-linked diacylglycerol	DG(O-24:5)	0.042	0.099	1.95	Positive
10.95_429.3677m/z	Ether-linked diacylglycerol	DG(O-26:3)	0.004	0.035	1.82	Positive
17.49_888.7895m/z	Triacylglycerol	TG 53:3	0.004	0.036	1.63	Positive
17.54_844.7406n	Triacylglycerol	TG 16:0_17:1_18:1	0.009	0.049	1.63	Positive
6.73_383.3236m/z	Ceramide non-hydroxyfatty acid-sphingosine	Cer_NS(22:3;2O)	0.032	0.087	1.61	Positive
15.00_565.5469m/z	Ether-linked diacylglycerol	DG(O-34:0)	0.000	0.011	1.59	Positive
17.46_914.8049m/z	Triacylglycerol	TG 18:1_18:2_19:1	0.001	0.022	1.58	Positive
18.07_890.8051m/z	Triacylglycerol	TG 53:2	0.003	0.033	1.57	Positive
17.57_836.7589m/z	Triacylglycerol	TG 15:0_16:0_18:1	0.009	0.050	1.55	Positive
17.21_882.7569n	Triacylglycerol	TG 18:1_18:1_18:2	0.004	0.034	1.52	Positive
18.13_864.7897m/z	Triacylglycerol	TG 16:0_17:0_18:1	0.002	0.027	1.51	Positive
17.74_884.7730n	Triacylglycerol	TG 54:3	0.007	0.043	1.51	Positive
18.43_860.7727n	Triacylglycerol	TG 16:0_18:0_18:1	0.004	0.036	1.51	Positive
17.26_874.7749m/z	Triacylglycerol	TG 16:0_18:1_18:2	0.018	0.067	1.50	Positive
17.79_858.7576n	Triacylglycerol	TG 16:0_18:1_18:1	0.016	0.062	1.49	Positive
17.85_850.7761m/z	Triacylglycerol	TG 16:0_16:0_18:1	0.014	0.059	1.49	Positive
16.58_904.7388n	Triacylglycerol	TG 16:0_18:2_22:5	0.003	0.033	1.48	Positive
16.62_857.7314n	Triacylglycerol	TG 54:6	0.014	0.059	1.47	Positive
17.06_834.7437m/z	Triacylglycerol	TG 14:0_17:1_18:1	0.038	0.094	1.46	Positive
17.03_859.7516n	Triacylglycerol	TG 54:5	0.004	0.036	1.46	Positive
16.40_868.7278m/z	Triacylglycerol	TG 14:0_16:0_22:6	0.033	0.088	1.46	Positive
18.36_886.7880n	Triacylglycerol	TG 16:0_18:1_20:1	0.004	0.037	1.46	Positive
16.62_852.7096n	Triacylglycerol	TG 52:5	0.043	0.099	1.45	Positive
14.44_652.6496m/z	Ceramide non-hydroxyfatty acid-dihydrosphingosine	Cer_NDS(42:0;2O)	0.002	0.026	1.45	Positive

16.80_872.7600m/z	Triacylglycerol	TG 16:1_18:1_18:2	0.023	0.074	1.45	Positive
14.61_583.5583m/z	Ether-linked diacylglycerol	DG(O-34:0)	0.005	0.039	1.44	Positive
17.08_808.7283m/z	Triacylglycerol	TG 14:0_15:0_18:1	0.043	0.100	1.44	Positive
4.22_330.3326m/z	Sphinganine	SPB(20:0;2O)	0.005	0.037	1.44	Positive
17.01_886.7686m/z	Triacylglycerol	TG 17:1_18:1_18:2	0.003	0.030	1.40	Positive
15.73_591.5628m/z	Ether-linked diacylglycerol	DG(O-36:1)	0.009	0.049	1.37	Positive
13.53_1674.2007m/z	Ganglioside GM3	GM3(68:1;2O)	0.013	0.056	1.37	Positive
14.97_624.6205m/z	Ceramide non-hydroxyfatty acid-dihydrosphingosine	Cer_NDS(40:0;2O)	0.001	0.025	1.37	Positive
18.00_877.7973n	Triacylglycerol	TG 18:1_18:1_19:1	0.009	0.050	1.36	Positive
15.58_813.6944n	Hexosylceramide non-hydroxyfatty acid-dihydrosphingosine	HexCer_NDS(18:0/24:0;2O)	0.000	0.017	1.35	Positive
16.35_946.7718m/z	Triacylglycerol	TG 18:1_18:2_22:6	0.001	0.017	1.34	Positive
16.19_1633.2599m/z	Ganglioside GM3	GM3(67:1;2O)	0.019	0.069	1.33	Positive
4.14_299.2790n	Sphingosine	SPB(18:1;2O)	0.001	0.021	1.33	Positive
16.60_883.7495n	Triacylglycerol	TG 13:1_19:0_22:5	0.013	0.057	1.31	Positive
15.66_1608.2386m/z	Ganglioside GM3	GM3(69:1;2O)	0.010	0.051	1.30	Positive
14.72_783.6419n	Hexosylceramide non-hydroxyfatty acid-sphingosine	HexCer_NS(18:1_22:0;2O)	0.001	0.020	1.30	Positive
18.28_912.8024n	Triacylglycerol	TG 18:1_18:1_20:1	0.021	0.071	1.29	Positive
15.58_652.6515m/z	Ceramide non-hydroxyfatty acid-dihydrosphingosine	Cer_NDS(42:0;2O)	0.002	0.029	1.28	Positive
14.79_596.5896m/z	Ceramide non-hydroxyfatty acid-dihydrosphingosine	Cer_NDS(38:0;2O)	0.011	0.053	1.26	Positive
17.69_910.7864n	Triacylglycerol	TG 18:1_18:1_20:2	0.005	0.038	1.26	Positive
15.58_665.6233n	Cholesteryl ester	CE(18:2)	0.022	0.073	1.25	Positive
14.94_811.6803n	Hexosylceramide non-hydroxyfatty acid-dihydrosphingosine	HexCer_NDS(18:0/24:1;2O)	0.004	0.036	1.25	Positive
4.11_567.3202n	Lysophophatidylcholine	LPC 22:6	0.031	0.086	1.25	Positive
15.05_797.6637n	Hexosylceramide non-hydroxyfatty acid-sphingosine	HexCer_NS(18:1_23:0;2O)	0.002	0.028	1.24	Positive
15.36_811.6800n	Hexosylceramide non-hydroxyfatty acid-sphingosine	HexCer_NS(18:1_24:0;2O)	0.001	0.021	1.24	Positive
16.75_930.7554n	Triacylglycerol	TG 58:8	0.007	0.043	1.23	Positive

22.87_846.6105m/z	Phosphatidylserine	PS 40:1	0.018	0.068	1.23	Positive
17.38_926.8046m/z	Triacylglycerol	TG 16:0_18:1_22:4	0.008	0.047	1.23	Positive
15.45_624.6206m/z	Ceramide non-hydroxyfatty acid-dihydrosphingosine	Cer_NDS(40:0;2O)	0.018	0.067	1.22	Positive
16.77_903.7264m/z	Ether-linked triacylglycerol	TG O-54:6	0.005	0.039	1.21	Positive
4.42_301.2946n	Sphinganine	SPB(18:0;2O)	0.002	0.030	1.20	Positive
17.39_796.7288m/z	Triacylglycerol	TG 14:0_16:0_16:0	0.043	0.099	1.18	Positive
15.64_825.6933n	Hexosylceramide non-hydroxyfatty acid-sphingosine	HexCer_NS(18:1_25:0;2O)	0.009	0.048	1.16	Positive
13.53_809.6648n	Hexosylceramide non-hydroxyfatty acid-sphingosine	HexCer_NS(18:1_24:1;2O)	0.005	0.039	1.15	Positive
22.87_844.5957m/z	Phosphatidylserine	PS 40:2	0.016	0.062	1.15	Positive
14.80_563.5322m/z	Ether-linked diacylglycerol	DG(O-34:1)	0.003	0.030	1.15	Positive
14.56_799.6443n	Hexosylceramide non-hydroxyfatty acid-sphingosine	HexCer_NS(18:1_22:1;2O)	0.002	0.030	1.14	Positive
14.56_637.5928n	Ceramide non-hydroxyfatty acid-sphingosine	Cer_NS(18:1_22:1;2O)	0.001	0.019	1.14	Positive
14.69_809.6654n	Hexosylceramide non-hydroxyfatty acid-sphingosine	HexCer_NS(18:1_24:1;2O)	0.018	0.068	1.13	Positive
15.08_774.5901m/z	Phosphatidylethanolamine	PE 20:0_18:1	0.002	0.026	1.13	Positive
13.52_568.5588m/z	Ceramide non-hydroxyfatty acid-dihydrosphingosine	Cer_NDS(36:0;2O)	0.049	0.106	1.13	Positive
13.88_554.5200n	Ether-linked diacylglycerol	DG(O-32:0)	0.030	0.085	1.13	Positive
13.53_889.6200n	Sulfatide	SHexCer(18:1_24:1;2O)	0.007	0.043	1.13	Positive
22.87_817.5732n	Phosphatidylserine	PS 40:4	0.029	0.083	1.12	Positive
11.67_870.5511n	Phosphatidylglycerol	PG 44:10	0.007	0.044	1.10	Positive
15.08_1510.1392m/z	Ganglioside GM3	GM3(62:1;2O)	0.047	0.104	1.10	Positive
14.56_1599.2035n	Ganglioside GM3	GM3(66:2;2O)	0.012	0.056	1.10	Positive
15.05_1560.1744m/z	Ganglioside GM3	GM3(63:1;2O)	0.008	0.046	1.09	Positive
15.58_1596.2473m/z	Ganglioside GM3	GM3(68:0;2O)	0.045	0.102	1.09	Positive
15.05_799.5993n	Phosphatidylethanolamine	PE 18:1_22:1	0.003	0.030	1.09	Positive
14.69_647.6126n	Ceramide non-hydroxyfatty acid-sphingosine	Cer_NS(18:1_24:1;2O)	0.040	0.097	1.09	Positive
22.75_837.6693m/z	N-acyl glycyl serine	NAGlySer(47:5)	0.012	0.055	1.08	Positive

13.81_592.5582m/z	Ceramide non-hydroxyfatty acid-sphingosine	Cer_NS(18:1_20:1;2O)	0.014	0.058	1.08	Positive
18.08_868.5967m/z	Phosphatidylserine	PS 42:4	0.024	0.075	1.07	Positive
15.20_648.6206m/z	Ceramide non-hydroxyfatty acid-sphingosine	Cer_NS(18:1_24:1;2O)	0.049	0.106	1.07	Positive

Table 7. Lipid Compounds with Altered Abundance Recorded in Positive Mode. Levels in P6 Sciatic nerves $p75^{KO}$ compared to WT control. All lipids significantly altered (P≤ 0.05 by Anova) and with structure confidence level L3a or above. m/z; mass (m) to charge (z) ratio.

Bibliography

Aerts, J. M. *et al.* (2008) 'Elevated globotriaosylsphingosine is a hallmark of Fabry disease', *Proceedings of the National Academy of Sciences of the United States of America*. National Academy of Sciences, 105(8), pp. 2812–2817. doi: 10.1073/pnas.0712309105.

Akinrodoye, M. A. and Lui, F. (2020) *Neuroanatomy, Somatic Nervous System*, *StatPearls*. Available at: http://www.ncbi.nlm.nih.gov/pubmed/32310487 (Accessed: 15 January 2021).

Alaamery, M. *et al.* (2020) 'Role of sphingolipid metabolism in neurodegeneration', *Journal of Neurochemistry*. Blackwell Publishing Ltd, p. jnc.15044. doi: 10.1111/jnc.15044.

Alé, A. *et al.* (2016) 'Inhibition of the neuronal NFκB pathway attenuates bortezomib-induced neuropathy in a mouse model', *NeuroToxicology*. Elsevier B.V., 55, pp. 58–64. doi: 10.1016/j.neuro.2016.05.004.

Alić, I. *et al.* (2016) 'Neural stem cells from mouse strain Thy1 YFP-16 are a valuable tool to monitor and evaluate neuronal differentiation and morphology', *Neuroscience Letters*, 634, pp. 32–41. doi: 10.1016/j.neulet.2016.10.001.

Allen, J. A., Halverson-Tamboli, R. A. and Rasenick, M. M. (2007) 'Lipid raft microdomains and neurotransmitter signalling', *Nature Reviews Neuroscience*. Nature Publishing Group, pp. 128–140. doi: 10.1038/nrn2059.

Arora, D. K. *et al.* (2007) 'Evidence of postnatal neurogenesis in dorsal root ganglion: Role of nitric oxide and neuronal restrictive silencer transcription factor', *Journal of Molecular Neuroscience*, 32(2). doi: 10.1007/s12031-007-0014-7.

Arthur-Farraj, P. J. *et al.* (2012) 'c-Jun reprograms Schwann cells of injured nerves to generate a repair cell essential for regeneration.', *Neuron*, 75(4), pp. 633–47. doi: 10.1016/j.neuron.2012.06.021.

Atkinson, D. *et al.* (2017) 'Sphingosine 1-phosphate lyase deficiency causes Charcot-Marie-Tooth neuropathy', *Neurology*, 88(6), pp. 533–542. doi: 10.1212/WNL.0000000000003595.

Aufschnaiter, A. *et al.* (2017) 'Mitochondrial lipids in neurodegeneration.', *Cell and tissue research*. Springer, 367(1), pp. 125–140. doi: 10.1007/s00441-016-2463-1.

Azhary, H. *et al.* (2010) *Peripheral Neuropathy: Differential Diagnosis and Management*, *American Family Physician*. Available at: http://www.aafp.org/afpsort.xml. (Accessed: 20 November 2020).

Baba, H. and Ishibashi, T. (2019) 'The Role of Sulfatides in Axon–Glia Interactions', in *Advances in Experimental Medicine and Biology*. Springer, pp. 165–179. doi: 10.1007/978-981-32-9636-7_11.

Bai, Y., Patzko, A. and Shy, M. E. (2013) ‘Unfolded protein response, treatment and CMT1B’, *Rare Diseases*. Informa UK Limited, 1(1), p. e24049. doi: 10.4161/rdis.24049.

Ballout, R. A. *et al.* (2020) ‘Statins for Smith-Lemli-Opitz syndrome’, *Cochrane Database of Systematic Reviews*. John Wiley and Sons Ltd, 2020(1). doi: 10.1002/14651858.CD013521.

Barber, C. N. and Raben, D. M. (2019) ‘Lipid Metabolism Crosstalk in the Brain: Glia and Neurons’, *Frontiers in Cellular Neuroscience*, 13, p. 212. doi: 10.3389/fncel.2019.00212.

Basso, L. *et al.* (2019) ‘Peripheral neurons: Master regulators of skin and mucosal immune response’, *European Journal of Immunology*. doi: 10.1002/eji.201848027.

Bekircan-Kurt, C. E., Tan, E. and Erdem Özdamar, S. (2015) ‘The activation of rage and NF-ΚB in nerve biopsies of patients with axonal and vasculitic neuropathy’, *Noropsikiyatri Arsivi*. Turkish Neuropsychiatric Society, 52(3), pp. 279–282. doi: 10.5152/npa.2015.8801.

Bentley, C. A. and Lee, K.-F. (2018) ‘p75 Is Important for Axon Growth and Schwann Cell Migration during Development’, *The Journal of Neuroscience*. Society for Neuroscience, 20(20), pp. 7706–7715. doi: 10.1523/jneurosci.20-20-07706.2000.

Bergmann, I. *et al.* (1997) ‘Analysis of Cutaneous Sensory Neurons in Transgenic Mice Lacking the Low Affinity Neurotrophin Receptor p75’, *European Journal of Neuroscience*. John Wiley & Sons, Ltd, 9(1), pp. 18–28. doi: 10.1111/j.1460-9568.1997.tb01349.x.

Bergmann, I. *et al.* (1998) ‘Nerve growth factor evokes hyperalgesia in mice lacking the low-affinity neurotrophin receptor p75’, *Neuroscience Letters*, 255(2). doi: 10.1016/S0304-3940(98)00713-7.

Bermingham, J. R. *et al.* (1996) ‘Tst-1/Oct-6/SCIP regulates a unique step in peripheral myelination and is required for normal respiration’, *Genes and Development*. Cold Spring Harbor Laboratory Press, 10(14), pp. 1751–1762. doi: 10.1101/gad.10.14.1751.

Biegstraaten, M. *et al.* (2012) ‘Small fiber neuropathy in Fabry disease’, *Molecular Genetics and Metabolism*. Academic Press, pp. 135–141. doi: 10.1016/j.ymgme.2012.03.010.

Björkhem, Ingemar; Dieter, Lütjohann; Diczfalusy, Ulf; Ståhle, L. A. and Gunvor; Wahren, J. (1998) ‘Cholesterol homeostasis in human brain: turnover of 24S-hydroxycholesterol and evidence for a cerebral origin of most of this oxysterol in the circulation’, *Journal of lipid research*, (39), pp. 1594–1600. Available at: https://www-jlr-org.proxy.library.vanderbilt.edu/content/39/8/1594.short (Accessed: 28 December 2020).

Bocca, C. *et al.* (2019) ‘Lipidomics Reveals Triacylglycerol Accumulation Due to Impaired Fatty Acid Flux in Opa1-Disrupted Fibroblasts’, *Journal of Proteome Research*. American Chemical Society, 18(7), pp. 2779–2790. doi: 10.1021/acs.jproteome.9b00081.

Bogenmann, E. *et al.* (2011) ‘Generation of mice with a conditional allele for the p75NTR neurotrophin receptor gene’, *genesis*, 49(11), pp. 862–869. doi: 10.1002/dvg.20747.

Bonetto, G. and Di Scala, C. (2019) ‘Importance of Lipids for Nervous System Integrity: Cooperation between Gangliosides and Sulfatides in Myelin Stability’, *The Journal of neuroscience : the official journal of the Society for Neuroscience*. NLM (Medline), pp. 6218–6220. doi: 10.1523/JNEUROSCI.0377-19.2019.

Bosio, A., Binczek, E. and Stoffel, W. (2002) ‘Functional breakdown of the lipid bilayer of the myelin membrane in central and peripheral nervous system by disrupted galactocerebroside synthesis’, *Proceedings of the National Academy of Sciences*. doi: 10.1073/pnas.93.23.13280.

Boyd, K. J., Alder, N. N. and May, E. R. (2018) ‘Molecular Dynamics Analysis of Cardiolipin and Monolysocardiolipin on Bilayer Properties’, *Biophysical Journal*. Biophysical Society, 114(9), pp. 2116–2127. doi: 10.1016/j.bpj.2018.04.001.

Brann, A. B. *et al.* (2002) ‘Nerve growth factor-induced p75-mediated death of cultured hippocampal neurons is age-dependent and transduced through ceramide generated by neutral sphingomyelinase.’, *The Journal of biological chemistry*. American Society for Biochemistry and Molecular Biology, 277(12), pp. 9812–8. doi: 10.1074/jbc.M109862200.

Breiden, B. and Sandhoff, K. (2020) ‘Mechanism of Secondary Ganglioside and Lipid Accumulation in Lysosomal Disease’, *International journal of molecular sciences*. NLM (Medline). doi: 10.3390/ijms21072566.

Brittain, E. L. *et al.* (2016) ‘Fatty acid metabolic defects and right ventricular lipotoxicity in human pulmonary arterial hypertension’, *Circulation*, 133(20). doi: 10.1161/CIRCULATIONAHA.115.019351.

Brown, M. S. and Goldstein, J. L. (1997) ‘The SREBP pathway: Regulation of cholesterol metabolism by proteolysis of a membrane-bound transcription factor’, *Cell*. doi: 10.1016/S0092-8674(00)80213-5.

Cai, Z. *et al.* (2006) ‘Paranodal pathology in Tangier disease with remitting-relapsing multifocal neuropathy’, *Journal of Clinical Neuroscience*. Churchill Livingstone, 13(4), pp. 492–497. doi: 10.1016/j.jocn.2005.07.009.

Camargo, N., Smit, A. B. and Verheijen, M. H. G. (2009) ‘SREBPs: SREBP function in glia-neuron interactions’, *FEBS Journal*. doi: 10.1111/j.1742-4658.2008.06808.x.

Cameron, N. and Cotter, M. (2008) ‘Pro-Inflammatory Mechanisms in Diabetic Neuropathy: Focus on the Nuclear Factor Kappa B Pathway’, *Current Drug Targets*. Bentham Science Publishers Ltd., 9(1), pp. 60–67. doi: 10.2174/138945008783431718.

Campomanes, P., Zoni, V. and Vanni, S. (2019) ‘Local accumulation of diacylglycerol alters membrane properties nonlinearly due to its transbilayer activity’, *Communications Chemistry*. Springer Nature, 2(1), pp. 1–8. doi: 10.1038/s42004-019-0175-7.

Cantuti Castelvetri, L. *et al.* (2013) 'The sphingolipid psychosine inhibits fast axonal transport in Krabbe disease by activation of GSK3β and deregulation of molecular motors.', *The Journal of neuroscience : the official journal of the Society for Neuroscience*. Society for Neuroscience, 33(24), pp. 10048–56. doi: 10.1523/JNEUROSCI.0217-13.2013.

Cashman, C. R. and Höke, A. (2015a) 'Mechanisms of distal axonal degeneration in peripheral neuropathies', *Neuroscience Letters*. Elsevier Ireland Ltd, pp. 33–50. doi: 10.1016/j.neulet.2015.01.048.

Cashman, C. R. and Höke, A. (2015b) 'Mechanisms of distal axonal degeneration in peripheral neuropathies', *Neuroscience Letters*. Elsevier Ireland Ltd, pp. 33–50. doi: 10.1016/j.neulet.2015.01.048.

Castelvetri, L. C. *et al.* (2011) 'Axonopathy is a compounding factor in the pathogenesis of Krabbe disease', *Acta Neuropathologica*, 122(1), pp. 35–48. doi: 10.1007/s00401-011-0814-2.

Cesmebasi, A. (2015) 'Anatomy of the Dorsal Root Ganglion', in *Nerves and Nerve Injuries*. Elsevier, pp. 471–476. doi: 10.1016/B978-0-12-410390-0.00034-2.

Chamberlain, K. A. and Sheng, Z. (2019) 'Mechanisms for the maintenance and regulation of axonal energy supply', *Journal of Neuroscience Research*, 97(8), pp. 897–913. doi: 10.1002/jnr.24411.

Chan, J. R. *et al.* (2004) 'NGF controls axonal receptivity to myelination by Schwann cells or oligodendrocytes', *Neuron*, 43(2). doi: 10.1016/j.neuron.2004.06.024.

Chao, M. V. (2003) 'Neurotrophins and their receptors: A convergence point for many signalling pathways', *Nature Reviews Neuroscience*, 4(4), pp. 299–309. doi: 10.1038/nrn1078.

Charruyer, A. *et al.* (2005) 'UV-C light induces raft-associated acid sphingomyelinase and JNK activation and translocation independently on a nuclear signal', *Journal of Biological Chemistry*. J Biol Chem, 280(19), pp. 19196–19204. doi: 10.1074/jbc.M412867200.

Chen, L.-W. *et al.* (2003) 'The two faces of IKK and NF-κB inhibition: prevention of systemic inflammation but increased local injury following intestinal ischemia-reperfusion', *Nature Medicine*, 9(5), pp. 575–581. doi: 10.1038/nm849.

Chen, Z. *et al.* (2017) 'p75 Is Required for the Establishment of Postnatal Sensory Neuron Diversity by Potentiating Ret Signaling.', *Cell reports*. NIH Public Access, 21(3), pp. 707–720. doi: 10.1016/j.celrep.2017.09.037.

Choi, L. *et al.* (2015) 'The Fabry disease-associated lipid lyso-Gb3 enhances voltage-gated calcium currents in sensory neurons and causes pain', *Neuroscience Letters*. Elsevier Ireland Ltd, pp. 163–168. doi: 10.1016/j.neulet.2015.01.084.

Chrast Roman *et al.* (2011) ‘Lipid metabolism in myelinating glial cells: lessons from human inherited disorders and mouse models.’, *Journal of lipid research*. American Society for Biochemistry and Molecular Biology, 52(3), pp. 419–34. doi: 10.1194/jlr.R009761.

Citri, A., Skaria, K. B. and Yarden, Y. (2003) ‘The deaf and the dumb: The biology of ErbB-2 and ErbB-3’, *Experimental Cell Research*. doi: 10.1016/S0014-4827(02)00101-5.

St. Clair, J. W. and London, E. (2019) ‘Effect of sterol structure on ordered membrane domain (raft) stability in symmetric and asymmetric vesicles’, *Biochimica et Biophysica Acta - Biomembranes*. Elsevier B.V., 1861(6), pp. 1112–1122. doi: 10.1016/j.bbamem.2019.03.012.

Clayton, B. L. L. and Popko, B. (2016) ‘Endoplasmic reticulum stress and the unfolded protein response in disorders of myelinating glia’, *Brain Research*, 1648(Pt B), pp. 594–602. doi: 10.1016/j.brainres.2016.03.046.

Coggeshall, R. E. *et al.* (1984) ‘An empirical method for converting nucleolar counts to neuronal numbers’, *Journal of Neuroscience Methods*, 12(2). doi: 10.1016/0165-0270(84)90011-6.

Coleman, M. (2005) ‘Axon degeneration mechanisms: Commonality amid diversity’, *Nature Reviews Neuroscience*. Nature Publishing Group, pp. 889–898. doi: 10.1038/nrn1788.

Corraliza-Gomez, M., Sanchez, D. and Ganfornina, M. D. (2019) ‘Lipid-Binding Proteins in Brain Health and Disease’, *Frontiers in Neurology*. Frontiers Media S.A., p. 1152. doi: 10.3389/fneur.2019.01152.

Cosgaya, J. M., Chan, J. R. and Shooter, E. M. (2002) ‘The Neurotrophin Receptor p75NTR as a Positive Modulator of Myelination’, *Science*. American Association for the Advancement of Science, 298(5596), pp. 1245–1248. doi: 10.1126/SCIENCE.1076595.

Court, F. A. *et al.* (2008) ‘Schwann Cell to Axon Transfer of Ribosomes: Toward a Novel Understanding of the Role of Glia in the Nervous System’, *Journal of Neuroscience*, 28(43), pp. 11024–11029. doi: 10.1523/jneurosci.2429-08.2008.

Cozma, C. *et al.* (2017) ‘C26-Ceramide as highly sensitive biomarker for the diagnosis of Farber Disease’, *Scientific Reports*. Nature Publishing Group, 7(1), pp. 1–13. doi: 10.1038/s41598-017-06604-2.

Crestani, M. *et al.* (1998) ‘Transcriptional activation of the cholesterol 7α-hydroxylase gene (CYP7A) by nuclear hormone receptors’, *Journal of Lipid Research*, 39(11), pp. 2192–2200.

Crowley, C. *et al.* (1994) ‘Mice lacking nerve growth factor display perinatal loss of sensory and sympathetic neurons yet develop basal forebrain cholinergic neurons’, *Cell*. Cell, 76(6), pp. 1001–1011. doi: 10.1016/0092-8674(94)90378-6.

Czuba, E. *et al.* (2017) ‘Cholesterol as a modifying agent of the neurovascular unit structure and function under physiological and pathological conditions’, *Metabolic Brain Disease*, 32(4), pp. 935–948. doi: 10.1007/s11011-017-0015-3.

D’Antonio, M. *et al.* (2013) ‘Resetting translational homeostasis restores myelination in Charcot-Marie-Tooth disease type 1B mice.’, *The Journal of experimental medicine*, 210(4), pp. 821–38. doi: 10.1084/jem.20122005.

Dali, C. í *et al.* (2015) ‘Sulfatide levels correlate with severity of neuropathy in metachromatic leukodystrophy’, *Annals of Clinical and Translational Neurology*. Wiley, 2(5), pp. 518–533. doi: 10.1002/acn3.193.

Darling, N. J. and Cook, S. J. (2014) ‘The role of MAPK signalling pathways in the response to endoplasmic reticulum stress’, *Biochimica et Biophysica Acta - Molecular Cell Research*. Elsevier, pp. 2150–2163. doi: 10.1016/j.bbamcr.2014.01.009.

Davies, A. M. (1998) ‘Neuronal survival: Early dependence on Schwann cells’, *Current Biology*. Cell Press, 8(1), pp. R15–R18. doi: 10.1016/S0960-9822(98)70009-0.

DeClue, J. E. *et al.* (2000) ‘Epidermal growth factor receptor expression in neurofibromatosis type 1- related tumors and NF1 animal models’, *Journal of Clinical Investigation*, 105(9). doi: 10.1172/JCI7610.

Dewachter, I. *et al.* (2002) ‘Neuronal Deficiency of Presenilin 1 Inhibits Amyloid Plaque Formation and Corrects Hippocampal Long-Term Potentiation but Not a Cognitive Defect of Amyloid Precursor Protein [V7171] Transgenic Mice’, *Journal of Neuroscience*. Society for Neuroscience, 22(9), pp. 3445–3453. doi: 10.1523/jneurosci.22-09-03445.2002.

DiVincenzo, C. *et al.* (2014) ‘The allelic spectrum of Charcot-Marie-Tooth disease in over 17,000 individuals with neuropathy.’, *Molecular genetics & genomic medicine*, 2(6), pp. 522–9. Available at: http://www.pubmedcentral.nih.gov/articlerender.fcgi?artid=4303222&tool=pmcentrez&rendertype=abstract.

Dobrowsky, R. T. *et al.* (1994) ‘Activation of the sphingomyelin cycle through the low-affinity neurotrophin receptor’, *Science*, 265(5178). doi: 10.1126/science.8079174.

Dodge, J. C. (2017) ‘Lipid involvement in neurodegenerative diseases of the motor system: Insights from lysosomal storage diseases’, *Frontiers in Molecular Neuroscience*. Frontiers Media S.A. doi: 10.3389/fnmol.2017.00356.

Le Douarin, N. M. and Dupin, E. (1993) ‘Cell lineage analysis in neural crest ontogeny’, *Journal of Neurobiology*, 24(2), pp. 146–161. doi: 10.1002/neu.480240203.

Duncan, A. L. (2020) ‘Monolysocardiolipin (MLCL) interactions with mitochondrial membrane proteins’, *Biochemical Society Transactions*. Portland Press Ltd, pp. 993–1004. doi: 10.1042/BST20190932.

Duncan, I. D. and Radcliff, A. B. (2016) ‘Inherited and acquired disorders of myelin: The underlying myelin pathology’, *Experimental Neurology*. doi: 10.1016/j.expneurol.2016.04.002.

Dyck, P. J. and Lambert, E. H. (2014) ‘Lower Motor and Primary Sensory Neuron Diseases With Peroneal Muscular Atrophy’.

Epstein, J., Sanderson, I. R. and Macdonald, T. T. (2010) ‘Curcumin as a therapeutic agent: the evidence from in vitro, animal and human studies.’, *The British journal of nutrition*, 103(11), pp. 1545–57. doi: 10.1017/S0007114509993667.

Erickson, R. P. (2013) ‘Current controversies in Niemann-Pick C1 disease: Steroids or gangliosides; neurons or neurons and glia’, *Journal of Applied Genetics*. Springer, pp. 215–224. doi: 10.1007/s13353-012-0130-0.

Fariñas, I. *et al.* (1996) ‘Lack of neurotrophin-3 results in death of spinal sensory neurons and premature differentiation of their precursors’, *Neuron*. Cell Press, 17(6), pp. 1065–1078. doi: 10.1016/S0896-6273(00)80240-8.

Felten, D. L., O’Banion, M. K. and Maida, M. S. (2016a) ‘Peripheral Nervous System’, in *Netter’s Atlas of Neuroscience*. Elsevier, pp. 153–231. doi: 10.1016/B978-0-323-26511-9.00009-6.

Felten, D. L., O’Banion, M. K. and Maida, M. S. (2016b) ‘Spinal Cord’, in *Netter’s Atlas of Neuroscience*. Elsevier, pp. 233–246. doi: 10.1016/B978-0-323-26511-9.00010-2.

Feltri, M. L., Poitelon, Y. and Previtali, S. C. (2015) ‘How Schwann Cells Sort Axons New Concepts’, *The Neuroscientist*, p. 1073858415572361. doi: 10.1177/1073858415572361.

Feng, G. *et al.* (2000) ‘Imaging neuronal subsets in transgenic mice expressing multiple spectral variants of GFP’, *Neuron*. Cell Press, 28(1), pp. 41–51. doi: 10.1016/S0896-6273(00)00084-2.

Fisher-Wellman, K. *et al.* (2020) ‘On the nature of ceramide-mitochondria interactions – Dissection using comprehensive mitochondrial phenotyping’, *Cellular Signalling*. Elsevier BV, 78, p. 109838. doi: 10.1016/j.cellsig.2020.109838.

Fliesler, S. and Xu, L. (2018) ‘Oxysterols and Retinal Degeneration in a Rat Model of Smith-Lemli-Opitz Syndrome: Implications for an Improved Therapeutic Intervention’, *Molecules*, 23(10), p. 2720. doi: 10.3390/molecules23102720.

Fobker, M. *et al.* (2001) ‘Accumulation of cardiolipin and lysocardiolipin in fibroblasts from Tangier disease subjects’, *FEBS Letters*. No longer published by Elsevier, 500(3), pp. 157–162. doi: 10.1016/S0014-5793(01)02578-9.

Fortun, J. *et al.* (2006) ‘Alterations in degradative pathways and protein aggregation in a neuropathy model based on PMP22 overexpression’, *Neurobiology of Disease*. Academic Press, 22(1), pp. 153–164. doi: 10.1016/j.nbd.2005.10.010.

Fridman, V. and Reilly, M. M. (2015) ‘Inherited Neuropathies’, *Seminars in Neurology*, 35(4), pp. 407–423. doi: 10.1055/s-0035-1558981.

Fu, Q. *et al.* (1998) ‘Control of Cholesterol Biosynthesis in Schwann Cells’, *J. Neurochem*. John Wiley & Sons, Ltd (10.1111), 71(2). doi: 10.1046/j.1471-4159.1998.71020549.x.

Fukuda, Y., Li, Y. and Segal, R. A. (2017) 'A mechanistic understanding of axon degeneration in chemotherapy-induced peripheral neuropathy', *Frontiers in Neuroscience*. Frontiers Media S.A. doi: 10.3389/fnins.2017.00481.

Funakoshi, H. *et al.* (1993) 'Differential expression of mRNAs for neurotrophins and their receptors after axotomy of the sciatic nerve', *Journal of Cell Biology*, 123(2). doi: 10.1083/jcb.123.2.455.

Gaoua, W. *et al.* (2000) 'Cholesterol deficit but not accumulation of aberrant sterols is the major cause of the teratogenic activity in the Smith-Lemli-Opitz syndrome animal model.', *Journal of lipid research*. American Society for Biochemistry and Molecular Biology, 41(4), pp. 637–46. Available at: http://www.ncbi.nlm.nih.gov/pubmed/10744785 (Accessed: 17 February 2019).

Garbay, B. *et al.* (2000) 'Myelin synthesis in the peripheral nervous system', *Progress in Neurobiology*. Pergamon, pp. 267–304. doi: 10.1016/S0301-0082(99)00049-0.

Garofalo, K. *et al.* (2011) 'Oral L-serine supplementation reduces production of neurotoxic deoxysphingolipids in mice and humans with hereditary sensory autonomic neuropathy type 1.', *The Journal of clinical investigation*. American Society for Clinical Investigation, 121(12), pp. 4735–45. doi: 10.1172/JCI57549.

Genaro-Mattos, T. C. *et al.* (2018) 'Dichlorophenyl piperazines, including a recently-approved atypical antipsychotic, are potent inhibitors of DHCR7, the last enzyme in cholesterol biosynthesis', *Toxicology and Applied Pharmacology*, 349. doi: 10.1016/j.taap.2018.04.029.

Genaro-Mattos, T. C. *et al.* (2019) 'Maternal aripiprazole exposure interacts with 7-dehydrocholesterol reductase mutations and alters embryonic neurodevelopment', *Molecular Psychiatry*, 24(4). doi: 10.1038/s41380-019-0368-6.

George, D., Ahrens, P. and Lambert, S. (2018) 'Satellite glial cells represent a population of developmentally arrested Schwann cells', *GLIA*, 66(7). doi: 10.1002/glia.23320.

Ghosh, S. and Dass, J. F. P. (2016) 'Study of pathway cross-talk interactions with NF-κB leading to its activation via ubiquitination or phosphorylation: A brief review', *Gene*. Elsevier B.V., pp. 97–109. doi: 10.1016/j.gene.2016.03.008.

Gibson, C. L. *et al.* (2018) 'Global untargeted serum metabolomic analyses nominate metabolic pathways responsive to loss of expression of the orphan metallo β-lactamase, MBLAC1', *Molecular Omics*. Royal Society of Chemistry, 14(3), pp. 142–155. doi: 10.1039/c7mo00022g.

Gill, J. S. and Windebank, A. J. (1998) 'Suramin induced ceramide accumulation leads to apoptotic cell death in dorsal root ganglion neurons', *Cell Death and Differentiation*. Nature Publishing Group, 5(10), pp. 876–883. doi: 10.1038/sj.cdd.4400410.

Gill, J. S. and Windebank, A. J. (2000) 'Ceramide initiates NFκB-mediated caspase activation in neuronal apoptosis', *Neurobiology of Disease*. Academic Press Inc., 7(4), pp. 448–461. doi: 10.1006/nbdi.2000.0312.

Ginanneschi, F. *et al.* (2013) ‘Polyneuropathy in cerebrotendinous xanthomatosis and response to treatment with chenodeoxycholic acid’, *Journal of Neurology*. Springer, 260(1), pp. 268–274. doi: 10.1007/s00415-012-6630-3.

Giudetti, A. M. *et al.* (2020) ‘An altered lipid metabolism characterizes Charcot-Marie-Tooth type 2B peripheral neuropathy’, *Biochimica et Biophysica Acta - Molecular and Cell Biology of Lipids*. Elsevier B.V., 1865(12), p. 158805. doi: 10.1016/j.bbalip.2020.158805.

Godel, T. *et al.* (2017) ‘Human dorsal root ganglion in vivo morphometry and perfusion in Fabry painful neuropathy’, *Neurology*. Lippincott Williams and Wilkins, 89(12), pp. 1274–1282. doi: 10.1212/WNL.0000000000004396.

Gonçalves, N. P., Yan, Y., *et al.* (2020) ‘Modulation of Small RNA Signatures in Schwann-Cell-Derived Extracellular Vesicles by the p75 Neurotrophin Receptor and Sortilin’, *Biomedicines*. MDPI AG, 8(11), p. 450. doi: 10.3390/biomedicines8110450.

Gonçalves, N. P., Jager, S. E., *et al.* (2020) ‘Schwann cell p75 neurotrophin receptor modulates small fiber degeneration in diabetic neuropathy’, *Glia*. John Wiley and Sons Inc, 68(12), pp. 2725–2743. doi: 10.1002/glia.23881.

Gonçalves, N. P., Vægter, C. B. and Pallesen, L. T. (2018) ‘Peripheral Glial Cells in the Development of Diabetic Neuropathy.’, *Frontiers in neurology*. Frontiers Media SA, 9, p. 268. doi: 10.3389/fneur.2018.00268.

Gonzalez, S. *et al.* (2014) ‘In vivo introduction of transgenes into mouse sciatic nerve cells in situ using viral vectors’, *Nature Protocols*. Nature Publishing Group, 9(5), pp. 1160–1169. doi: 10.1038/nprot.2014.073.

Goodrum, J. F. *et al.* (1994) *Fate of Myelin Lipids during Degeneration and Regeneration of Peripheral Nerve: An Autoradiographic Study*, *The Journal of Neuroscience*. Available at: https://www.jneurosci.org/content/jneuro/14/1/357.full.pdf (Accessed: 22 July 2019).

Goodrum, J. F. *et al.* (2000) ‘Peripheral nerve regeneration and cholesterol reutilization are normal in the low-density lipoprotein receptor knockout mouse’, *Journal of Neuroscience Research*. J Neurosci Res, 59(4), pp. 581–586. doi: 10.1002/(SICI)1097-4547(20000215)59:4<581::AID-JNR14>3.0.CO;2-P.

Gregg, E. W. *et al.* (2004) ‘Prevalence of lower-extremity disease in the U.S. adult population ≥40 years of age with and without diabetes: 1999-2000 National Health and Nutrition Examination Survey’, *Diabetes Care*, 27(7). doi: 10.2337/diacare.27.7.1591.

Griffin, J. W. and Thompson, W. J. (2008) ‘Biology and pathology of nonmyelinating Schwann cells.’, *Glia*, 56(14), pp. 1518–31. doi: 10.1002/glia.20778.

Griffiths, W. J. *et al.* (2017) ‘Sterols and oxysterols in plasma from Smith-Lemli-Opitz syndrome patients’, *Journal of Steroid Biochemistry and Molecular Biology*, 169, pp. 77–87. doi: 10.1016/j.jsbmb.2016.03.018.

Gumbinas, M., Larsen, M. and Liu, H. M. (1975) 'Peripheral neuropathy in classic niemann-pick disease: Ultrastructure of nerves and skeletal muscles', *Neurology*, 25(2), pp. 107–113. doi: 10.1212/wnl.25.2.107.

Haldar, S. *et al.* (2012) 'Differential Effect of Cholesterol and Its Biosynthetic Precursors on Membrane Dipole Potential', *Biophysical Journal*. Cell Press, 102(7), pp. 1561–1569. doi: 10.1016/J.BPJ.2012.03.004.

Hamburger, V. (1992) 'History of the discovery of neuronal death in embryos', *Journal of Neurobiology*, 23(9). doi: 10.1002/neu.480230904.

Hanani, M. and Spray, D. C. (2020) 'Emerging importance of satellite glia in nervous system function and dysfunction', *Nature Reviews Neuroscience*. Nature Research, pp. 485–498. doi: 10.1038/s41583-020-0333-z.

Hanemann, C. O. *et al.* (2000) 'Mutation-dependent alteration in cellular distribution of peripheral myelin protein 22 in nerve biopsies from Charcot–Marie–Tooth type 1A', *Brain*. Oxford University Press, 123(5), pp. 1001–1006. doi: 10.1093/brain/123.5.1001.

Harrington, A. W., Kim, J. Y. and Yoon, S. O. (2002) 'Activation of Rac GTPase by p75 is necessary for c-jun N-terminal kinase-mediated apoptosis', *Journal of Neuroscience*, 22(1). doi: 10.1523/jneurosci.22-01-00156.2002.

Henne, W. M., Reese, M. L. and Goodman, J. M. (2018) 'The assembly of lipid droplets and their roles in challenged cells', *The EMBO Journal*. EMBO, 37(12). doi: 10.15252/embj.201898947.

Hichor, M. *et al.* (2018) 'Liver X Receptor exerts a protective effect against the oxidative stress in the peripheral nerve', *Scientific Reports*. Nature Publishing Group, 8(1). doi: 10.1038/s41598-018-20980-3.

Hicks, C. W. and Selvin, E. (2019) 'Epidemiology of Peripheral Neuropathy and Lower Extremity Disease in Diabetes', *Current Diabetes Reports*. doi: 10.1007/s11892-019-1212-8.

Hinder, L. M. *et al.* (2014) 'Long-chain acyl coenzyme a synthetase 1 overexpression in primary cultured schwann cells prevents long chain fatty acid-induced oxidative stress and mitochondrial dysfunction', *Antioxidants and Redox Signaling*. Mary Ann Liebert Inc., pp. 588–600. doi: 10.1089/ars.2013.5248.

Hirata, H *et al.* (2001) 'Nerve growth factor signaling of p75 induces differentiation and ceramide-mediated apoptosis in Schwann cells cultured from degenerating nerves.', *Glia*, 36(3), pp. 245–58. Available at: http://www.ncbi.nlm.nih.gov/pubmed/11746763 (Accessed: 18 February 2019).

Hirata, Hitoshi *et al.* (2001) 'Nerve growth factor signaling of p75 induces differentiation and ceramide-mediated apoptosis in Schwann cells cultured from degenerating nerves', *Glia*. John Wiley & Sons, Ltd, 36(3), pp. 245–258. doi: 10.1002/glia.1113.

Honda, M. *et al.* (1998) '7-dehydrocholesterol down-regulates cholesterol biosynthesis in cultured Smith-Lemli-Opitz syndrome skin fibroblasts', *Journal of Lipid Research*, 39(3). doi: 10.1016/S0022-2275(20)33302-2.

Horton, J. D., Goldstein, J. L. and Brown, M. S. (2002) 'SREBPs: Activators of the complete program of cholesterol and fatty acid synthesis in the liver', *Journal of Clinical Investigation*. doi: 10.1172/JCI0215593.

Huffnagel, I. C. *et al.* (2019) 'Disease progression in women with X-linked adrenoleukodystrophy is slow', *Orphanet Journal of Rare Diseases*. BioMed Central Ltd., 14(1), p. 30. doi: 10.1186/s13023-019-1008-6.

Hughes, R. A. C. (2002) 'Regular review: Peripheral neuropathy', *BMJ*, 324(7335). doi: 10.1136/bmj.324.7335.466.

Ichim, G., Tauszig-Delamasure, S. and Mehlen, P. (2012) 'Neurotrophins and cell death', *Experimental Cell Research*. doi: 10.1016/j.yexcr.2012.03.006.

Jaegle, M. *et al.* (2003) 'The POU proteins Brn-2 and Oct-6 share important functions in Schwann cell development.', *Genes & development*, 17(11), pp. 1380–91. doi: 10.1101/gad.258203.

Jani, T. S. *et al.* (2010) 'Inhibition of NF-kappaB signaling by quinacrine is cytotoxic to human colon carcinoma cell lines and is synergistic in combination with tumor necrosis factor-related apoptosis-inducing ligand (TRAIL) or oxaliplatin', *The Journal of Biological Chemistry*, 285(25), pp. 19162–19172. doi: 10.1074/jbc.M109.091645.

Jansen, G. A. *et al.* (1997) 'Refsum disease is caused by mutations in the phytanoyl-coa hydroxylase gene', *Nature Genetics*. Nature Publishing Group, 17(2), p. 193. doi: 10.1038/ng1097-190.

Jessen, K. R. K. *et al.* (2016) 'the Repair Schwann Cell and Its Function in Regenerating Nerves', *Journal of Physiology*, 594(13). doi: 10.1113/JP270874.This.

Jessen, K. R. and Mirsky, R. (2019) 'Schwann Cell Precursors; Multipotent Glial Cells in Embryonic Nerves.', *Frontiers in molecular neuroscience*. Frontiers Media SA, 12, p. 69. doi: 10.3389/fnmol.2019.00069.

Jessen, K. R., Mirsky, R. and Lloyd, A. C. (2015) 'Schwann Cells: Development and Role in Nerve Repair'. Cold Spring Harbor Laboratory Press, 7(7), p. a020487. doi: 10.1101/cshperspect.a020487.

Jessen, K. R., Mirsky, R. and Salzer, J. (2008) 'Introduction. Schwann cell biology.', *Glia*, 56(14), pp. 1479–80. doi: 10.1002/glia.20779.

Jha, M. K. and Morrison, B. M. (2018) 'Glia-neuron energy metabolism in health and diseases: New insights into the role of nervous system metabolic transporters', *Experimental Neurology*. doi: 10.1016/j.expneurol.2018.07.009.

Jin, Y. *et al.* (2018) 'Reactive oxygen species induces lipid droplet accumulation in hepg2 cells by increasing perilipin 2 expression', *International Journal of Molecular Sciences*. MDPI AG, 19(11). doi: 10.3390/ijms19113445.

Jones, K. R. *et al.* (1994a) 'Targeted disruption of the BDNF gene perturbs brain and sensory neuron development but not motor neuron development', *Cell*. NIH Public Access, 76(6), pp. 989–999. doi: 10.1016/0092-8674(94)90377-8.

Jones, K. R. *et al.* (1994b) ‘Targeted disruption of the BDNF gene perturbs brain and sensory neuron development but not motor neuron development’, *Cell*. NIH Public Access, 76(6), pp. 989–999. doi: 10.1016/0092-8674(94)90377-8.

Jurevics, H. *et al.* (1998) ‘Regenerating sciatic nerve does not utilize circulating cholesterol’, *Neurochemical Research*, pp. 401–406. doi: 10.1023/A:1022469803426.

Kang, H. *et al.* (2014) ‘Terminal schwann cells participate in neuromuscular synapse remodeling during reinnervation following nerve injury’, *Journal of Neuroscience*. Society for Neuroscience, 34(18), pp. 6323–6333. doi: 10.1523/JNEUROSCI.4673-13.2014.

Kasemeir-Kulesa, J. C., Kulesa, P. M. and Lefcort, F. (2005) ‘Imaging neural crest cell dynamics during formation of dorsal root ganglia and sympathetic ganglia’, *Development*, 132(2), pp. 235–245. doi: 10.1242/dev.01553.

Kastriti, M. E. and Adameyko, I. (2017) ‘Specification, plasticity and evolutionary origin of peripheral glial cells’, *Current Opinion in Neurobiology*. Elsevier Current Trends, 47, pp. 196–202. doi: 10.1016/J.CONB.2017.11.004.

Katona, I. *et al.* (2009) ‘PMP22 expression in dermal nerve myelin from patients with CMT1A’, *Brain*. Oxford University Press, 132(7), pp. 1734–1740. doi: 10.1093/brain/awp113.

Keller, R. K., Arnold, T. P. and Fliesler, S. J. (2004) ‘Formation of 7-dehydrocholesterol-containing membrane rafts in vitro and in vivo, with relevance to the Smith-Lemli-Opitz syndrome.’, *Journal of lipid research*. NIH Public Access, 45(2), pp. 347–55. doi: 10.1194/jlr.M300232-JLR200.

Kemp, S., Berger, J. and Aubourg, P. (2012) ‘X-linked adrenoleukodystrophy: Clinical, metabolic, genetic and pathophysiological aspects’, *Biochimica et Biophysica Acta - Molecular Basis of Disease*. Biochim Biophys Acta, pp. 1465–1474. doi: 10.1016/j.bbadis.2012.03.012.

Kim, J. B. (2014) ‘Channelopathies’, *Korean Journal of Pediatrics*. Korean Pediatric Society, pp. 1–18. doi: 10.3345/kjp.2014.57.1.1.

Kim, J. Y. *et al.* (2003) ‘The role of ErbB2 signaling in the onset of terminal differentiation of oligodendrocytes in vivo’, *Journal of Neuroscience*, 23(13). doi: 10.1523/jneurosci.23-13-05561.2003.

Kim, M. *et al.* (2018) ‘Maf links neuregulin1 signaling to cholesterol synthesis in myelinating schwann cells’, *Genes and Development*. Cold Spring Harbor Laboratory Press, 32(9–10), pp. 645–657. doi: 10.1101/gad.310490.117.

Klein, R. *et al.* (1993) ‘Targeted disruption of the trkB neurotrophin receptor gene results in nervous system lesions and neonatal death’, *Cell*, 75(1). doi: 10.1016/S0092-8674(05)80088-1.

Kleinecke, S. *et al.* (2017) ‘Peroxisomal dysfunctions cause lysosomal storage and axonal Kv1 channel redistribution in peripheral neuropathy’, *eLife*. eLife Sciences Publications Ltd, 6. doi: 10.7554/eLife.23332.

Komen, J. C. *et al.* (2007) ‘Phytanic acid impairs mitochondrial respiration through protonophoric action’, *Cellular and Molecular Life Sciences*. Springer, 64(24), pp. 3271–3281. doi: 10.1007/s00018-007-7357-7.

Korade, Z. *et al.* (2007) ‘Expression and p75 neurotrophin receptor dependence of cholesterol synthetic enzymes in adult mouse brain’, *Neurobiology of Aging*, 28(10). doi: 10.1016/j.neurobiolaging.2006.06.026.

Korade, Z. *et al.* (2010) ‘Biological activities of 7-dehydrocholesterol-derived oxysterols: implications for Smith-Lemli-Opitz syndrome’, 51(11), pp. 3259–69. doi: 10.1194/jlr.M009365.

Kramer, R., Bielawski, J., Kistner-Griffin, E., *et al.* (2015) ‘Neurotoxic 1-deoxysphingolipids and paclitaxel-induced peripheral neuropathy’, *FASEB Journal*. FASEB, 29(11), pp. 4461–4472. doi: 10.1096/fj.15-272567.

Kramer, R., Bielawski, J., Kistner-Griffin, E., *et al.* (2015) ‘Neurotoxic 1-deoxysphingolipids and paclitaxel-induced peripheral neuropathy’, *The FASEB Journal*. FASEB, 29(11), pp. 4461–4472. doi: 10.1096/fj.15-272567.

Kucenas, S. (2015) ‘Perineurial glia’, *Cold Spring Harbor Perspectives in Biology*. Cold Spring Harbor Laboratory Press, 7(6), pp. 1–14. doi: 10.1101/cshperspect.a020511.

Landrieu, P. and Saïd, G. (1984) ‘Peripheral neuropathy in type A Niemann-Pick disease - A morphological study’, *Acta Neuropathologica*. Springer-Verlag, 63(1), pp. 66–71. doi: 10.1007/BF00688472.

Lawson, S. N. and Biscoe, T. J. (1979) ‘Development of mouse dorsal root ganglia: an autoradiographic and quantitative study’, *Journal of Neurocytology*, 8(3), pp. 265–274. doi: 10.1007/BF01236122.

LeBlanc, S. E. *et al.* (2005) ‘Regulation of cholesterol/lipid biosynthetic genes by Egr2/Krox20 during peripheral nerve myelination’, *Journal of Neurochemistry*. Wiley/Blackwell (10.1111), 93(3), pp. 737–748. doi: 10.1111/j.1471-4159.2005.03056.x.

Leclerc, A., Matveeff, L. and Emery, E. (2020) ‘Syringomyelia and hydromyelia: Current understanding and neurosurgical management’, *Revue Neurologique*. Elsevier Masson SAS. doi: 10.1016/j.neurol.2020.07.004.

Ledonne, A. and Mercuri, N. B. (2020) ‘On the modulatory roles of neuregulins/ErbB signaling on synaptic plasticity’, *International Journal of Molecular Sciences*. MDPI AG. doi: 10.3390/ijms21010275.

Lee, K. F. *et al.* (1992) ‘Targeted mutation of the gene encoding the low affinity NGF receptor p75 leads to deficits in the peripheral sensory nervous system.’, *Cell*, 69(5), pp. 737–49. Available at: http://www.ncbi.nlm.nih.gov/pubmed/1317267 (Accessed: 12 February 2019).

Lee, K. F., Davies, A. M. and Jaenisch, R. (1994) ‘p75-deficient embryonic dorsal root sensory and neonatal sympathetic neurons display a decreased sensitivity to NGF.’, *Development (Cambridge, England)*, 120(4), pp. 1027–33. Available at: http://www.ncbi.nlm.nih.gov/pubmed/7600951 (Accessed: 12 February 2019).

Lee, S. *et al.* (2018) ‘Elevated Peripheral Myelin Protein 22, Reduced Mitotic Potential, and Proteasome Impairment in Dermal Fibroblasts from Charcot-Marie-Tooth Disease Type 1A Patients’, *American Journal of Pathology*. Elsevier Inc., 188(3), pp. 728–738. doi: 10.1016/j.ajpath.2017.10.021.

Lemke, G. and Chao, M. (1988) ‘Axons regulate Schwann cell expression of the major myelin and NGF receptor genes.’, 102(3), pp. 499–504. Available at: http://www.ncbi.nlm.nih.gov/pubmed/2846259 (Accessed: 18 February 2019).

Levi-Montalcini, R. (1966) ‘The nerve growth factor: its mode of action on sensory and sympathetic nerve cells.’, *Harvey lectures*.

Li, H.-Y., Say, E. H. M. and Zhou, X.-F. (2007) ‘Isolation and Characterization of Neural Crest Progenitors from Adult Dorsal Root Ganglia’, *STEM CELLS*, 25(8). doi: 10.1634/stemcells.2007-0080.

Li, J. *et al.* (2012) ‘Lysocardiolipin acyltransferase 1 (ALCAT1) controls mitochondrial DNA fidelity and biogenesis through modulation of MFN2 expression’, *Proceedings of the National Academy of Sciences of the United States of America*. National Academy of Sciences, 109(18), pp. 6975–6980. doi: 10.1073/pnas.1120043109.

Li, J. *et al.* (2013) ‘The PMP22 gene and its related diseases.’, *Molecular neurobiology*, 47(2), pp. 673–98. doi: 10.1007/s12035-012-8370-x.

Li, J. (2015) ‘Molecular regulators of nerve conduction - Lessons from inherited neuropathies and rodent genetic models’, *Experimental Neurology*, 267, pp. 209–218. doi: 10.1016/j.expneurol.2015.03.009.

Limpert, A. S. and Carter, B. D. (2010) ‘Axonal Neuregulin 1 Type III Activates NF-κB in Schwann Cells during Myelin Formation’, 285(22). doi: 10.1074/jbc.M109.098780.

Lin, W. and Stone, S. (2020) ‘Unfolded protein response in myelin disorders’, *Neural Regeneration Research*. Wolters Kluwer Medknow Publications, pp. 636–645. doi: 10.4103/1673-5374.266903.

Liu, L. *et al.* (2015) ‘Glial lipid droplets and ROS induced by mitochondrial defects promote neurodegeneration’, *Cell*. Cell Press, 160(1–2), pp. 177–190. doi: 10.1016/j.cell.2014.12.019.

Lopez-Verrilli, M. A. and Court, F. A. (2012) ‘Transfer of vesicles from Schwann cells to axons: A novel mechanism of communication in the peripheral nervous system’, *Frontiers in Physiology*. doi: 10.3389/fphys.2012.00205.

Lossi, L., Castagna, C. and Merighi, A. (2015a) ‘Neuronal cell death: An overview of its different forms in central and peripheral neurons’, *Methods in Molecular Biology*. Humana Press Inc., 1254, pp. 1–18. doi: 10.1007/978-1-4939-2152-2_1.

Lossi, L., Castagna, C. and Merighi, A. (2015b) 'Neuronal Cell Death: An Overview of Its Different Forms in Central and Peripheral Neurons', in. Humana Press, New York, NY, pp. 1–18. doi: 10.1007/978-1-4939-2152-2_1.

Lv, W. *et al.* (2018) 'Schwann Cell Plasticity is Regulated by a Weakened Intrinsic Antioxidant Defense System in Acute Peripheral Nerve Injury', *Neuroscience*. doi: 10.1016/j.neuroscience.2018.04.018.

Marcos, J. *et al.* (2007) 'Cholesterol Biosynthesis from Birth to Adulthood in a Mouse Model for 7-dehydrosterol reductase deficiency (Smith-Lemli- Opitz Syndrome', *Steroids*. NIH Public Access, 72(11–12), pp. 802–8. doi: 10.1016/j.steroids.2007.07.002.

Marmigère, F. and Carroll, P. (2014) 'Neurotrophin Signalling and Transcription Programmes Interactions in the Development of Somatosensory Neurons', in, pp. 329–353. doi: 10.1007/978-3-642-45106-5_13.

Marol, G. S. *et al.* (2004) 'Neural crest boundary cap cells constitute a source of neuronal and glial cells of the PNS', *Nature Neuroscience*. Nature Publishing Group, 7(9), pp. 930–938. doi: 10.1038/nn1299.

Marshall, L. L. *et al.* (2014) 'Increased lipid droplet accumulation associated with a peripheral sensory neuropathy', *Journal of Chemical Biology*. Springer Verlag, 7(2), pp. 67–76. doi: 10.1007/s12154-014-0108-y.

Martini, R. *et al.* (2008) 'Interactions between Schwann cells and macrophages in injury and inherited demyelinating disease.', *Glia*, 56(14), pp. 1566–77. doi: 10.1002/glia.20766.

Maurel, P. and Salzer, J. L. (2000) 'Axonal regulation of Schwann cell proliferation and survival and the initial events of myelination requires PI 3-kinase activity', *Journal of Neuroscience*, 20(12). doi: 10.1523/jneurosci.20-12-04635.2000.

Meeker, R. B. and Williams, K. S. (2015) 'The p75 neurotrophin receptor: At the crossroad of neural repair and death', *Neural Regeneration Research*. Editorial Board of Neural Regeneration Research, 10(5), pp. 721–725. doi: 10.4103/1673-5374.156967.

Meeker, R. and Williams, K. (2014) 'Dynamic Nature of the p75 Neurotrophin Receptor in Response to Injury and Disease', *Journal of Neuroimmune Pharmacology*. doi: 10.1007/s11481-014-9566-9.

Mellinghoff, I. K. *et al.* (2004) 'HER2/neu kinase-dependent modulation of androgen receptor function through effects on DNA binding and stability', *Cancer Cell*, 6(5). doi: 10.1016/j.ccr.2004.09.031.

Mercan, M. *et al.* (2018) 'Peripheral neuropathy in Tangier disease: A literature review and assessment', *Journal of the Peripheral Nervous System*. Blackwell Publishing Inc., 23(2), pp. 88–98. doi: 10.1111/jns.12265.

Michailov, G. V. *et al.* (2004) ‘Axonal Neuregulin-1 Regulates Myelin Sheath Thickness’, *Science*, 304(5671). doi: 10.1126/science.1095862.

Mignarri, A. *et al.* (2016) ‘Evaluation of cholesterol metabolism in cerebrotendinous xanthomatosis’, *Journal of Inherited Metabolic Disease*. Springer Netherlands, 39(1), pp. 75–83. doi: 10.1007/s10545-015-9873-1.

Mirsky, R. *et al.* (2002) ‘Schwann cells as regulators of nerve development.’, *Journal Of Physiology Paris*. EDITIONS SCIENTIFIQUES MEDICALES ELSEVIER, 96(1–2), pp. 17–24. Available at: http://discovery.ucl.ac.uk/185912/.

Mirsky, R. *et al.* (2008) ‘Novel signals controlling embryonic Schwann cell development, myelination and dedifferentiation’, in *Journal of the Peripheral Nervous System*, pp. 122–135. doi: 10.1111/j.1529-8027.2008.00168.x.

Montani, L. *et al.* (2018) ‘De novo fatty acid synthesis by Schwann cells is essential for peripheral nervous system myelination’, *The Journal of Cell Biology*, 217(4), pp. 1353–1368. doi: 10.1083/jcb.201706010.

de Moraes, E. R., Kushmerick, C. and Naves, L. A. (2017) ‘Morphological and functional diversity of first-order somatosensory neurons.’, *Biophysical reviews*. Springer, 9(5), pp. 847–856. doi: 10.1007/s12551-017-0321-3.

Morton, P. D. *et al.* (2012) ‘Nuclear factor-κB activation in schwann cells regulates regeneration and remyelination’, *Glia*. John Wiley & Sons, Ltd, 60(4), pp. 639–650. doi: 10.1002/glia.22297.

Morton, P. D. *et al.* (2013) ‘Activation of NF-κB in Schwann cells is dispensable for myelination In vivo’, *Journal of Neuroscience*. Society for Neuroscience, 33(24), pp. 9932–9936. doi: 10.1523/JNEUROSCI.2483-12.2013.

Muratori, L. *et al.* (2015) ‘Generation of new neurons in dorsal root Ganglia in adult rats after peripheral nerve crush injury’, *Neural Plasticity*, 2015, p. 860546. doi: 10.1155/2015/860546.

Murinson, B. B. and Griffin, J. W. (2004) ‘C-fiber structure varies with location in peripheral nerve.’, *Journal of neuropathology and experimental neurology*, 63(3), pp. 246–54. Available at: http://www.ncbi.nlm.nih.gov/pubmed/15055448 (Accessed: 4 March 2019).

Murray, S. S., Bartlett, P. F. and Cheema, S. S. (1999) ‘Differential loss of spinal sensory but not motor neurons in the p75NTR knockout mouse’, *Neuroscience Letters*. Elsevier, 267Murray,(1), pp. 45–48. doi: 10.1016/S0304-3940(99)00330-4.

Di Muzio, A. *et al.* (2003) ‘Dysmyelinating sensory-motor neuropathy in merosin-deficient congenital muscular dystrophy’, *Muscle & Nerve*. John Wiley & Sons, Ltd, 27(4), pp. 500–506. doi: 10.1002/mus.10326.

Nagai, K. (2015) ‘Phytanic acid induces Neuro2a cell death via histone deacetylase activation and mitochondrial dysfunction’, *Neurotoxicology and Teratology*. Elsevier Inc., 48, pp. 33–39. doi: 10.1016/j.ntt.2015.01.006.

Nascimento, A. I., Mar, F. M. and Sousa, M. M. (2018) 'The intriguing nature of dorsal root ganglion neurons: Linking structure with polarity and function', *Progress in Neurobiology*. Pergamon, 168, pp. 86–103. doi: 10.1016/J.PNEUROBIO.2018.05.002.

Nelis, E. *et al.* (1996) 'Estimation of the mutation frequencies in Charcot-Marie-Tooth disease type 1 and hereditary neuropathy with liability to pressure palsies: a European collaborative study', *European journal of human genetics: EJHG*, 4(1), pp. 25–33. Available at: http://www.ncbi.nlm.nih.gov/pubmed/8800924.

Ng, B. K. *et al.* (2007) 'Anterograde transport and secretion of brain-derived neurotrophic factor along sensory axons promote schwann cell myelination', *Journal of Neuroscience*, 27(28). doi: 10.1523/JNEUROSCI.0563-07.2007.

Nickols, J. C. *et al.* (2003) 'Activation of the transcription factor NF-κB in Schwann cells is required for peripheral myelin formation', *Nature Neuroscience*, 6(2), pp. 161–167. doi: 10.1038/nn995.

Nie, S. *et al.* (2014) *Cerebrotendinous xanthomatosis: a comprehensive review of pathogenesis, clinical manifestations, diagnosis, and management*. doi: 10.1186/s13023-014-0179-4.

Njajou, O. T. *et al.* (2009) 'Association between oxidized LDL, obesity and type 2 diabetes in a population-based cohort, the health, aging and body composition study', *Diabetes/Metabolism Research and Reviews*. Diabetes Metab Res Rev, 25(8), pp. 733–739. doi: 10.1002/dmrr.1011.

Nykjaer, A. *et al.* (2004) 'Sortilin is essential for proNGF-induced neuronal cell death', *Nature*, 427(6977), pp. 843–848. doi: 10.1038/nature02319.

Okamoto, Y. *et al.* (2013) 'Curcumin facilitates a transitory cellular stress response in Trembler-J mice.', *Human molecular genetics*, 22(23), pp. 4698–705. doi: 10.1093/hmg/ddt318.

Oppenheim, R. W. (1991) 'Cell death during development of the nervous system', *Annual Review of Neuroscience*. doi: 10.1146/annurev.ne.14.030191.002321.

Otero, J. E. *et al.* (2012) 'Constitutively active canonical NF-κB pathway induces severe bone loss in mice', *PLoS ONE*. Public Library of Science, 7(6). doi: 10.1371/journal.pone.0038694.

Paassen, B. W. van *et al.* (2014) 'PMP22 related neuropathies: Charcot-Marie-Tooth disease type 1A and Hereditary Neuropathy with liability to Pressure Palsies', *Orphanet Journal of Rare Diseases*, 9(1), p. 38. doi: 10.1186/1750-1172-9-38.

Palmada, M. *et al.* (2002) 'c-jun is essential for sympathetic neuronal death induced by NGF withdrawal but not by p75 activation', *Journal of Cell Biology*, 158(3). doi: 10.1083/jcb.200112129.

Pareek, S. *et al.* (1997) 'Neurons promote the translocation of peripheral myelin protein 22 into myelin', *Journal of Neuroscience*. Society for Neuroscience, 17(20), pp. 7754–7762. doi: 10.1523/jneurosci.17-20-07754.1997.

Pareyson, D. and Marchesi, C. (2009) 'Diagnosis, natural history, and management of Charcot–Marie–Tooth disease', *The Lancet Neurology*, 8(7), pp. 654–667. doi: 10.1016/S1474-4422(09)70110-3.

Pareyson, D., Scaioli, V. and Laurà, M. (2006) 'Clinical and electrophysiological aspects of Charcot-Marie-Tooth disease', *NeuroMolecular Medicine*, 8(1–2), pp. 3–22. doi: 10.1385/NMM:8:1-2:3.

Penno, A. *et al.* (2010) 'Hereditary sensory neuropathy type 1 is caused by the accumulation of two neurotoxic sphingolipids.', *The Journal of biological chemistry*. American Society for Biochemistry and Molecular Biology, 285(15), pp. 11178–87. doi: 10.1074/jbc.M109.092973.

Perez-Matos, M. C., Morales-Alvarez, M. C. and Mendivil, C. O. (2017) 'Lipids: A Suitable Therapeutic Target in Diabetic Neuropathy?', *Journal of Diabetes Research*. Hindawi Publishing Corporation. doi: 10.1155/2017/6943851.

Perez-Matos, M C, Morales-Alvarez, M. C. and Mendivil, C. O. (2017) 'Lipids: A Suitable Therapeutic Target in Diabetic Neuropathy?' doi: 10.1155/2017/6943851.

Pertusa, M. *et al.* (2007a) 'Transcriptional control of cholesterol biosynthesis in Schwann cells by axonal neuregulin 1.', *The Journal of biological chemistry*. American Society for Biochemistry and Molecular Biology, 282(39), pp. 28768–78. doi: 10.1074/jbc.M701878200.

Pertusa, M. *et al.* (2007b) 'Transcriptional control of cholesterol biosynthesis in schwann cells by axonal neuregulin 1', *Journal of Biological Chemistry*. JBC Papers in Press, 282(39), pp. 28768–28778. doi: 10.1074/jbc.M701878200.

Pfeffer, B. A. *et al.* (2016) 'Differential cytotoxic effects of 7-dehydrocholesterol-derived oxysterols on cultured retina-derived cells: Dependence on sterol structure, cell type, and density.', *Experimental eye research*, 145, pp. 297–316. doi: 10.1016/j.exer.2016.01.016.

Pfeiffer, K. *et al.* (2003) 'Cardiolipin Stabilizes Respiratory Chain Supercomplexes', *Journal of Biological Chemistry*. J Biol Chem, 278(52), pp. 52873–52880. doi: 10.1074/jbc.M308366200.

Pham, D. D. *et al.* (2016) 'P75 neurotrophin receptor signaling activates sterol regulatory element-binding protein-2 in hepatocyte cells via p38 mitogen-activated protein kinase and caspase-3', *Journal of Biological Chemistry*, 291(20). doi: 10.1074/jbc.M116.722272.

Poitelon, Y., Kopec, A. M. and Belin, S. (2020) 'Myelin Fat Facts: An Overview of Lipids and Fatty Acid Metabolism', *Cells*. Multidisciplinary Digital Publishing Institute, 9(4), p. 812. doi: 10.3390/cells9040812.

Pope, S., Land, J. M. and Heales, S. J. R. (2008) 'Oxidative stress and mitochondrial dysfunction in neurodegeneration; cardiolipin a critical target?', *Biochimica et Biophysica Acta - Bioenergetics*. Elsevier, pp. 794–799. doi: 10.1016/j.bbabio.2008.03.011.

Porter, F. D. (2008) ‘Smith–Lemli–Opitz syndrome: pathogenesis, diagnosis and management’, *European Journal of Human Genetics*. Nature Publishing Group, 16(5), pp. 535–541. doi: 10.1038/ejhg.2008.10.

Porter, F. D. and Herman, G. E. (2011) ‘Malformation syndromes caused by disorders of cholesterol synthesis.’, *Journal of lipid research*. American Society for Biochemistry and Molecular Biology, 52(1), pp. 6–34. doi: 10.1194/jlr.R009548.

Posse de Chaves, E. I. (2006) ‘Sphingolipids in apoptosis, survival and regeneration in the nervous system’, *Biochimica et Biophysica Acta - Biomembranes*. Elsevier, pp. 1995–2015. doi: 10.1016/j.bbamem.2006.09.018.

Powers, J. M. *et al.* (2001) ‘The dorsal root ganglia in adrenomyeloneuropathy: Neuronal atrophy and abnormal mitochondria’, *Journal of Neuropathology and Experimental Neurology*. American Association of Neuropathologists Inc., 60(5), pp. 493–501. doi: 10.1093/jnen/60.5.493.

Prabhu, A. V., Sharpe, L. J. and Brown, A. J. (2014) ‘The sterol-based transcriptional control of human 7-dehydrocholesterol reductase (DHCR7): Evidence of a cooperative regulatory program in cholesterol synthesis’, *Biochimica et Biophysica Acta - Molecular and Cell Biology of Lipids*. Elsevier, 1841(10), pp. 1431–1439. doi: 10.1016/j.bbalip.2014.07.006.

Qin, Z. *et al.* (2020) ‘Partial deletion of p75 ^{NTR} in large-diameter DRG neurons exerts no influence upon the survival of peripheral sensory neurons *in vivo*’, *Journal of Neuroscience Research*. J Neurosci Res, p. jnr.24665. doi: 10.1002/jnr.24665.

Raghunath, A. *et al.* (2018) ‘Antioxidant response elements: Discovery, classes, regulation and potential applications’, *Redox Biology*. doi: 10.1016/j.redox.2018.05.002.

Van Rappard, D. F., Boelens, J. J. and Wolf, N. I. (2015) ‘Metachromatic leukodystrophy: Disease spectrum and approaches for treatment’, *Best Practice and Research: Clinical Endocrinology and Metabolism*. doi: 10.1016/j.beem.2014.10.001.

Redmann, M. *et al.* (2018) ‘Methods for assessing mitochondrial quality control mechanisms and cellular consequences in cell culture’, *Redox Biology*. Elsevier B.V., 17, pp. 59–69. doi: 10.1016/j.redox.2018.04.005.

Reilly, M. (2009) ‘Classification and diagnosis of the inherited neuropathies’, *Annals of Indian Academy of Neurology*. Wolters Kluwer -- Medknow Publications, pp. 80–88. doi: 10.4103/0972-2327.53075.

Reinhold, A. K. and Rittner, H. L. (2020) ‘Characteristics of the nerve barrier and the blood dorsal root ganglion barrier in health and disease’, *Experimental Neurology*. Academic Press Inc. doi: 10.1016/j.expneurol.2020.113244.

Renner, F. and Schmitz, M. L. (2009) ‘Autoregulatory feedback loops terminating the NF-κB response’, *Trends in Biochemical Sciences*. Trends Biochem Sci, pp. 128–135. doi: 10.1016/j.tibs.2008.12.003.

Riethmacher, D. *et al.* (1997) ‘Severe neuropathies in mice with targeted mutations in the ErbB3 receptor’, *Nature*, 389(6652). doi: 10.1038/39593.

Rombach, S. M. *et al.* (2010) ‘Plasma globotriaosylsphingosine: Diagnostic value and relation to clinical manifestations of Fabry disease’, *Biochimica et Biophysica Acta - Molecular Basis of Disease*. Biochim Biophys Acta, 1802(9), pp. 741–748. doi: 10.1016/j.bbadis.2010.05.003.

Saher, G. *et al.* (2005) ‘High cholesterol level is essential for myelin membrane growth’, *Nature Neuroscience*. Nature Publishing Group, 8(4), pp. 468–475. doi: 10.1038/nn1426.

Saher, G. and Simons, M. (2010) ‘Cholesterol and Myelin Biogenesis’, in. Springer, Dordrecht, pp. 489–508. doi: 10.1007/978-90-481-8622-8_18.

Saporta, M. a C. *et al.* (2012) ‘MpzR98C arrests Schwann cell development in a mouse model of early-onset Charcot-Marie-Tooth disease type 1B.’, *Brain : a journal of neurology*, 135(Pt 7), pp. 2032–47. doi: 10.1093/brain/aws140.

Sasaki, Y. *et al.* (2006) ‘Canonical NF-κB Activity, Dispensable for B Cell Development, Replaces BAFF-Receptor Signals and Promotes B Cell Proliferation upon Activation’, *Immunity*. Immunity, 24(6), pp. 729–739. doi: 10.1016/j.immuni.2006.04.005.

Schmitt, S., Cantuti Castelvetri, L. and Simons, M. (2014) ‘Metabolism and functions of lipids in myelin ☆’. doi: 10.1016/j.bbalip.2014.12.016.

Schmitt, S., Cantuti Castelvetri, L. and Simons, M. (2015a) ‘Metabolism and functions of lipids in myelin’, *Biochimica et Biophysica Acta (BBA) - Molecular and Cell Biology of Lipids*. Elsevier B.V., 1851(8), pp. 999–1005. doi: 10.1016/j.bbalip.2014.12.016.

Schmitt, S., Cantuti Castelvetri, L. and Simons, M. (2015b) ‘Metabolism and functions of lipids in myelin’, *Biochimica et Biophysica Acta - Molecular and Cell Biology of Lipids*. Elsevier B.V., pp. 999–1005. doi: 10.1016/j.bbalip.2014.12.016.

Schuchman, E. H. and Desnick, R. J. (2017) ‘Types A and B Niemann-Pick disease’, *Molecular Genetics and Metabolism*. Academic Press Inc., pp. 27–33. doi: 10.1016/j.ymgme.2016.12.008.

Schwartzlow, C. and Kazamel, M. (2019) ‘Hereditary Sensory and Autonomic Neuropathies: Adding More to the Classification’. doi: 10.1007/s11910-019-0974-3.

Shih, V. F. S. *et al.* (2009) ‘Kinetic control of negative feedback regulators of NF-κB/RelA determines their pathogen- and cytokine-receptor signaling specificity’, *Proceedings of the National Academy of Sciences of the United States of America*. National Academy of Sciences, 106(24), pp. 9619–9624. doi: 10.1073/pnas.0812367106.

Shy, M. E. *et al.* (2004) ‘Phenotypic clustering in MPZ mutations’, *Brain: a journal of neurology*, 127(Pt 2), pp. 371–384. doi: 10.1093/brain/awh048.

Singh, A. *et al.* (2019) ‘Oxidative stress: A key modulator in neurodegenerative diseases’, *Molecules*. MDPI AG. doi: 10.3390/molecules24081583.

Sitarska, D. and Ługowska, A. (2019) ‘Laboratory diagnosis of the Niemann-Pick type C disease: an inherited neurodegenerative disorder of cholesterol metabolism’, *Metabolic Brain Disease*, 34(5), pp. 1253–1260. doi: 10.1007/s11011-019-00445-w.

Skaper, S. D. (2018) ‘Neurotrophic factors: An overview’, in *Methods in Molecular Biology*. Humana Press Inc., pp. 1–17. doi: 10.1007/978-1-4939-7571-6_1.

Smeyne, R. J. *et al.* (1994) ‘Severe sensory and sympathetic neuropathies in mice carrying a disrupted Trk/NGF receptor gene’, *Nature*. Nature, 368(6468), pp. 246–249. doi: 10.1038/368246a0.

Smith, A. G. and Singleton, J. R. (2013) ‘Obesity and hyperlipidemia are risk factors for early diabetic neuropathy’, *Journal of Diabetes and its Complications*. J Diabetes Complications, 27(5), pp. 436–442. doi: 10.1016/j.jdiacomp.2013.04.003.

Smith, D. *et al.* (2009) ‘Nuclear factor-κB activation in axons and schwann cells in experimental sciatic nerve injury and its role in modulating axon regeneration: Studies with etanercept’, *Journal of Neuropathology and Experimental Neurology*. PMC Canada manuscript submission, 68(6), pp. 691–700. doi: 10.1097/NEN.0b013e3181a7c14e.

Spassieva, S. and Bieberich, E. (2016) ‘Lysosphingolipids and sphingolipidoses: Psychosine in Krabbe’s disease’, *Journal of Neuroscience Research*. John Wiley and Sons Inc., pp. 974–981. doi: 10.1002/jnr.23888.

Starck, L. *et al.* (2007) ‘Beneficial effects of dietary supplementation in a disorder with defective synthesis of cholesterol. A case report of a girl with Smith-Lemli-Opitz syndrome, polyneuropathy and precocious puberty’, *Acta Paediatrica*. John Wiley & Sons, Ltd (10.1111), 88(7), pp. 729–733. doi: 10.1111/j.1651-2227.1999.tb00033.x.

Stassart, R. M. *et al.* (2013) ‘A role for Schwann cell-derived neuregulin-1 in remyelination.’, *Nature neuroscience*, 16(1), pp. 48–54. doi: 10.1038/nn.3281.

Stavrou, M. *et al.* (2020) ‘Genetic mechanisms of peripheral nerve disease’, *Neuroscience Letters*. Neurosci Lett, p. 135357. doi: 10.1016/j.neulet.2020.135357.

Stucky, C. L. and Koltzenburg, M. (1997) ‘The low-affinity neurotrophin receptor p75 regulates the function but not the selective survival of specific subpopulations of sensory neurons’, *Journal of Neuroscience*. Society for Neuroscience, 17(11), pp. 4398–4405. doi: 10.1523/jneurosci.17-11-04398.1997.

Sunami, E. *et al.* (2001) ‘Morphological characteristics of Schwann cells in the islets of Langerhans of the murine pancreas’, *Archives of Histology and Cytology*. Japan Society of Histological Documentation, 64(2), pp. 191–201. doi: 10.1679/aohc.64.191.

Sundaram, V. K., Massaad, C. and Grenier, J. (2019) ‘Liver X receptors and their implications in the physiology and pathology of the peripheral nervous system’, *International Journal of Molecular Sciences*. MDPI AG. doi: 10.3390/ijms20174192.

Suryavanshi, S. V. and Kulkarni, Y. A. (2017) 'NF-κβ: A potential target in the management of vascular complications of diabetes', *Frontiers in Pharmacology*. Frontiers Media S.A. doi: 10.3389/fphar.2017.00798.

Suzuki, Kunihiko and Suzuki, Kinuko (1995) 'The Twitcher Mouse: A Model for Krabbe Disease and for Experimental Therapies', *Brain Pathology*. Brain Pathol, 5(3), pp. 249–258. doi: 10.1111/j.1750-3639.1995.tb00601.x.

Takahashi, M. and Osumi, N. (2005) 'Identification of a novel type II classical cadherin: Rat cadherin19 is expressed in the cranial ganglia and Schwann cell precursors during development', *Developmental Dynamics*, 232(1). doi: 10.1002/dvdy.20209.

Tam, A. B. *et al.* (2012) 'ER stress activates NF-κB by integrating functions of basal IKK activity, IRE1 and PERK.', *PloS one*, 7(10), p. e45078. doi: 10.1371/journal.pone.0045078.

Tapinos, N., Ohnishi, M. and Rambukkana, A. (2006) 'ErbB2 receptor tyrosine kinase signaling mediates early demyelination induced by leprosy bacilli', *Nature Medicine*. Nature Publishing Group, 12(8), pp. 961–966. doi: 10.1038/nm1433.

Taso, O. V. *et al.* (2019a) 'Lipid peroxidation products and their role in neurodegenerative diseases', *Annals of Research Hospitals*. AME Publishing Company, 3, pp. 2–2. doi: 10.21037/arh.2018.12.02.

Taso, O. V. *et al.* (2019b) 'Lipid peroxidation products and their role in neurodegenerative diseases', *Annals of Research Hospitals*. AME Publishing Company, 3, pp. 2–2. doi: 10.21037/arh.2018.12.02.

Taveggia, C. *et al.* (2005) 'Neuregulin-1 type III determines the ensheathment fate of axons', *Neuron*, 47(5). doi: 10.1016/j.neuron.2005.08.017.

Tep, C. *et al.* (2012) 'Brain-derived neurotrophic factor (BDNF) induces polarized signaling of small GTPase (Rac1) protein at the onset of schwann cell myelination through partitioning-defective 3 (Par3) protein', *Journal of Biological Chemistry*. doi: 10.1074/jbc.M111.312736.

Tep, C. *et al.* (2013) 'Oral administration of a small molecule targeted to block proNGF binding to p75 promotes myelin sparing and functional recovery after spinal cord injury', *Journal of Neuroscience*, 33(2). doi: 10.1523/JNEUROSCI.0399-12.2013.

Tesfaye, S. *et al.* (2005) 'Vascular Risk Factors and Diabetic Neuropathy', *New England Journal of Medicine*. Massachusetts Medical Society, 352(4), pp. 341–350. doi: 10.1056/nejmoa032782.

Timmerman, V., Strickland, A. V and Züchner, S. (2014) 'Genetics of Charcot-Marie-Tooth (CMT) Disease within the Frame of the Human Genome Project Success', *Genes*, 5(1), pp. 13–32. doi: 10.3390/genes5010013.

Toda, K. *et al.* (1989) 'Accumulation of lysosulfatide (sulfogalactosylsphingosine) in tissues of a boy with metachromatic leukodystrophy', *Biochemical and Biophysical Research Communications*. Biochem Biophys Res Commun, 159(2), pp. 605–611. doi: 10.1016/0006-291X(89)90037-5.

Tooth, H. H. (1886) *The peroneal type of progressive muscular atrophy.* London: Lewis.

Tracey, T. J. *et al.* (2018) 'Neuronal lipid metabolism: Multiple pathways driving functional outcomes in health and disease', *Frontiers in Molecular Neuroscience*. Frontiers Media S.A. doi: 10.3389/fnmol.2018.00010.

Tulenko, T. N. *et al.* (2006) 'A membrane defect in the pathogenesis of the Smith-Lemli-Opitz syndrome.', *Journal of lipid research*. American Society for Biochemistry and Molecular Biology, 47(1), pp. 134–43. doi: 10.1194/jlr.M500306-JLR200.

Turk, B. R. *et al.* (2020) 'X-linked adrenoleukodystrophy: Pathology, pathophysiology, diagnostic testing, newborn screening and therapies', *International Journal of Developmental Neuroscience*. John Wiley and Sons Inc., 80(1), pp. 52–72. doi: 10.1002/jdn.10003.

Ueda, H. (2020) 'Pathogenic mechanisms of lipid mediator lysophosphatidic acid in chronic pain', *Progress in Lipid Research*. Elsevier BV, 81, p. 101079. doi: 10.1016/j.plipres.2020.101079.

Vaegter, C. B. *et al.* (2011) 'Sortilin associates with Trk receptors to enhance anterograde transport and neurotrophin signaling', *Nature Neuroscience*. NIH Public Access, 14(1), pp. 54–63. doi: 10.1038/nn.2689.

Vance, J. M. *et al.* (1991) 'Localization of Charcot-Marie-Tooth disease type 1a (CMT1A) to chromosome 17p11.2', *Genomics*, 9(4), pp. 623–628. doi: 10.1016/0888-7543(91)90355-I.

Verhamme, C. *et al.* (2011) *Myelin and axon pathology in a long-term study of PMP22-overexpressing mice.*, *Journal of neuropathology and experimental neurology*. doi: 10.1097/NEN.0b013e318217eba0.

Verheijen, M. H. G. *et al.* (2003) 'Local regulation of fat metabolism in peripheral nerves.', *Genes & development*. Cold Spring Harbor Laboratory Press, 17(19), pp. 2450–64. doi: 10.1101/gad.1116203.

Verheijen, M. H. G. *et al.* (2009) 'SCAP is required for timely and proper myelin membrane synthesis', *Proceedings of the National Academy of Sciences*, 106(50), pp. 21383–21388. doi: 10.1073/pnas.0905633106.

Viader, A. (2012) 'The role of Schwann cell mitochondrial metabolism in Schwann cell biology and axonal survival.', *Dissertation Abstracts International: Section B: The Sciences and Engineering*, 73(4-B), p. 2019. Available at: http://gateway.proquest.com/openurl?url_ver=Z39.88-2004&rft_val_fmt=info:ofi/fmt:kev:mtx:dissertation&res_dat=xri:pqm&rft_dat=xri:pqdiss:3487544%5Cnhttp://ovidsp.ovid.com/ovidweb.cgi?T=JS&PAGE=reference&D=psyc7&NEWS=N&AN=2012-99200-180.

Viader, A. *et al.* (2013) 'Aberrant Schwann cell lipid metabolism linked to mitochondrial deficits leads to axon degeneration and neuropathy.', *Neuron*. NIH Public Access, 77(5), pp. 886–98. doi: 10.1016/j.neuron.2013.01.012.

Vincent, A. M. *et al.* (2004) ‘Oxidative stress in the pathogenesis of diabetic neuropathy’, *Endocrine Reviews*. Oxford Academic, pp. 612–628. doi: 10.1210/er.2003-0019.

Vincent, A. M., Hayes, J. M., *et al.* (2009) ‘Dyslipidemia-induced neuropathy in mice: The role of oxLDL/LOX-1’, *Diabetes*. American Diabetes Association, 58(10), pp. 2376–2385. doi: 10.2337/db09-0047.

Vincent, A. M., Kato, K., *et al.* (2009) ‘Sensory Neurons and Schwann Cells Respond to Oxidative Stress by Increasing Antioxidant Defense Mechanisms’, *Antioxidants & Redox Signaling*, 11(3), pp. 425–438. doi: 10.1089/ars.2008.2235.

Visigalli, D. *et al.* (2015) ‘Alternative Splicing in the Human PMP22 Gene: Implications in CMT1A Neuropathy’, *Human Mutation*, p. n/a-n/a. doi: 10.1002/humu.22921.

Visigalli, D. *et al.* (2020) ‘Exploiting Sphingo- and Glycerophospholipid Impairment to Select Effective Drugs and Biomarkers for CMT1A’, *Frontiers in Neurology*. Frontiers Media S.A., 11, p. 903. doi: 10.3389/fneur.2020.00903.

Wang, L., Chopp, M., Szalad, A., Lu, X. R., *et al.* (2020) ‘Exosomes derived from Schwann cells ameliorate peripheral neuropathy in type 2 diabetic mice’, *Diabetes*, 69(4). doi: 10.2337/db19-0432.

Wang, L., Chopp, M., Szalad, A., Lu, X., *et al.* (2020) ‘Exosomes Derived From Schwann Cells Ameliorate Peripheral Neuropathy in Type II Diabetic Mice’, *Diabetes*, p. db190432. doi: 10.2337/db19-0432.

Wang, W. *et al.* (2020) ‘Activation of sphingosine 1-phosphate receptor 2 attenuates chemotherapy-induced neuropathy’, *Journal of Biological Chemistry*. American Society for Biochemistry and Molecular Biology Inc., 295(4), pp. 1143–1152. doi: 10.1074/jbc.RA119.011699.

Webster, H. D. (1971) ‘The geometry of peripheral myelin sheaths during their formation and growth in rat sciatic nerves.’, *The Journal of cell biology*. The Rockefeller University Press, 48(2), pp. 348–67. Available at: http://www.ncbi.nlm.nih.gov/pubmed/4928020 (Accessed: 22 February 2019).

Weerasuriya, A. and Mizisin, A. P. (2011) ‘The Blood-Nerve Barrier: Structure and Functional Significance’, in. Humana Press, pp. 149–173. doi: 10.1007/978-1-60761-938-3_6.

Wei, Z. *et al.* (2019) ‘Proteomics analysis of Schwann cell-derived exosomes: a novel therapeutic strategy for central nervous system injury’, *Molecular and Cellular Biochemistry*. Springer New York LLC, 457(1–2), pp. 51–59. doi: 10.1007/s11010-019-03511-0.

Welte, M. A. (2015) ‘Expanding roles for lipid droplets’, *Current Biology*. Cell Press, pp. R470–R481. doi: 10.1016/j.cub.2015.04.004.

White, F. A. *et al.* (1996) ‘Synchronous onset of NGF and TrkA survival dependence in developing dorsal root ganglia’, *Journal of Neuroscience*. Society for Neuroscience, 16(15), pp. 4662–4672. doi: 10.1523/jneurosci.16-15-04662.1996.

Wiggin, T. D. *et al.* (2009) 'Elevated triglycerides correlate with progression of diabetic neuropathy', *Diabetes*. American Diabetes Association, 58(7), pp. 1634–1640. doi: 10.2337/db08-1771.

Wilson, E. R. *et al.* (2018) 'Hereditary sensory neuropathy type 1-associated deoxysphingolipids cause neurotoxicity, acute calcium handling abnormalities and mitochondrial dysfunction in vitro', *Neurobiology of Disease*, 117, pp. 1–14. doi: 10.1016/j.nbd.2018.05.008.

Woldeyesus, M. T. *et al.* (1999) 'Peripheral nervous system defects in erbB2 mutants following genetic rescue of heart development', *Genes and Development*, 13(19). doi: 10.1101/gad.13.19.2538.

Woronicz, J. D. *et al.* (1997) 'IκB kinase-β: NF-κB activation and complex formation with IκB kinase-α and NIK', *Science*. American Association for the Advancement of Science, 278(5339), pp. 866–869. doi: 10.1126/science.278.5339.866.

Xu, G. *et al.* (2009) 'Oxidation of cholesterol and β and prevention by natural antioxidants', *Journal of Agricultural and Food Chemistry*, 57(19). doi: 10.1021/jf902552s.

Xu, L. *et al.* (2012a) 'DHCEO accumulation is a critical mediator of pathophysiology in a Smith-Lemli-Opitz syndrome model', *Neurobiology of Disease*, 45(3). doi: 10.1016/j.nbd.2011.12.011.

Xu, L. *et al.* (2012b) 'DHCEO accumulation is a critical mediator of pathophysiology in a Smith-Lemli-Opitz syndrome model', *Neurobiology of Disease*, 45(3), pp. 923–929. doi: 10.1016/j.nbd.2011.12.011.

Xu, L., Davis, T. A. and Porter, N. A. (2009) 'Rate constants for peroxidation of polyunsaturated fatty acids and sterols in solution and in liposomes', *Journal of the American Chemical Society*, 131(36). doi: 10.1021/ja9029076.

Yang, D. P. *et al.* (2012) 'p38 MAPK activation promotes denervated Schwann cell phenotype and functions as a negative regulator of Schwann cell differentiation and myelination.', *The Journal of neuroscience : the official journal of the Society for Neuroscience*, 32(21), pp. 7158–68. doi: 10.1523/JNEUROSCI.5812-11.2012.

Yoon, C., Korade, Z. and Carter, B. D. (2008) 'Protein kinase A-induced phosphorylation of the p65 subunit of nuclear factor-kappaB promotes Schwann cell differentiation into a myelinating phenotype', *The Journal of Neuroscience: The Official Journal of the Society for Neuroscience*, 28(14), pp. 3738–3746. doi: 10.1523/JNEUROSCI.4439-07.2008.

Yu, F. P. S. *et al.* (2018) 'Acid ceramidase deficiency: Farber disease and SMA-PME', *Orphanet Journal of Rare Diseases*. BioMed Central Ltd. doi: 10.1186/s13023-018-0845-z.

Zappatini-Tommasi, L. *et al.* (1992) 'Farber disease: an ultrastructural study - Report of a case and review of the literature', *Virchows Archiv A Pathological Anatomy and Histopathology*. Springer-Verlag, pp. 281–290. doi: 10.1007/BF01600282.

Zhou, M. *et al.* (2018) ‘Effects of RSC96 Schwann Cell-Derived Exosomes on Proliferation, Senescence, and Apoptosis of DorsZhou, M. et al. (2018) “Effects of RSC96 Schwann Cell-Derived Exosomes on Proliferation, Senescence, and Apoptosis of Dorsal Root Ganglion Cells In Vitro”, M’, *Medical Science Monitor*, 24, pp. 7841–7849. doi: 10.12659/MSM.909509.

Zhou, Y. *et al.* (2019) ‘A neutral lipid-enriched diet improves myelination and alleviates peripheral nerve pathology in neuropathic mice’, *Experimental Neurology*. Academic Press Inc., 321, p. 113031. doi: 10.1016/j.expneurol.2019.113031.

Zuchner, S. (2003) ‘A novel nonsense mutation in the ABC1 gene causes a severe syringomyelia-like phenotype of Tangier disease’, *Brain*. Oxford Academic, 126(4), pp. 920–927. doi: 10.1093/brain/awg074.

Zyss, J. *et al.* (2012) ‘Clinical and electrophysiological characteristics of neuropathy associated with Tangier disease’, *Journal of Neurology*. Springer-Verlag, 259(6), pp. 1222–1226. doi: 10.1007/s00415-011-6340-2.